P-06-01

Oskarshamn site investigation

Mineralogical, chemical and redox features of red-staining adjacent to fractures

Results from drill cores KSH01A+B and KSH03A+B

Henrik Drake
Department of Geology, Earth Sciences Centre,
Göteborg University

Eva-Lena Tullborg
Terralogica AB

January 2006

Svensk Kärnbränslehantering AB
Swedish Nuclear Fuel
and Waste Management Co
Box 5864
SE-102 40 Stockholm Sweden
Tel 08-459 84 00
+46 8 459 84 00
Fax 08-661 57 19
+46 8 661 57 19

ISSN 1651-4416
SKB P-06-01

Oskarshamn site investigation

Mineralogical, chemical and redox features of red-staining adjacent to fractures

Results from drill cores KSH01A+B and KSH03A+B

Henrik Drake
Department of Geology, Earth Sciences Centre,
Göteborg University

Eva-Lena Tullborg
Terralogica AB

January 2006

Keywords: Red-staining, Simpevarp, Wall rock alteration, Hydrothermal alteration, Oxidation, Mineralogy, Whole rock chemistry, Mössbauer spectroscopy, SEM-EDS, Reducing capacity.

Abstract

The present study is part of the site investigation program run by the Swedish Nuclear Fuel and Waste Management Co (SKB) in the Simpevarp/Laxemar area 30 km N of Oskarshamn, SE Sweden. Two drill-cores, KSH01A+B and KSH03A+B from the Simpevarp peninsula have been sampled for detailed studies of red-staining in fine-grained dioritoid, quartz monzodiorite and Ävrö granite adjacent to fractures. This is a very common feature in the Simpevarp/Laxemar area and is caused by hydrothermal alteration in combination with oxidation.

Thin sections of 24 samples, comprising twelve red-stained samples and twelve samples of reference rock were investigated and point-counted using petrographic microscope and SEM-EDS. Whole rock chemical analyses of major, minor and trace elements were performed using ICP-AES and ICP-QMS, in order to distinguish which elements that were depleted, enriched or unaffected during alteration. Mössbauer spectroscopy was carried out in order to make out the total Fe^{3+}/Fe_{tot}-ratio in the red-stained rock compared to the reference rock. This indicates how much reducing capacity that is remaining in the red-stained rock. A comparison of the results from the present study with the results from a similar study in the Laxemar subarea is found in /Drake and Tullborg 2006c/.

The red-staining is mainly caused by minute inclusions of Fe^{3+}-rich minerals, mainly hematite. These are mainly hosted in porous secondary K-feldspar and albite that completely replace primary plagioclase. Accompanying this alteration is replacement of magnetite by hematite and of biotite by chlorite, formation of secondary sericite, prehnite, titanite and epidote, as well as an increase in micro-porosity and micro-fractures. The red-staining is thought to occur at temperatures of c. 280–400°C, based on e.g. indications from earlier studies on temperatures of chloritization, plagioclase alteration and the low-temperature paragenesis in general e.g. /Liou et al. 1983, Frey et al. 1991, Deer et al. 1992, Slaby 1992, Spear 1993, Lee and Parsons 1997, Bucher and Frey 2002, Wilamowski 2002/. Intense local red-staining caused by hematite and possibly also Fe-oxyhydroxide in micro-fractures is thought to be formed subsequently to the major red-staining event, presumably at lower temperatures. Primary quartz, K-feldspar and titanite remained rather fresh during alteration. The reference rock is often hydrothermally altered as well, characterized by partial to complete replacement of biotite by chlorite and of magnetite by hematite, which shows that the hydrothermal alteration often reaches further into the wall rock than the red-staining does.

The red-stained rock is significantly enriched in K, Na, Rb, and H_2O and partially enriched in Ba, F and U. The increase in K, Na, Rb, Ba, and H_20 is associated to formation of secondary adularia, albite and water-bearing minerals like chlorite, prehnite and sericite. The red-stained rock is highly depleted in Ca, Sr, Cs, Be, Ga and Cr while more moderate depletion is evident for Al, Th, and S. The depletion is mainly associated to break down of plagioclase, alteration of biotite, hornblende and augite and oxidation of magnetite and subordinately pyrite. The total Fe-content as well as related elements such as Ti, Mg, Sc, V, Co and other elements like Si, P, Y and REE:s remained fairly constant. Mössbauer analyses reveal that Fe^{3+}-contents are elevated in the red-stained rock compared to the reference rock, due to oxidation of magnetite to hematite and an increased amount of Fe^{3+}-bearing epidote in the red-stained rock. Increase of chlorite in the red-stained rock also affects this ratio. The total increase in Fe^{3+}/Fe_{tot}, generally about 3–10%, is however not as high as the macroscopic features of the red-stained rock might suggest. Ävrö granite samples generally have the largest amounts of Fe^{3+}/Fe_{tot} as well as the largest increase in Fe^{3+}/Fe_{tot}, mainly due to high epidote-contents.

Sammanfattning

Svensk Kärnbränslehantering AB (SKB) utför för närvarande platsundersökningar i Simpevarp/Laxemar området i Oskarshamns kommun, med syfte att hitta en lämplig plats för slutförvaring av utbränt kärnbränsle. Prover har tagits från borrkärnorna KSH01A+B och KSH03A+B från Simpevarpshalvön i syfte att undersöka rödfärgningen av finkornig dioritoid, kvartsmonzodiorit och Ävrö granit runt sprickor. Rödfärgning orsakad av hydrotermal omvandling i kombination med oxidering är vanligt förekommande i Simpevarp/Laxemar-området.

Tunnslip från 24 prover, tolv rödfärgade och tolv referensprover, har undersökts med petrografiskt mikroskop (inklusive ”point-counting”) och SEM-EDS. Kemiska analyser, med hjälp av ICP-AES och ICP-QMS, har utförts för att undersöka vilka ämnen som anrikats, urlakats eller varit konstanta under hydrotermalomvandlingen och rödfärgningen. För att utröna skillnader i Fe^{3+}/Fe_{tot}-kvoten mellan de rödfärgade proverna och referensproverna har Mössbauer spektroskopianalyser utförts. Detta ger indikation på hur mycket reducerande kapacitet som finns kvar i det rödfärgade berget. En jämförelse av resultaten från denna studie med resultaten från en liknande studie från Laxemarområdet finns i /Drake and Tullborg 2006c/.

Rödfärgningen runt sprickor är främst orsakad av mikroskopiskt till submikroskopiskt små Fe^{3+}-rika mineral, huvudsakligen hematit, vilka mestadels sitter i porös kalifältspat och albit, vilka har ersatt ursprunglig plagioklas. Hematitisering av magnetit, kloritisering av biotit, bildande av sekundär prehnit, titanit och epidot och ökning av mikroporositet och antalet mikrosprickor är också karaktäristiskt för det rödfärgade berget. Rödfärgningen har troligen skett vid temperaturer runt 280–400°C, baserat på temperaturangivelser från tidigare studier av kloritisering av biotit, prehnit- och epidotbildning, nedbrytning/omvandling av plagioklas och lågtemperaturparagenesen i övrigt /Liou et al. 1983, Frey et al. 1991, Deer et al. 1992, Slaby 1992, Spear 1993, Lee and Parsons 1997, Bucher and Frey 2002, Wilamowski 2002/. Intensiv lokal rödfärgning i mikrosprickor fyllda med hematit och möjligen Fe-oxyhydroxider, tolkas som ett senare fenomen, troligen bildat vid lägre temperaturer än den huvudsakliga rödfärgningen. Kvarts, kalifältspat och titanit har huvudsakligen inte påverkats av hydrotermalomvandlingen. Referensproverna är ofta inte helt opåverkade utan visar prov på kloritisering av biotit, vilket visar att hydrotermalomvandlingen ofta sträcker sig längre ut i sidoberget än rödfärgningen.

Det rödfärgade berget är mycket anrikat på K, Na, Rb, H_2O och till viss del också på Ba, F och U. Anrikningen av K, Na, Rb, Ba och H_2O är relaterad till bildandet av sekundär adularia, albit och vattenrika mineral som klorit, prehnit och sericit. Det rödfärgade berget är urlakat på Ca, Al, Sr, Cs, Be, Ga, Cr och S. Urlakningen av dessa ämnen är huvudsakligen relaterad till nedbrytning av plagioklas, biotit, hornblände och augit och oxidering av magnetit och till viss del pyrit. Det totala Fe-innehållet är, i likhet med Fe-relaterade ämnen som Ti, Mg, Sc, V, Co och några övriga ämnen såsom Si, P, Y och REE, konstanta under hydrotermalomvandlingen. Mössbauer analyser visar att Fe^{3+}/Fe_{tot}-kvoten är förhöjd i det rödfärgade berget jämfört med referens berget, vilket bl.a. tyder på oxidering av magnetit och en förhöjd halt av epidot i det rödfärgade berget. Ökningen av klorit påverkar också denna kvot. Ökningen i Fe^{3+}/Fe_{tot}, vanligen 3–10 %, är dock lägre än vad det intensivt rödfärgade berget låter påskina. Högst Fe^{3+}/Fe_{tot}-kvot finns i Ävrö granitprover, vilka även har högst ökning av Fe^{3+}/Fe_{tot}-kvoten.

Contents

1 Introduction

The Swedish Nuclear Fuel and Waste Management Co. (SKB) is currently carrying out site investigations in the Simpevarp/Laxemar area in the Oskarshamn region on the Swedish East Coast. The site is situated in an area dominated by granitoids belonging to the Transscandinavian Igneous Belt (TIB). Two drill-cores, KSH01A+B and KSH03A+B from the Simpevarp peninsula (Figure 1-1), have been sampled for detailed studies of red-stained wall rock occurring adjacent to fractures. The red-staining is caused by hydrothermal alteration in combination with oxidation and is a very common feature in the Simpevarp/Laxemar area, and has been described briefly from drill cores e.g. /Drake and Tullborg 2004, Mattsson and Thunehed 2004/ and from field observations /Wahlgren et al. 2004/. The red-staining is more frequent in the Simpevarp area than in the Laxemar area. Earlier studies of red-stained rock from Äspö HRL, have been carried out by /Eliasson 1993, Mazurek et al. 1995, Tullborg 1995, Stosnach and Mengel 1998/.

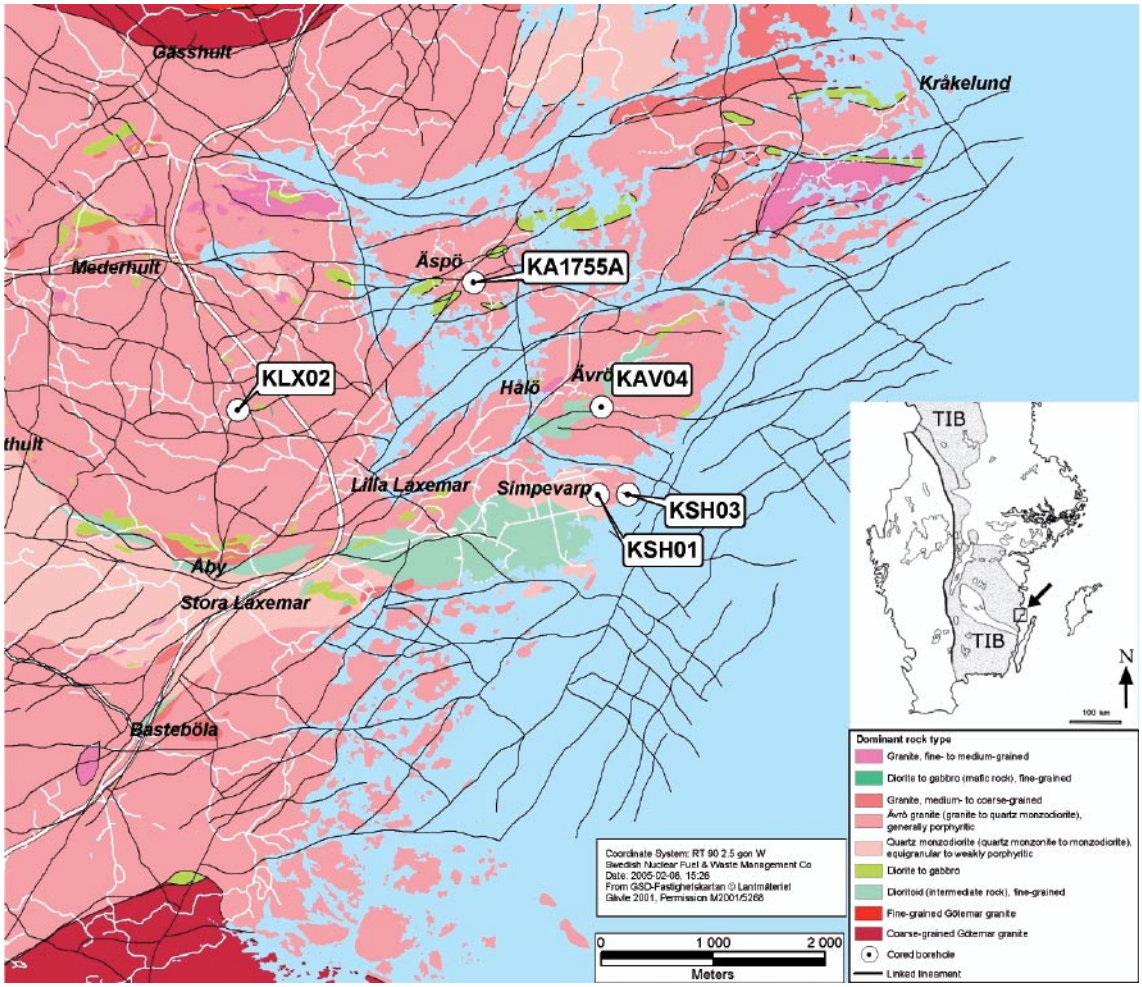

Figure 1-1. *Map showing the location of bore holes KSH01A+B and KSH03A+B. The small map shows southern Sweden and the location of the study area (arrow) and TIB, modified from /Kornfält et al. 1997/.*

A total number of 12 samples of fine-grained dioritic rocks to coarse-grained granodioritic rocks (mapped as “fine-grained dioritoid”, “quartz monzodiorite” and “Ävrö granite”, respectively) were collected from the drill cores. Each sample was divided into an “unaltered” reference rock and an altered red-stained rock. Thin sections were prepared from each of these 24 samples. The thin sections were investigated and point-counted using petrographic microscope. Scanning electron microscope (SEM) equipped with an energy dispersive spectrometer (EDS) was used for high resolution investigation and analysis of the different minerals.

Whole rock chemical analyses of major, minor and trace elements, using ICP-AES and ICP-QMS, were performed on each of the 24 samples in order to distinguish which elements were depleted, enriched or constant in the red-stained sample, compared to the reference rock, during alteration.

In order to make out the Fe^{3+}/Fe_{tot}-ratio in silicates and oxides in the red-stained rock compared to the reference rock, and in order to find out how much reducing capacity that is left in the red-stained rock after oxidation, Mössbauer spectroscopy were carried out on all of the 24 samples.

Although there are some contradicting results, a generalized model of the processes causing the red-staining can be suggested by comparison and evaluation of the thin section investigations, the chemical analyses and the results from Mössbauer spectroscopy.

This report also includes a chapter on how the features of the oxidation and hydrothermal alteration affect a nuclear repository. This includes changes in reducing capacity, porosity, sorption, rock mechanics and thermal conductivity.

Comparison of the results from the present study with investigations of red-stained wall rock from the Laxemar subarea is found in Section 7.7 in /Drake and Tullborg 2006c/.

The work was carried out in accordance with activity plan SKB PS 400-04-018. In Table 1-1 controlling documents for performing this activity are listed. Both activity plan and method descriptions are SKB’s internal controlling documents.

Table 1-1. Controlling documents for the performance of the activity.

Activity plan	**Number**	**Version**
Sprickmineralogiska undersökningar	AP PS 400-04-018	1.0
Method descriptions	**Number**	**Version**
Sprickmineralogi	SKB MD 144.000	1.0

2 Objective and scope

The aim of the study is to describe the mineralogical, chemical and redox features of the red-stained rock adjacent to fractures, compared to the relatively unaltered rock, approximately one decimetre away. By combining results from several different analytical methods, such as microscopy, SEM-EDS, whole rock chemistry analyses and Mössbauer spectroscopy, the general features and processes causing the red-staining can be recognized. For instance microscopy shows which minerals that have been altered and/or replaced and shows also the secondary minerals formed during the alteration. Whole rock chemical analyses show which elements are depleted, enriched or constant during alteration. Changes in reducing capacity caused by the hydrothermal oxidation are of certain interest in this study and are largely determined by Fe(II) available in the rock. Other elements contributing reducing capacity are S^{2-} (usually present as pyrite) and Mn^{2+} present in chlorite. Elements like U and V are also redox sensitive but present in very low amounts. Mössbauer spectroscopy shows how much of the Fe^{2+} that is oxidized to Fe^{3+} and thereby how much reducing capacity that is left in the red-stained rock.

The properties and features of the red-stained rock and the processes behind the red-staining provide useful information of a phenomenon that is widespread in all rock types in the area. Since the red-stained rock make up such a high portion of the rocks in the area, especially in association with major deformation zones it is important to understand these properties, features and principal processes in the planning of a nuclear waste repository. This report includes a chapter on how the features of the oxidation and hydrothermal alteration affect a nuclear repository. This includes changes in reducing capacity, porosity, sorption, rock mechanics and thermal conductivity.

3 Geological setting

The bedrock in the Simpevarp/Laxemar area north of Oskarshamn is dominated by Småland granitoids and dioritoids of the Transscandinavian Igneous Belt (TIB) e.g. /Gaal and Gorbatschev 1987, Kornfält and Wikman 1987, Kornfält et al. 1997, Wahlgren et al. 2004/. This belt is found between the older Svecofennian (c. 1.9 Ga) crust to the east-northeast and the younger, Gothian rocks to the west e.g. /Larson and Berglund 1992/. The TIB granitoids and volcanics were formed during several pulses of magmatism between 1.85 and 1.66 Ga. They were formed at three major magmatic events; TIB 1 (1.81–1.77 Ga), TIB 2 (1.72–1.69 Ga) and TIB 3 (1.69–1.66 Ga) /Larson and Berglund 1992, Åhäll and Larson 2000/. The Småland granitoids in the Simpevarp/Laxemar/Äspö area belong to the TIB 1 and have been dated with U-Pb-dating to 1,804 +/–4 Ma (zircon) /Kornfält et al. 1997/ and 1,802 +/–4 Ma (zircon), 1,793 +/–4 (titanite) and 1,800 +/–4 Ma (titanite and zircon) /Wahlgren et al. 2004/. Other intrusions are e.g. Götemar /Kresten and Chyssler 1976, Åberg et al. 1984/ and Uthammar. These coarse-grained granites were emplaced at 1,452 +11/–9 Ma (Götemar) and 1,441 +5/–3 Ma (Uthammar) /Åhäll 2001/. Dating and determination of a paleomagnetic pole of the "Äspö diorite" from Äspö HRL, show that the rock has not been heated above 550–600°C since its crystallization /Maddock et al. 1993/.

The bedrock surface at the Simpevarp peninsula (cf. Figure 1-1) is dominated by the rock types "fine-grained dioritoid, (intermediate magmatic rock)" in the southern part, "Ävrö granite (granite to quartz monzodiorite), generally porphyritic" in the eastern part and "quartz monzodiorite (quartz monzonite to quartzdiorite), equigranular to partly porphyritic" in the northern part /Wahlgren et al. 2004/. The lithology in drill core KSH01A+B is dominated by "quartz monzodiorite" in the upper 200 m, "fine-grained dioritoid" in section 200–600 m and by "Ävrö granite and "quartz monzodiorite" in section 600–1,000 m, while the lithology in KSH03A+B is dominated by "quartz monzodiorite" in the interval 0–270 m and by "Ävrö granite" from 270 m and downwards /Ehrenborg and Stejskal 2004ab/. These dominant rock types have similar and overlapping chemical compositions and are thus mainly distinguished by grain size and texture /Wahlgren et al. 2004/.

Structurally, the rock types on the Simpevarp peninsula are more or less well preserved, although some local occurrences of decimetre to a couple of metres wide, low-grade, ductile shear zones, may occur /Wahlgren et al. 2004/. Many of the rocks have suffered from a low-grade, metamorphic alteration, shown by sericitization and/or saussuritization of plagioclase and chloritization of biotite. A characteristic phenomenon that affects all rock types on the peninsula is an extensive, inhomogeneous red staining caused by oxidation in association with hydrothermal alteration. Geological surface mapping of the neighbouring Laxemar area reveals that similar red-staining is observed in this area as well, although not to the same extent as on the Simpevarp peninsula /Nilsson et al. 2004/.

In KSH01A+B, red-staining caused by oxidation is most extensive in the section 204–628 m, dominated by "fine-grained dioritoid" and in KSH03A+B red-staining is most extensive in the section 25–360 m /Ehrenborg and Stejskal 2004ab/.

The dominant rock types of the Simpevarp peninsula are interpreted to be formed more or less synchronously, based on mixing and mingling relationships, diffuse contacts and ages for the quartz monzodiorite and the Ävrö granite /Kornfält et al. 1997, Wahlgren et al. 2004/. Based on field relationships, /Wahlgren et al. 2004/ established a chronostratigraphy for the rock types, where the fine-grained dioritoid is oldest followed by the younger quartz monzodiorite and even younger Ävrö granite.

3.1 Related fracture mineralogy and timing

Studies of the fracture mineralogy from drill cores KSH01, KSH03, KAS04, KA1755A, KLX02 and ongoing studies of KLX03, KLX04 and KLX06, show that the red-staining is present in the entire Äspö-Laxemar-Simpevarp area although more widespread and extensive adjacent to fractures in the Simpevarp area /Drake and Tullborg 2004, 2005, 2006a/. Further, this red-staining of wall rock has been identified adjacent to fractures filled with minerals of generations 1–4 (Table 3-1), in particular by prehnite of generation 4 /Drake and Tullborg 2005/. In contrast, red-stained wall rock is generally not observed when pyrite of generation 3 (early hydrothermal pyrite) is present in the fracture filling. The fracture mineral generations have not been dated but the mylonites of generation 1 are inferred to be older than the Götemar granite (1,450 Ma cf. above). e.g. /Tullborg 1997, Stanfors et al. 1999/. K-Ar datings of biotite and whole-rock samples from SE Sweden /Åberg 1978, 1988/ suggest that the mylonites are older than c. 1.5 Ga. Generation 2 and 3 might be related to the intrusion of the Götemar granite and re-activation of mylonites /Tullborg 1997, Drake and Tullborg 2005/. It can thus be proposed that hydrothermal conditions that were favourable for oxidizing and red-staining of the wall rock have occurred during several episodes, possibly during a long period of time in the early geological record of the region. The red-staining took place at semi-ductile to brittle conditions. The most extensive red-staining and also the last red-staining event was related to wide spread prehnite crystallization in fractures. Based on datings of wall rock and fracture fillings /Maddock et al. 1993/ it can be proposed that the feldspar alteration in the altered wall rock is at least older than 1,100 Ma and probably c. 1,400 Ma.

Table 3-1. Schematic fracture filling model for drill cores KSH01A+B, KSH03A+B, KLX02, KLX03, KLX04, KLX05, KLX06, KAS04 and KA1755A modified from /Drake and Tullborg 2006a/.

1. **Quartz- and Epidote-rich mylonite**, occasionally including muscovite, titanite, Fe-Mg-chlorite, albite, (apatite), (calcite), (K-feldspar).
2. **Cataclasite**
   - **a** Early **epidote**-rich, with quartz, titanite, Fe-Mg-chlorite, (K-feldspar), (albite).
   - **b.** Late **hematite**-rich, with epidote, **K-feldspar**, quartz, albite, **chlorite**.
3. Euhedral **quartz**, **epidote, Fe/Mg chlorite, calcite**, pyrite, fluorite, muscovite, (K-feldspar).
4. **Prehnite**, (fluorite)
5. **a. Calcite**, (fluorite, hematite).
   - **b. Dark red/brown filling – Adularia, Mg-chlorite** (also as ML-clay with Illite), **hematite** (quartz), (apatite); sometimes cataclastic.
   - **c. Calcite, adularia, laumontite, Mg-chlorite, quartz, illite** (also as ML-clay with chlorite), **hematite**, (albite).
6. **Calcite, adularia, Fe-chlorite, hematite, fluorite, quartz, pyrite**, **barite**, **gypsum**, harmotome, REE-carbonate, apophyllite, illite/chlorite (ML-clay), corrensite, chalcopyrite, galena, sphalerite, Ti-oxide, U-silicate, laumontite, Cu-oxide, sylvite, (Fe-oxyhydroxide), (Mg-chlorite), (apatite), (wolframite).
7. **Calcite**, pyrite, Fe-oxyhydroxides (near surface).

4 Earlier studies

In drill core KSH02, Simpevarp, /Mattsson and Thunehed 2004/ investigated geophysical and petrophysical properties of hydrothermally red-stained dioritoid and compared these to unaltered dioritoid. /Drake and Tullborg 2004/ investigated fracture mineralogy and the mineralogical features of red-stained rock from drill core KSH01A+B, Simpevarp.

Earlier studies of altered, predominantly red-stained rocks from Äspö HRL, have been carried out by e.g./Eliasson 1993, Mazurek et al. 1995, Tullborg 1995, Stosnach and Mengel 1998, Landström et al. 2001/. Although the dominant rock types differ somewhat between Äspö and Simpevarp, with a higher amount of fine-grained dioritoid and quartz monzodiorite at the Simpevarp peninsula and a higher amount of Ävrö granite at Äspö, the red-staining features are reported to be similar at both of the sites.

A number of studies on fracture minerals and altered wall rock conclude that the most significant red-staining of the rock occurs in association with hydrothermal alteration of plagioclase adjacent to fractures /Eliasson 1993, Mazurek et al. 1995, Tullborg 1995, Stosnach and Mengel 1998, Drake and Tullborg 2004/. The plagioclase is originally grey but is red-stained adjacent to many fractures. Red-staining may also occur along grain boundaries and in micro-fractures /Eliasson 1993, Mazurek et al. 1995/. The red-staining is mainly caused by very fine-grained hematite and/or Fe-oxyhydroxide which are present as inclusions in the altered plagioclase /Eliasson 1993, Tullborg 1995, Drake and Tullborg 2004/. These minute Fe^{3+}-rich minerals along with other fine-grained alteration products like sericite and an increased porosity, give the plagioclase crystals a clouded appearance. /Eliasson 1993/ estimates that the major red-staining event, caused by Fe-oxyhydroxide precipitation in the altered plagioclases took place at temperatures of about 150–250°C. /Landström et al. 2001/ showed that the hydrothermal alteration of the wall rock, indicated by the chloritization of biotite and alteration of plagioclase, not always coincide with the extension of the red-staining – the hydrothermal alteration often reaches further into the wall rock than the red-staining does.

Analyses of whole rock chemistry of red-stained wall rock have been compared to relatively fresh rock nearby /Eliasson 1993, Tullborg 1995, Stosnach and Mengel 1998, Landström et al. 2001/. From these studies it is shown that REE and several other trace elements remain fairly constant during the alteration. /Eliasson 1993, Landström et al. 2001/ report increases in Na, Cs and LOI and a decrease in Ca in the red-stained rock compared to the unaltered rock. /Eliasson 1993/ also reports increase in K and constant values of Ti and Al. /Tullborg 1995/ reports increase in LOI, a slight loss in Na and K, while Ca was constant. /Stosnach and Mengel 1998/ reports increase in e.g. K, Ba, Sr and Rb and depletion of Ca, Si and Cs, in the red-stained rock while Al, Ti, Mg, Fe_{tot}, Na and P are fairly constant during alteration. Sr is fixed in secondary epidote during alteration and Rb and K are fixed in sericite and K-feldspar.

/Tullborg 1995/ found that Fe_{tot} increases somewhat in the altered rock compared to the unaltered rock at Äspö and that the Fe^{2+}/Fe_{tot}-ratio is slightly lower in chlorite in the altered rock than in biotite in the unaltered rock. /Eliasson 1993/ found that the Fe^{3+}/Fe_{tot}-ratio increased in the red-stained rock compared to the unaltered rock, which reflects oxidation of magnetite and formation of hematite, and subordinate Fe-oxyhydroxides.

/Gebel et al. 1999/ investigated the distribution of trace elements on a grain size scale, in rocks from Äspö HRL. It was shown that titanite hosts nearly all bulk rock HREE (including Y), about 80% of the LREE, more than 70% of the Ti, 50% of the Th and about 40% of the U in granodioritic rocks at Äspö. Rb and Cs are mainly found in biotite and Ba is mainly found in K-feldspar. Biotite also contains about 50% of the Mn and Co. The REE-concentrations in biotite are very low. During the alteration process biotite reacts to chlorite, which seems to have significantly lower concentrations of Rb and Cs than biotite.

Petrophysical and geophysical investigations show an increase in porosity, a decrease in magnetization /Eliasson 1993, Mattsson and Thunehed 2004/ and density /Eliasson 1993, Mazurek et al. 1995, Mattsson and Thunehed 2004/. The electrical resistivity is also lower in the altered rock compared to the unaltered /Mattsson and Thunehed 2004/. These results indicate oxidation of magnetite and formation of secondary Fe^{3+}-bearing minerals and hydrous minerals in combination with increased secondary porosity in the secondary minerals and the altered primary minerals in the red-stained zone.

5 Equipment

The following equipment was used for sampling, sample preparation, microscopy, SEM-EDS and data processing.

- Scanning electron microscope (Zeiss DSM 940) with EDS (Oxford Instruments Link).
- Petrographic microscopes (Leica DMRXP and Leica DMLP).
- Microscope camera (Leica DFC 280).
- Digital camera (Konica Revio KD-420Z).
- Rock saws.
- Rock Labs swing mill.
- Point-counting equipment (Swift, Model F).
- Scanner (Epson 4180) and polaroid filters.
- Computer software (e.g. Corel Draw 11, Microsoft Word, Microsoft Excel, SolvCalc, NewPet, TriDraw).

All equipment listed above is property of Earth Sciences Centre, Göteborg University or is owned by the authors. For equipment used for whole rock chemistry analyses and Mössbauer spectroscopy, see the “Execution”-chapter below.

6 Execution

6.1 Sampling

The drill cores from the bore holes KSH01A+B (2 samples) and KSH03A+B (10 samples) were sampled for detailed study of the wall rock alteration. The drill cores are approximately 1,000 m long each and have diameters of about 50 mm.

Samples were collected from the most extensively and homogenously red-stained parts of the wall rock adjacent to fractures. Sampling was generally focused to the parts of the drill cores which where homogenous and intensely red-stained and free from sealed minor fractures. In addition, the adjacent reference rock had to be free from fractures, homogeneous and fresh. Samples free from minor- and micro-fractures, as well as truly fresh reference rock adjacent to the red-stained rock, were however very difficult to find. The intensity of the red-staining varies between the samples. Table 6-1 shows rough estimations of the red-staining intensity, sample volume, presence of sealed micro-fractures, grain-size and presence of pertithe- and quartz phenocrysts, for each sample. The sampled sections are mapped as "Ävrö granite", "quartz monzodiorite" and "fine-grained dioritoid" in the detailed Boremap drill core mappings /Ehrenborg and Stejskal 2004ab/. This broad range of rock types were sampled in order to investigate if the red-staining processes were of similar for all rock types.

Each of the 12 samples was divided into one red-stained sample (labeled "R" in this report) and one "unaltered" reference sample (labeled "G" in this report), resulting in a total of 24 samples. Sealed fractures and basic enclaves were removed by sawing and the samples were grinded to powder in a Rock labs swing mill at the Earth Sciences Centre in Göteborg, Sweden. The sample volume of each sample varied widely since homogenous red-staining is often limited to a rather small part of the wall rock and decreases when rock volumes with sealed minor fractures and heterogeneous parts are removed. Further, the diameter of the drill cores limits the sample volumes. For some of the red-stained parts, the volumes are about 0.2–0.7 kg, which is smaller than what is desired, especially for the more porphyritic samples. A small rock chip of each sample was sawed for thin-section preparation. Figure 6-1 illustrates how the drill core samples were normally prepared.

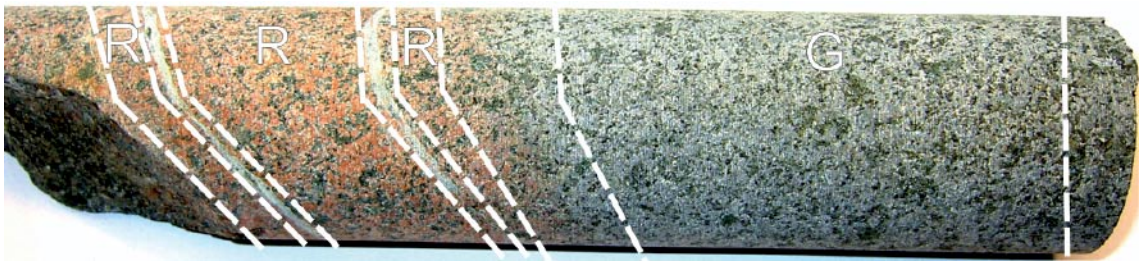

Figure 6-1. *Photo of drill core with intense red-staining adjacent to prehnite-filled fractures. The stippled lines indicate which parts of the sample, marked with "R" and "G" that were used in the study. "R" stands for "red-stained" and "G" for "grey – reference sample". Sample KSH03: 82 m. Drill core diameter is about 50 mm.*

Table 6-1.

Sample	Depth	Red-staining	Sample volume	Micro-fractures	Grain-size	Pheno-crysts
KSH03						
62	61.94–62.15	xx	x	xxx	Medium	
81	81.46–81.65	xx	xx	xx	Medium	
82	82.05–82.25	xxx	xx	x	Fine-Medium	
100	100.41–100.56	xxx	x	x	Medium	
128	128.08–128.23	xx	x	x	Fine-Medium	
144	144.49–144.89	xx	xxx	x	Coarse	Yes
172	171.85–172.05	xxx	xx	xx	Fine-Medium	
372	372.52–372.70	x	xx		Coarse	Yes
394	394.34–394.45	xx	x		Coarse	Yes
661	661.29–661.34	x	xx		Coarse	Yes
KSH01						
536-1	536.65–537.52	xxx	x	xxx	Fine-medium	
536-2	536.65–537.52	xxx	xxx		Fine	

x = faint/small/few, xx = medium, xxx = intense/big/numerous.

6.2 Thin section

Polished, 30 µm thick, thin-sections were prepared for each of the 24 samples, by Minoprep. The thin-sections were impregnated with blue ink, so that micro-fractures, voids and highly porous parts of the rock could be more easily traced.

The thin sections were examined using petrographic microscope and scanning electron microscope (SEM-EDS). Point-counting was performed with petrographic microscope, with 10 times magnification, on all samples. Oxides were identified and point-counted using the reflective light mode on the microscope.

Point-counting was carried out in order to obtain general information of the whole rock and to obtain modal mineral composition in the red-stained rock compared to the reference rock. The results from the point-counting are combined with the results from the chemical analyses. The SEM-EDS investigations provide e.g. high resolution pictures and analyses of fine-grained minerals in the thin sections.

The SEM-EDS microanalyses were carried out on an Oxford Instruments energy dispersive system mounted on a Zeiss DSM 940 SEM at the Earth Sciences Centre, Göteborg University, Sweden. Polished thin-sections were coated with carbon for electron conductivity. The acceleration voltage was 25 kV, the working distance 24 mm and the specimen current was about 0.7nA. The instrument was calibrated at least twice every hour using a cobalt standard linked to simple oxide and mineral standards, to confirm that the drift was acceptable. ZAF calculations were maintained by an on-line LINK ISIS computer system. These quantitative analyses give reliable mineral compositions but Fe^{2+} and Fe^{3+} are not distinguished and the H_2O content is not calculated. Detection limit is 0.1 oxide %, except for Na_2O (0.3 oxide %). Note that the SEM-EDS analyses used in this report show the Fe_{tot}-content as "FeO" (about 78% Fe) in contrast to the chemical analyses which gives the Fe content as Fe_2O_3 (about 0.70% Fe).

6.3 Chemical analyses

Each of the 24 samples were analysed for major, minor and trace element contents by Analytica AB. Six of the samples were analysed twice. The following is valid for Co, Cu, Ni, S and Zn: Digestion was done by microwave heating in closed teflon vessels with HNO_3/H_2O 1:1. The following is valid for the other elements: 0.125 g sample is fused with 0.375 g $LiBO_2$ and dissolved in dilute HNO_3. LOI (Loss on ignition) is carried out at 1,000°C. Concentrations of the elements are determined by ICP-AES and ICP-QMS. Analyses are carried out according to EPA methods (modified) 200.7 (ICP-AES) and 200.8 (ICP-QMS). Fluorine was measured with an ion selective electrode.

6.4 Mössbauer spectroscopy

Written by Prof. Hans Annersten, Uppsala University.

Rock powder from each of the 24 samples were analysed by Prof. Hans Annersten, Uppsala University, with a Mössbauer spectrometer.

Mössbauer spectroscopy is the resonant absorption of γ-rays. It is a highly selective analytical method that has especially been developed for the study of Fe in solid material e.g. minerals. The Mössbauer effect is a nuclear resonance effect that involves the recoil free emission of γ-rays from a radioactive source, in the case of iron, ^{57}Co that decays to the stable ^{57}Fe with an energy of 14.7 keV. ^{57}Fe in the sample (absorber) absorb this low energetic γ-ray. Natural iron contains 2% of this stable isotope. In order to achieve the right energy for recoilless resonant absorption of the γ-quanta, the Doppler effect modulates the emitted energy by accelerating the source towards the absorber sample. The Mössbauer spectrometer is therefore built by a source (^{57}Co diffused into Rh matrix) sitting on a vibrator that successively increase the acceleration to achieve resonant absorption in the iron containing absorber sample (powder or single crystals) and a detector measuring the transmitted radiation. Vibrator and detector are coupled through a computer and a spectrum where each channel shows the transmission as a function of velocity or energy. Resonant absorption will show up as absorption dips in the spectrum.

Absorption peaks are usually seen as doublets with two symmetric lines because there are two transitions from the ground state +/– 1/2 = > +/– 1/2 and +/– 1/2 = > +/– 3/2 in the exited state in ^{57}Fe. The splitting of the doublet is a measure of the crystal field and is characteristic for each mineral, yielding crystallographic information. In the case of magnetic materials e.g. Fe_3O_4 and Fe_2O_3, the different magnetic spins give rise to a six-line absorption pattern. In all experiments the chemical difference between the source and the absorber will result in a centroid shift of the absorption pattern. The value of the centroid shift gives information on the electron density around the nucleus and the d^5 and d^6 electron configuration of Fe^{3+} and Fe^{2+} make is possible to separate the two types of iron in the sample and hence determining the oxidation degree.

In summary the Mössbauer effect will allow determination of the type of coordination of iron in the mineral, the valence state of iron and the magnetic properties of iron. Mössbauer spectroscopy will to some extent also act as a fingerprint method for identifying solids in a multi-phase sample where only the iron containing phases of course will be observed. Normally 20–50 mg sample, depending on the iron content, is needed for a Mössbauer analysis but samples smaller than 5 mg can be analysed.

In the present study of powder samples absorbers from rocks were analysed 20–40 mg sample were pressed into Cu-holders between low absorbing Mylar films and mounted in the magic angle 54.7° to avoid textural effects from the flaky phyllosilicates. This result in symmetric absorption doublets and will make the fitting of strong overlapping absorption line more easy. Measuring time for each sample took 1–3 days depending on the iron content. Each spectra, 512 channels each, was analysed in computer and fitted using a least square fitting program that give the Mössbauer parameters centroid shift, quadrupole splitting, magnetic hyperfine field and intensity. Velocity scale of the spectrometer is calibrated against metallic iron.

Centroid shifts for ferrous iron are around 1.12 mm/s and for ferric iron between 0.35–0.45 mm/s. Quadrupole splitting are generally much higher for ferrous iron, 2.60 mm/s while splitting from ferric iron is between 0.60–1.0 mm/s. However ferric iron quadrupole splitting in epidote group minerals are the highest measured for ferric iron in silicates, 2.0 mm/s. This is an important diagnostic feature for identifying epidote in rock samples by use of Mössbauer spectroscopy. Magnetite and hematite are identified from their large magnetic hyperfine field 48 and 51 T respective. Examples of Mössbauer spectra containing different iron phases are shown in Figures 6-2 and 6-3.

Oxidation degree of the sample is calculated from the intensity ratios between the ferric iron and ferrous iron absorption pattern assuming similar recoil free fractions.

Detection limit for iron bound to magnetic oxides is 1% intensity and 3% for a meaningful fit. Iron bound into paramagnetic silicates has a detection limit of 3% of total intensity and 5% for a reasonable correct fit.

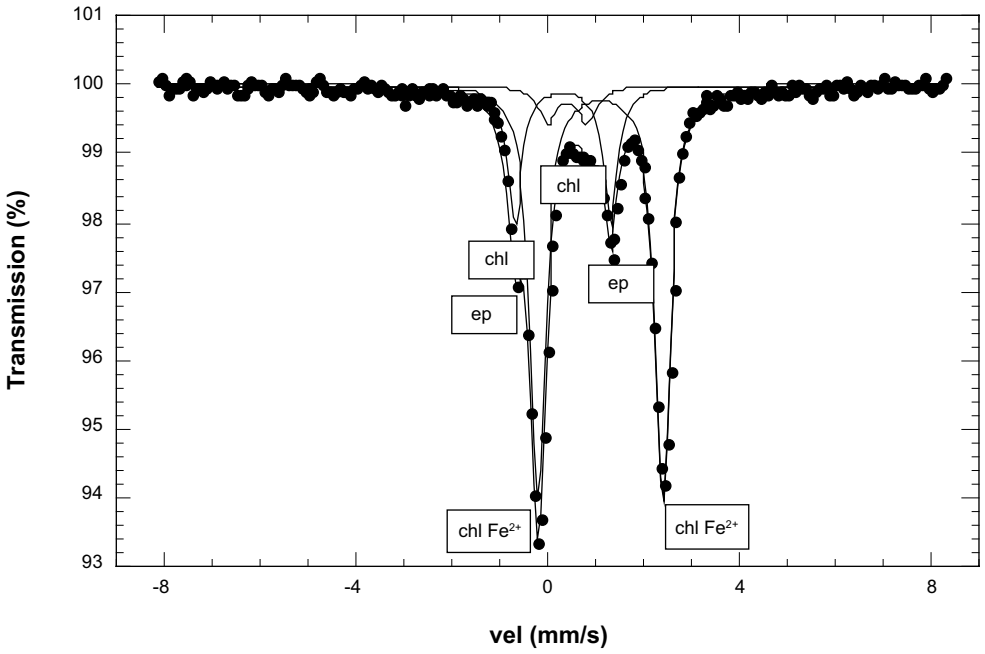

***Figure 6-2**. Sample containing Fe-Mg silicate (mainly chlorite) and epidote. "Chl" indicate doublet for ferric iron in chlorite.*

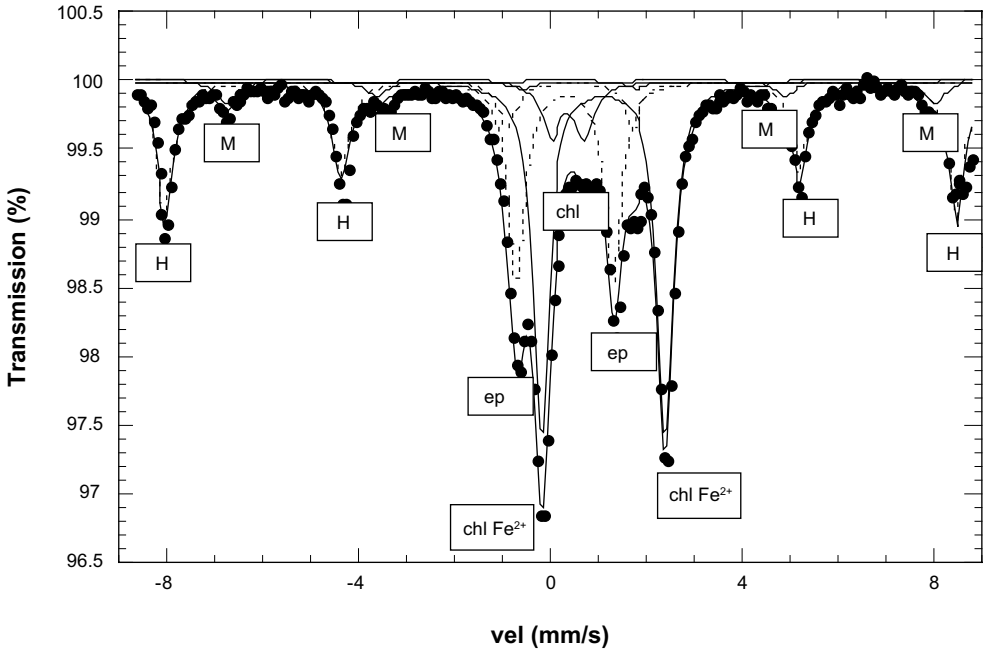

Figure 6-3. *Spectra of rock sample containing hematite (H), magnetite (M), epidote (ep), and Fe-Mg silicates (mainly chlorite [chl]). "Chl" indicate ferric iron in Fe-Mg silicates (mainly chlorite).*

7 Results and discussion

7.1 Mineralogy

The thin sections were point-counted in order to compare the mineralogy between the reference rock and the red-stained rock (Table 7-1). The point counting was carried out using an extended subdivision of the different mineral phases compared with what is usually applied for classification of rocks at the investigated sites /Wahlgren et al. 2004/. This was done in order to better describe the hydrothermal alteration. For example the oxides were point-counted as “opaque” minerals, but subdivided into “magnetite”, “magnetite+hematite”, “hematite”, “pyrite” and “ilmentite”. The classification “magnetite+hematite” was used when more than about 25% magnetite is present in hematitized magnetite.

Table 7-1. Modal composition, mineral content in %.

Sample	Pl	Alt.Pl	Kfsp	Alt.Kfsp	Qz	Op	Bt	Tit	Am+Px	Epi	Chl	Preh	Imp	No
62G	12.5	37.5	4.0	0.1	10.6	1.5	0.3	0.7	18.8	0.3	10.3	3.3		1541
62R	0.2	51.5	5.7		6.6	1.6	0.1	0.9	18.3	3.2	9.4	2.3		1527
81G	22.0	25.0	3.3		12.8	2.1	0.8		17.3	0.1	15.6	0.9		1541
81R	1.0	46.0	5.0		11.4	1.9	0.2	0.4	17.2	1.8	11.8	3.0	2.2	1542
82G	25.0	15.1	5.0	1.0	15.9	3.7	11.8		16.7	0.1	5.1	0.1	0.1	1541
82R	0.1	50.8	0.5	1.6	3.1	2.7	0.3	0.1	15.6	1.4	16.9	6.3	0.7	1542
100G	12.3	35.1	3.4	0.8	10.6	3.5	0.7	0.6	11.8	0.8	17.2	3.0		1579
100R	1.1	53.4	1.0	0.3	9.9	3.6	0.7	0.5	6.7	1.2	17.7	3.5	0.3	1540
128G	26.3	12.5	19.6	0.7	21.0	0.4	10.7	0.1	7.7	0.1	0.9			1563
128R	0.3	49.9	13.3		15.9	2.1	0.3		7.4	1.0	9.1	0.6		1553
144G#	22.6	18.1	15.2	0.1	33.3	1.4	2.0	0.8	2.7	0.2	3.2	0.2	0.1	1542
144R#	0.3	42.5	27.2	4.3	17.5	0.6		0.6	0.1	1.1	5.4	0.1	0.4	1575
172G	16.3	28.1	12.0	0.6	14.7	1.9	2.2	0.1	8.1	1.4	13.5	0.9		1544
172R	6.2	45.9	9.1		14.9	1.5	1.8	0.4	7.8	1.1	10.2	1.1		1544
372G#	14.2	34.6	12.4	0.2	16.6	1.4	1.0	3.0	1.8	4.4	10.1	0.3	0.1	1541
372R	1.5	49.4	7.5		17.1	2.3		1.8	0.1	6.2	11.3	2.0	0.8	1542
394G#	8.7	31.5	13.6	2.0	17.8	1.2	1.4	2.0	0.8	10.3	10.3	0.4		1541
394R#	2.6	40.2	9.8	2.4	20.0	0.7	0.1	1.9	0.1	9.4	12.3	0.3		1541
536-1G	9.1	36.8	6.7	0.1	25.4	0.6	6.7	0.1	7.5	0.1	6.7	0.1		1646
536-1R	1.8	36.4	0.7	14.0	28.6	0.3	1.4		0.7	0.3	14.4	1.2	0.3	1538
536-2G	27.0	15.6	10.9		16.8	0.8	15.4	0.1	12.4	0.2	0.8			1541
536-2R#	0.6	48.4	0.3	11.0	14.0	1.2	1.0		6.5	0.8	13.4	2.7	0.1	1530
661G#	16.8	43.3	5.7	0.6	12.4	0.6	0.6	1.4	0.7	5.5	11.5	0.5	0.3	1540
661R#	1.6	42.8	26.1	0.4	13.3	0.3	0.6	1.3	0.1	6.0	4.9	1.9	0.6	1541

G = reference sample, R = red-stained sample, # = Porphyritic sample, Pl = fresh plagioclase (in R = albite), Alt. Pl = altered plagioclase (in G: plagioclase, albite, sericite, prehnite, [epidote, K-feldspar], in R: albite, K-feldspar, sericite, prehnite [epidote]), Kfsp = fresh K-feldspar, Alt. Kfsp = altered K-feldspar, Qz = quartz, Op = Opaque minerals, Bt = biotite, Tit = titanite, Am+Px = amphibole and pyroxene, Epi = epidote, Chl = chlorite (incl. traces of titanite and biotite), Preh = prehnite, Imp = impregnated (voids, highly porous sections etc), No = number of counted points.

SEM-EDS investigations reveal that minerals counted as “altered plagioclase” in the reference rock are partly replaced by sericite, albite, prehnite, epidote and K-feldspar but that a big portion of the original plagioclase is still present, counted as “plagioclase”. Points counted as “altered plagioclase” in the red-stained rock samples are as a rule completely replaced in a pseudomorphic manner by albite and K-feldspar mainly and subordinately by sericite and prehnite and to an even lesser degree by epidote. The points counted as “plagioclase” are mostly fresh, secondary albite.

Chlorite is often replacing biotite, and to a lesser degree amphibole and pyroxene. The chloritization of biotite is pseudomorphic and include crystallisation of fine-grained secondary titanite, which is present along with the chlorite. These titanite crystals and small remnants of the original biotite can often be traced in thin section but are often too small to be point-counted. Biotite, secondary titanite, prehnite, K-feldspar, albite and epidote are underrepresented in the point-counting.

The thin sections are impregnated in order to reveal micro-porosity and micro-fractures. The parts that are big enough to point-count are counted as “impregnated”. The impregnated parts are often too small to give a fair comparison between the red-stained and the reference rock. Examinations of the thin sections show that the porosity is generally more common in the red-stained rock than in the unaltered rock. These observations are in correspondence with earlier studies of porosity and micro-fracturing in altered granite from Äspö, using the more advanced ^{14}C- and ^{3}H-PMMA-techniques /Kelokaski et al. 2001/. Micro-fractures filled with fracture minerals may occur in the thin sections are not counted.

Some of the rock types that are sampled are porphyritic, with large perthitic and quartz-rich phenocrysts, respectively. These samples have to be evaluated with care since the thin section used is too small to reflect the true modal composition.

According to the International Union of Geological Sciences /Le Maitre 2002/, the classification of rocks should be based on the modal composition. QAP-modal classification of the reference samples is found in Figure 7-1. In this classification all of the sericitized plagioclase is plotted as plagioclase. Since the plagioclase crystals of the red-stained samples generally are completely replaced by K-feldspar, albite and other secondary minerals, the red-stained samples could not be properly classified in the QAP-classification (Figure 7-1). The content of albite, K-feldspar and plagioclase, in the red samples differ quite a bit. The red-stained samples have been plotted in Figure 7-1, with the assumption that albite and K-feldspar make up half of the plagioclase pseudomorphs each, which is an over simplification. Nevertheless the plot illustrates how the feldspar composition has changed as a cause of the hydrothermal alteration.

7.1.2 Mineralogy of the reference rock

Macroscopically, the unaltered reference rocks are grey or sometimes reddish-grey, fine-medium to coarse-grained and sometimes porphyritic. The reference rock samples show quite different modal compositions, which change gradually with increasing differentiation of the rocks. However, in this report, the samples are generally divided into Ävrö granite, quartz monzodiorite and fine-grained dioritoid, based on the Boremap mapping /Ehrenborg and Stejskal 2004ab/, so that the alteration processes can be discussed easier. The rocks with a high amount of biotite, amphibole and pyroxene are darker in colour. These minerals are often found in clusters and in many samples these minerals have been partly or entirely replaced by chlorite which gives the rock a somewhat green colour. The epidote content varies widely between the samples.

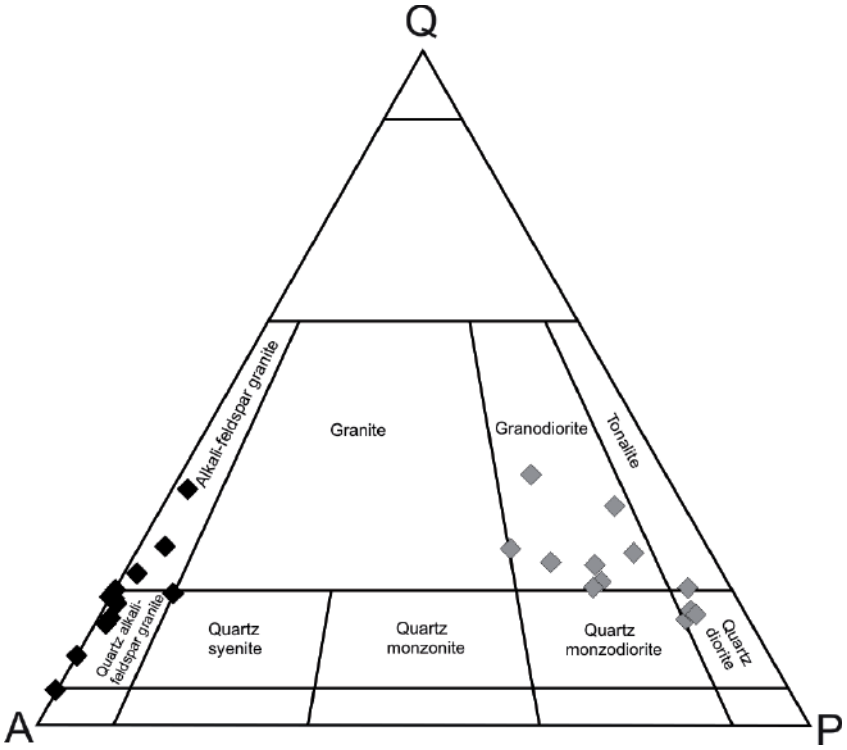

Figure 7-1. *QAP modal classification /Streckeisen 1976, 1978/ of reference samples (grey) and red-stained samples (black). See text for details.*

The reference samples show different contents of the main minerals plagioclase, K-feldspar, quartz, biotite and amphibole/pyroxene. Results are summarised in Figures 7-2, 7-3 and 7-4. In the quartz monzodiorite (62, 81, 82, 100, 128, 172) and diorite samples (536-1, 536-2) the plagioclase content is 39–52%, the K-feldspar content is 3.3–20%, the quartz content is commonly 10–21%, the amphibole plus pyroxene-content is 7.5–19%. In the more porphyritic Ävrö granite samples (144, 372, 394, 661, granodiorite to quartz monzodiorite) the modal composition is more varied, because of the phenocrysts in combination with the relatively small sample volume. In these samples the plagioclase content is 40–50% (60 in sample 661), K-feldspar content is 6–16% (but is probably higher since phenocrysts were not numerous in the thin section), the quartz content is 13–20% (33 in sample 144), the amphibole plus pyroxene content is 0.7–2.7%. The plagioclase crystals in the reference rock are often bigger than crystals of other minerals and are often altered to sericite, albite and epidote, in the centre of the crystal. 60% of the total plagioclase-counts in the reference rock have been counted as altered plagioclase. This alteration is however not as extensive as the alteration in the red-stained plagioclases, where the whole crystal is replaced. In the reference rock the original plagioclase is often present between the alteration products.

The modal contents of opaque-minerals (commonly magnetite) and titanite in all of the reference samples are 0.6–3.7% and 0–3%, respectively. The euhedral titanite crystals are quite large, up to 4 mm in length in as most. Titanite is most abundant in the Ävrö granite samples (1.3–3%) while the dioritoid samples more or less lack titanite. The quartz monzodiorite samples have titanite-contents of about 0.5% in average. The epidote content is generally low in the reference rock (about 0.5%) but the Ävrö granite samples (372, 394 and 661) show extremely high contents of euhedral epidote, 4.4%, 10.3%, and 5.5%, respectively. Prehnite is often present in the reference rock, commonly as a secondary mineral in altered plagioclase, but also as bigger individual aggregates which might be secondary as well.

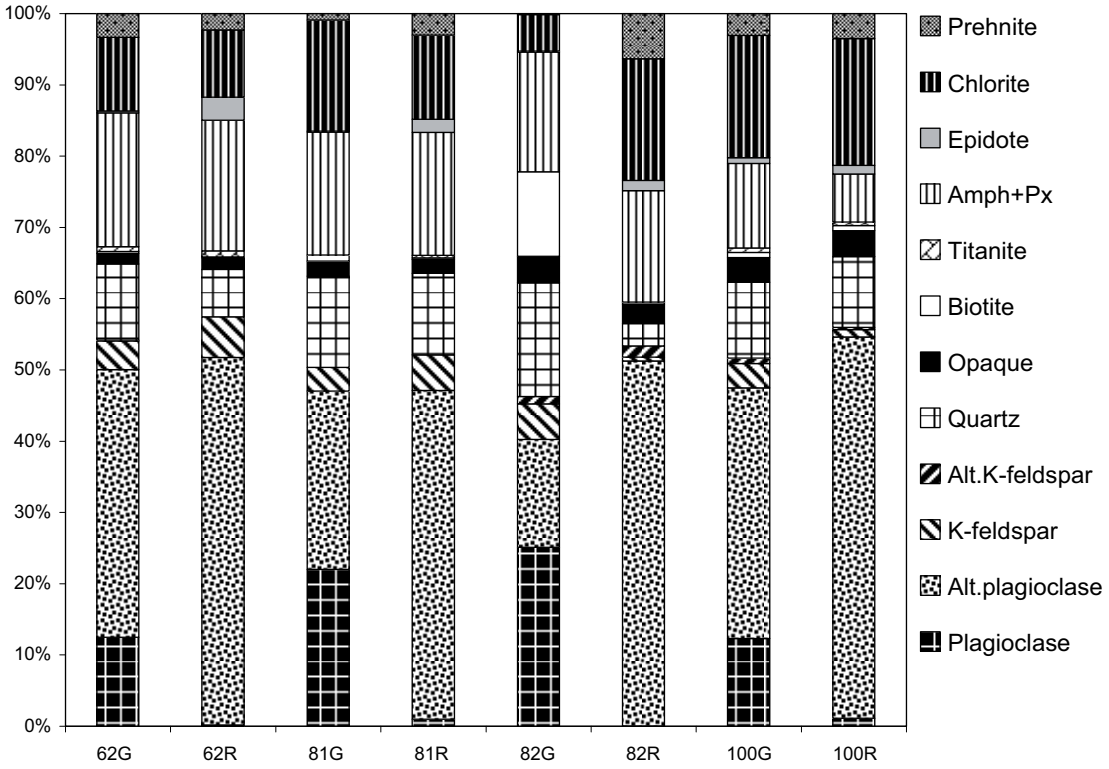

Figure 7-2. *Modal analyses of samples 62, 81, 82 and 100. G = reference sample, R = red-stained sample.*

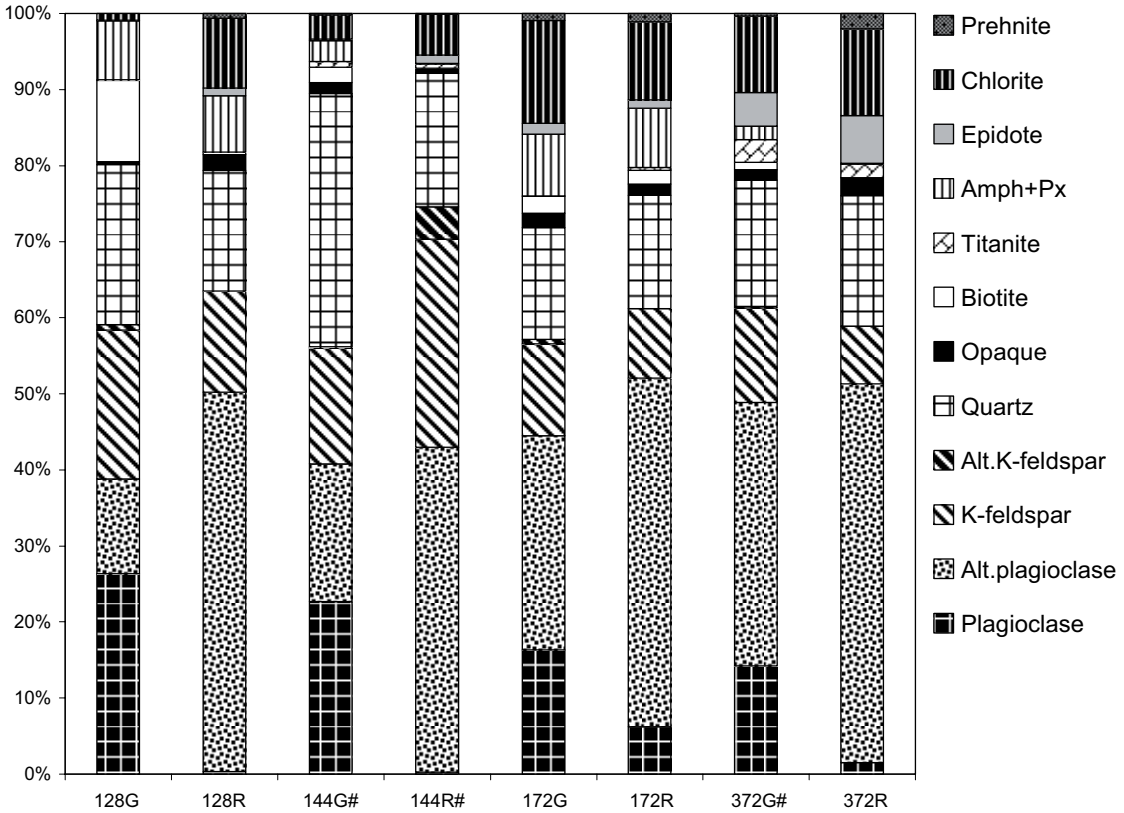

Figure 7-3*. Modal analyses of samples 128, 144, 172 and 372. G = reference sample, R = red-stained sample. # = Porphyritic.*

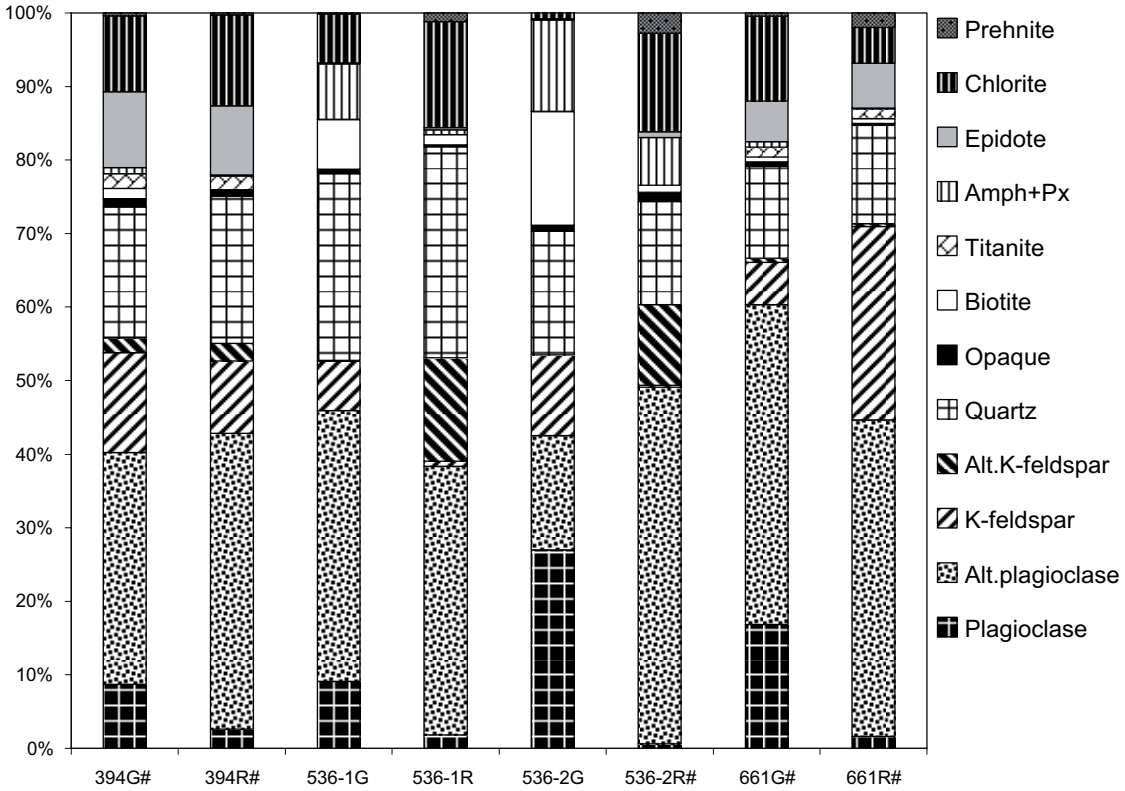

Figure 7-4*. Modal analyses of samples 394, 536-1, 536-2 and 661. G = reference sample, R = red-stained sample. # = Porphyritic.*

In almost two thirds of the reference samples the biotite has been completely altered to chlorite with fine-grained titanite and possibly Ti-oxide. In the samples where the biotite-content is still larger than the chlorite-content (81, 128, 536-2) the biotite-content is 10.7–15.4% and the chlorite content is 0.8–5%. In samples 144 and 536-1 the chlorite-content roughly equals that of biotite, 2–3% and 7% respectively. In the other 9 samples the biotite-content is 0.3–2.2% and the chlorite content 9–17%. This indicates that the hydrothermal alteration reaches further from the fracture rim than the red-staining does, as suggested by /Landström et al. 2001/.

7.1.3 Mineralogy of the red-stained rock

The mineralogy of the rock is gradually changed with decreasing distance from the fractures. The texture of the rock is however well preserved and secondary minerals replace original minerals in a pseudomorphic manner. The most prominent textural changes occur in micro-fractured sections. Some of the Ävrö granite samples show a week foliation, which affects the matrix whereas the phenocrysts are largely unaltered and rarely show any preferred orientation. Sample 661 shows some signs of local micro-fracturing and sub-grain formation in highly strained sections. Micro-fracturing of quartz is more frequent in 144R compared to other samples.

In Figures 7-2, 7-3 and 7-4 the results from comparisons of the modal composition are presented. The most striking features of the alteration adjacent to the fractures are plagioclase alteration, chloritization of biotite, hematite replacing magnetite and increased prehnite and epidote contents. The chloritization of biotite ranges further into the wall rock than the red-staining.

From point-counting it is evident that almost all fresh plagioclase have been completely altered and replaced by secondary minerals. The K-feldspar content varies widely and is increased in some red-stained samples and decreased in others. No sign of break-down or newly formed K-feldspar is noted, except in altered plagioclase. The quartz-content is roughly unchanged except for samples 62, 82 and 144 (porphyritic), where the content decreases in the red-stained rock. No major break down or secondary growth of quartz is however noted, except for in micro-fracturing and sub-grain formation in some samples. Many of the samples show a small decrease in the quartz-content of the red-stained samples, though. Quartz may be micro-fractured and thus counted as impregnation or as secondary minerals occurring in the micro-fractures.

The biotite content is always lower in the red-stained samples compared to the reference rock, although the biotite is commonly altered to chlorite in the reference rock as well. The chlorite content is higher or roughly the same in the red-stained samples as in the reference samples except for sample 62, 81, 172 and 661, where almost all biotite is altered to chlorite in the reference sample. Inhomogeneous mineral content between the thin sections gives relatively higher chlorite content in the reference samples, compared to the red-stained samples. The amphibole and pyroxene content is lower in all red-stained samples and are replaced by chlorite. However, in half of the samples this decrease is insignificant, which shows that amphibole and possibly also pyroxene were more resistant to the hydrothermal alteration than biotite.

The prehnite and epidote contents are higher in almost all of the red-stained samples compared to the reference samples. Micro-fractures and porous parts recognised as ink-impregnations are more common in the red-stained samples. They occur in cross cutting fractures in quartz, in porous parts of chlorite, prehnite, altered plagioclase, and along grain boundaries.

The modal titanite content is slightly higher in the red-stained rock as titanite is formed during chloritization of biotite although most of the biotite is already chloritized in the reference rock and the secondary titanite is often too small to be counted.

Magnetite is partly replaced by hematite in the red-stained samples; i.e. remnants of magnetite surrounded by hematite are common in the pseudomorphs. The magnetite in the reference samples is often fresh, unless in sample 100G where hematite has partially replaced the majority of the magnetite crystals. In Table 7-2 the opaque-minerals from the point-counting is presented. The Fe-oxides that are point-counted in the red-stained rock are both primary minerals and secondary minerals replacing the primary minerals.

Fine-grained Fe-oxides in plagioclase crystals are too small to be point-counted. Ilmenite and pyrite are present in some samples. Ilmenite is occasionally partially altered to titanite and Ti-oxide. Euhedral pyrite is more common in the reference samples than in the red-stained samples. This might be caused by oxidation of Fe^{2+} in pyrite. In sample 82R a slight increase of fine-grained pyrite, compared to 82G is noted. This pyrite is thought to be formed in this highly porous sample subsequent to the red-staining, at reducing conditions.

The clay mineral content is generally low. Clay minerals may be found in secondary prehnite, in altered plagioclase and K-feldspar and in micro-fractures along with hematite and/or Fe-oxyhydroxide.

Table 7-2. Detailed point-counting of the opaque minerals from Table 7-1.

Sample	Hematite	Magnetite	Hematite+magnetite	Ilmenite	Pyrite	Total counts
62G		13		3	2	18
62R	3	4	18			25
81G		18	6	5	4	33
81R	2	8				10
82G	2	42	5	6		55
82R	5	11	19	6	1	42
100G	5	1	45	2	2	55
100R	4		52			56
128G		5				5
128R	10		21			31
144G#	7		15			22
144R#	1	1	7	1		10
172G	1	20	6	1		28
172R	2	2	18	1		23
372G#		2	19			21
372R	20	0	16			36
394G#	1	16			1	18
394R#	1	6	3			10
536-1G	1	6	3			10
536-1R	1	1	2			4
536-2G	2	8	1			11
536-2R#		3	15		1	19
661G#		10				10
661R#	1	2	1			4

7.2 Mineralogical features

In this section the most important features of the minerals in the red-stained rock compared to the reference rock is discussed, along with micro-photographs, SEM-images and SEM-EDS analyses.

7.2.1 Quartz

Quartz was not heavily altered, dissolved or deformed during the hydrothermal alteration. However, the quartz crystals show a higher degree of micro-fractures in all red-stained samples compared to the reference samples, although the micro-fracturing is commonly discrete, except for in samples 144R and 661R (Figure 7-5). The micro-fractures are sometimes filled by fine-grained minerals, among others Fe-rich minerals. The quartz crystals remain transparent in the red-stained rock.

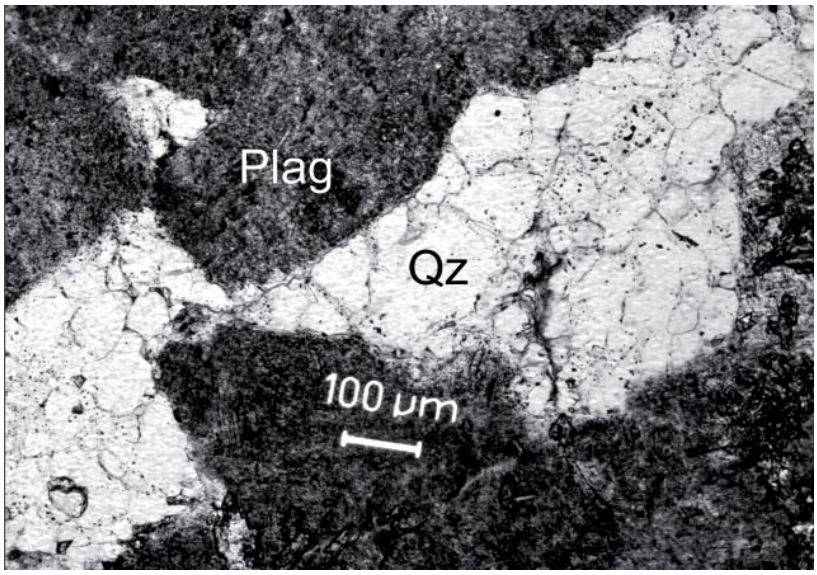

Figure 7-5. *Microphotograph, showing ink-impregnated micro-fractures in quartz, surrounded by red-stained plagioclase. Thin-section 661 R. Plain polarized light.*

7.2.2 K-feldspar

K-feldspar is present as primary and secondary crystals. The primary crystals are microcline crystals that are mostly preserved during alteration. The secondary K-feldspar, possibly adularia, is found along with albite in pseudomorphs after plagioclase in the red-stained rock. K-feldspar is also present as the major constituent of perthite phenocrysts (K-feldspar with albite inclusions), in porphyritic Ävrö granite samples (144, 372, 394, 661). The perthite is largely unaltered during the hydrothermal alteration, but micro-fractures and a small degree of secondary sericite may be present. Perthite and microcline crystals generally maintain their pinkish colour during alteration. In some samples the microcline crystals are somewhat clouded. This clouding is induced along the tweed-twin-planes and consists of extremely fine-grained crystals. These crystals are too fine-grained to be analysed or even traced with SEM-EDS, and may possibly be illite, Fe-oxides or Fe-oxyhydroxides. In sample 536-1R most of the microcline crystals are entirely clouded by fine-grained material and SEM-EDS analyses of the whole crystals show higher Fe-values than in microcline and perthite (Table 7-3).

An interesting observation is that the BaO-content is much higher in perthite than in the other K-feldspar phases. The values of BaO from all SEM-EDS-analyses of perthite in this study ranges from 0.6 to 2.3%. The K-feldspar found in altered plagioclase is discussed in the “Plagioclase”-section.

7.2.3 Primary and altered plagioclase

In the unaltered samples, fresh, unaltered plagioclase crystals are common, but in most cases they have been partially altered to sericite, albite, prehnite, epidote and rarely K-feldspar. The plagioclase crystals in the red-stained samples are as a rule completely replaced by the low temperature paragenesis of albite, K-feldspar, sericite, prehnite, hematite and more rarely epidote and very seldom calcite. Porous and clouded plagioclase is by far the most characteristic feature in the red-stained samples. The red-staining becomes very prominent since plagioclase originally makes up about 40–50% of the modal composition of the rock.

Table 7-3. Selected SEM-EDS analyses of K-feldspar.

Microcline	Na2O	Al2O3	SiO2	K2O	FeO	BaO	Total
144G	0.84	19.06	64.60	15.25		0.51	100.26
144R	0.56	18.85	64.25	15.72		0.39	99.77
K-feldspar in perthite							
144R	0.59	19.07	64.08	15.11		1.83	100.68
394R	0.66	19.34	63.92	15.04		1.99	100.95
Red-stained microcline							
536-1R(1)		18.65	64.25	16.66	0.26		99.82
536-1R(2)		18.65	64.27	16.55	0.50	0.29	100.26
K-feldspar in plagioclase pseudomorphs							
82R	0.73	19.23	63.60	15.57	0.20	0.23	99.55
100R(1)		18.91	63.97	16.20	0.05	0.63	99.70
100R(2)	0.33	20.57	61.49	15.46	0.39	0.76	99.00
128R	0.42	19.19	64.16	15.84	0.21		100.03
372R		19.06	65.21	15.69	0.14	0.29	100.40
661R		19.47	63.80	16.05	0.05	0.65	99.97

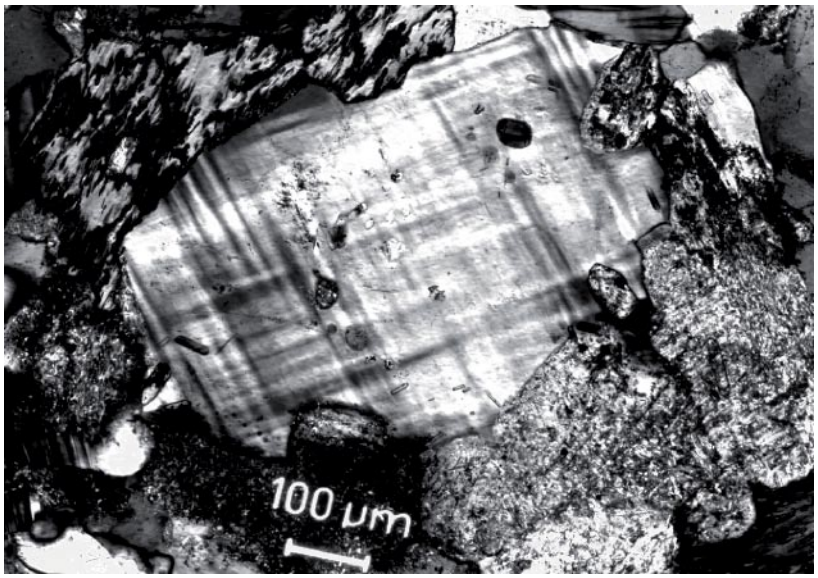

Figure 7-6. *Microphotograph of practically unaltered microcline with tweed-twinning. Thin section 144R, +nic.*

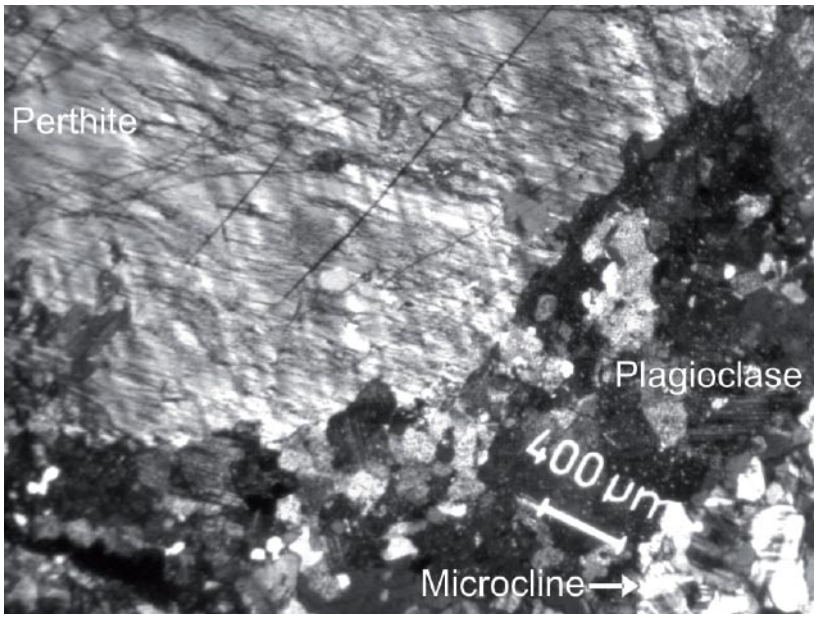

Figure 7-7. *Microphotograph of perthite phenocryst, red-stained plagioclase pseudomorphs and almost unaltered microcline. Thin section 144R, +nic.*

Plagioclase in reference samples

The primary anorthite-content of plagioclase is about 26–45%, and is highest in quartz monzodiorite to diorite samples. Representative analyses are found in Table 7-4. The FeO-content in the primary plagioclase is quite small and the average content is 0.15% (from 15 analyses).

The plagioclase crystals are normally twinned according to the albite-law. Carlsbad-twinning is also common. Typically, the primary plagioclase in the reference samples is partially replaced by alteration minerals such as sericite, albite and epidote, but a complete replacement is not observed (Figure 7-8). Plagioclase in the reference samples is usually colourless in plain polarised light. The sericitized and altered parts are somewhat more porous and clouded, which gives a slight increase in colouration (Figure 7-9). This faint colouration effect, increases gradually with increased alteration of the plagioclase in the reference samples. The primary plagioclase has low porosity (Figure 7-10) in contrast to the plagioclase pseudomorphs in the red-stained samples.

Whole crystal-analyses (SEM-EDS) of plagioclase (Table 7-5) mostly show higher K_2O-, FeO- and MgO-contents compared to the SEM-EDS-spot analyses of unaltered parts of plagioclase (Table 7-4). This increase is caused by sericite and possibly also K-feldspar increase in the more altered part of the crystal. The Na_2O-content and CaO-content are somewhat lower in the whole crystal-analyses, for the same reasons. Some crystals are fairly unaltered (172G (1), 536-2G, Table 7-5) whereas others are heavily sericitized showing K_2O-values as high as 5%. Average K_2O-content from 45 whole crystal-analyses is 2.21%.

Table 7-6 shows SEM-EDS analyses of sericite from the altered parts of plagioclase crystals in both reference samples and red-stained samples. The analyses are of rather poor quality because of the fine-grained nature of the sericite crystals, but it is evident that the BaO-content is generally higher in the red-stained samples.

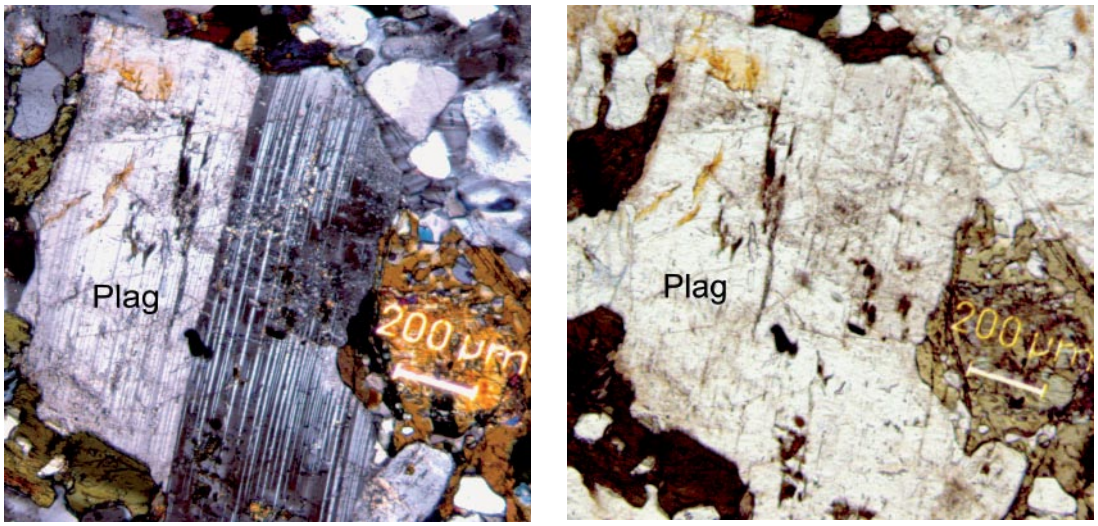

Figure 7-8. *Microphotographs of unaltered plagioclase from sample 128G, +nic (left), plain polarised light (right).*

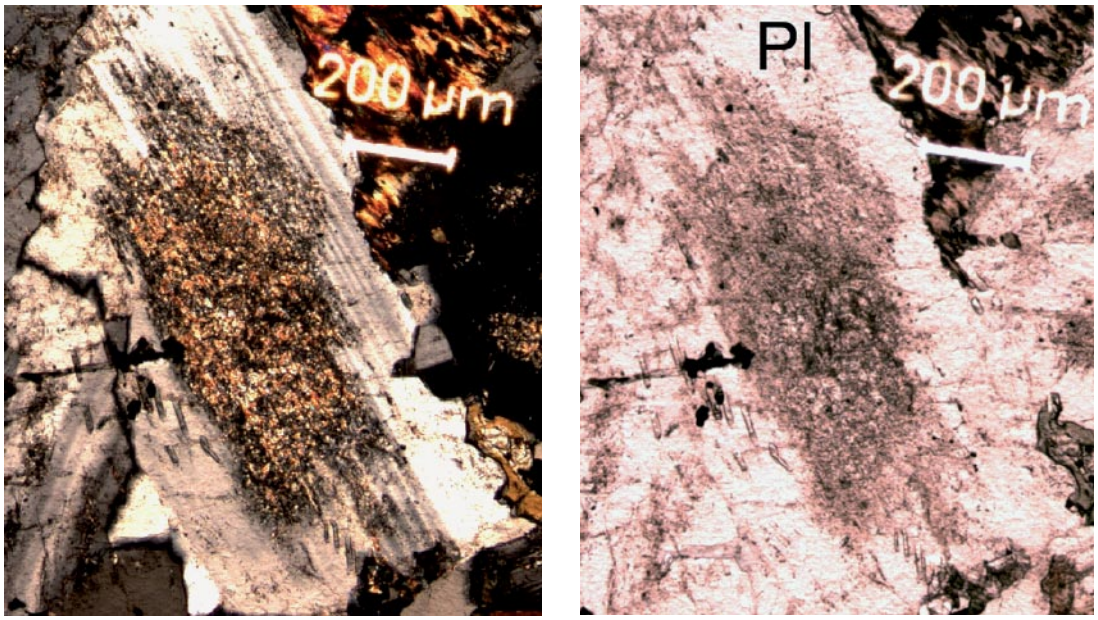

Figure 7-9. *Microphotographs of sericitized plagioclase from sample 82G, +nic (left), plain polarized light (right). Note the increased cloudiness and slight increase in coloration compared to unaltered plagioclase in Figure 7-8, although the colour setting of the camera differed a bit between these two samples.*

Table 7-4. Selected SEM-EDS analyses of unaltered plagioclase.

	Na_2O	Al_2O_3	SiO_2	K_2O	CaO	FeO	Total	An%
81G	7.38	26.49	59.41	0.23	7.15	0.12	100.79	35
82G	6.91	26.74	58.89	0.15	7.88	0.17	100.69	39
128G	6.94	26.72	58.86	0.19	7.46	0.17	100.33	38
172G	6.36	27.71	56.96	0.12	8.61	*	99.72	43
661G[1]	8.12	24.79	61.21	*	5.56	0.16	99.85	27
536-2G	6.52	27.38	57.72	0.32	8.45	0.20	100.59	42

[1] = Ävrö granite. * = Below detection limit.

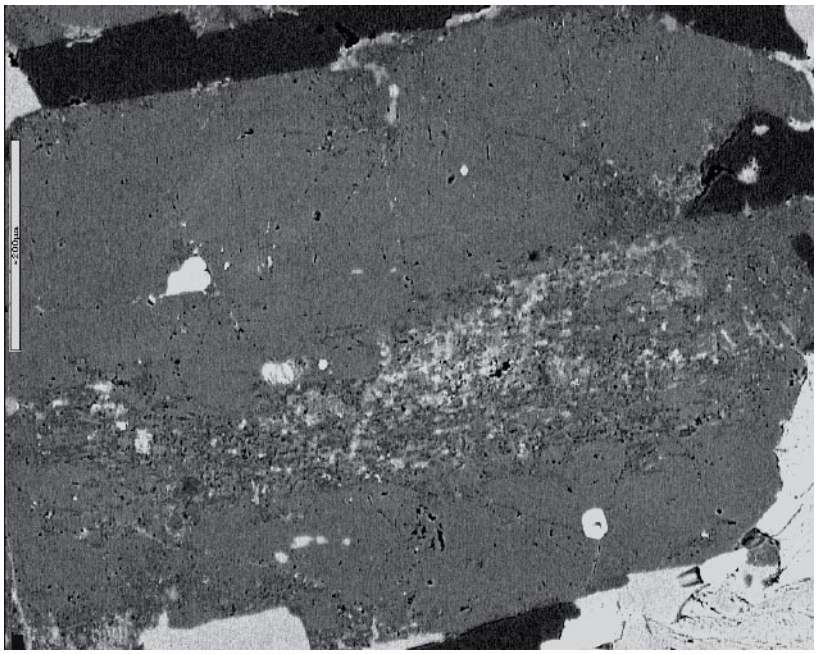

Figure 7-10. *Back-scattered SEM-image of partly sericitized plagioclase from sample 82G. Secondary minerals are sericite, albite and prehnite. The major part of the plagioclase crystal is unaltered and has low porosity. Scale marker bar is 200 µm.*

Table 7-5. Selected SEM-EDS analyses of whole plagioclase crystals from reference samples.

	Na_2O	MgO	Al_2O_3	SiO_2	K_2O	CaO	FeO	Total
62G	6.19	0.21	26.15	57.56	2.16	5.61	0.63	98.50
82G	5.59	*	27.64	56.79	1.82	7.32	0.51	99.69
128G	5.66	*	28.20	56.57	0.65	9.03	0.16	100.30
172G(1)[1]	5.55	0.23	27.42	56.53	2.24	6.26	0.39	98.75
172G(2)	6.22	*	26.30	58.15	1.85	6.71	0.34	99.57
172G(3)	6.62	*	26.96	58.36	0.51	7.56	0.18	100.20
372G	7.40	*	24.38	58.65	1.45	5.33	0.43	97.64
394G	7.64	*	24.70	60.86	1.19	4.62	0.33	99.33
536-1G(1)	6.54	0.21	26.55	58.58	2.35	5.21	0.40	99.84
536-1G(2)	6.29	*	26.72	58.16	2.25	5.58	0.39	99.38
536-2G	6.64	*	26.71	58.31	0.41	8.27	0.13	100.50
Av.(n=45)	6.27	0.13	26.4	58.41	2.21	5.68	0.54	99.70

[1] = Incl. 0.14 TiO2. Av.(n=45) = Average value from 45 analyses of whole plagioclase crystals. * = Below detection limit.

Table 7-6. Selected SEM-EDS analyses of sericite in plagioclase crystals.

	Na_2O	MgO	Al_2O_3	SiO_2	K_2O	CaO	FeO	BaO	Total
81G	0.49	0.39	32.73	49.24	10.58	0.49	3.14	*	97.04
100R	0.39	0.57	28.65	53.98	12.35	*	0.91	0.64	97.48
128G	0.84	0.84	31.38	51.19	10.16	0.85	1.83	*	97.09
144R	0.73	0.20	34.27	47.29	10.57	*	0.34	*	93.40
394R	0.52	1.44	31.72	46.98	10.53	*	3.70	0.78	95.67

* = Below detection limit.

Plagioclase in red-stained samples

Plagioclase in the red-stained samples is in most cases completely replaced by the secondary minerals albite, K-feldspar, sericite, prehnite, Fe-oxides and epidote (order of relative abundance). Albite and K-feldspar are by far the most abundant secondary minerals in the pseudomorphs. The primary-anorthite content is removed from plagioclase during alteration and forms prehnite, epidote or calcite, in the pseudomorphs, in voids, or in fracture fillings. The replacement of plagioclase is pseudomorphic and the crystal shape is maintained during alteration (Figure 7-11). The intensity of the red-staining varies widely within crystals and between different crystals.

The replacement of primary plagioclase is associated with an increased porosity within the secondary grains. This is clearly visible in the petrographic microscope using reflective light (Figure 7-12).

The primary albite-twinning of the plagioclase remains in many of the secondary pseudomorphs although the mineralogy is completely changed and no anorthite-component remains (Figure 7-13).

Comparisons of microphotographs and back-scattered SEM-images clearly show that the intensity of the red-staining within crystals is associated to secondary minerals. Figure 7-14 shows that the most intense red-staining in the pseudomorphs occurs where K-feldspar ("K" in Figure 7-14) is the dominant mineral. In albite-rich parts (e.g. "A", in Figure 7-14) of the crystal, the red-staining is weaker, although still intense compared to surrounding crystals. Another feature shown in Figure 7-14 is the dark brown/black/red micro-fractures filled with Fe-oxides and possibly Fe-oxyhydroxides ("M"), cutting through the earlier formed pseudomorphs. These fractures were obviously induced and filled subsequently to the replacement of plagioclase, and thus subsequently to the major red-staining of the plagioclases. It is however difficult to determine how long time it was between the red-staining of the plagioclase pseudomorphs and the sealing of the Fe-oxide/Fe-oxyhydroxide filled fractures.

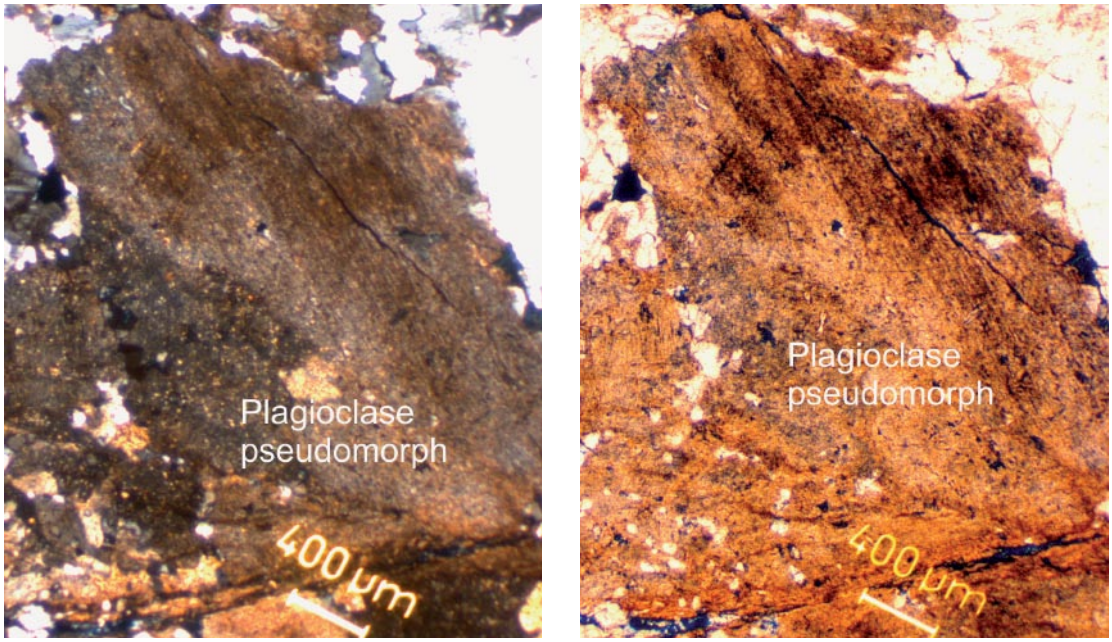

Figure 7-11. *Microphotographs of albite- and K-feldspar-rich pseudomorph after plagioclase, from sample 144R, +nic (left) and plain polarized light (right). Note the ink-impregnated micro-fractures cutting through the pseudomorphs.*

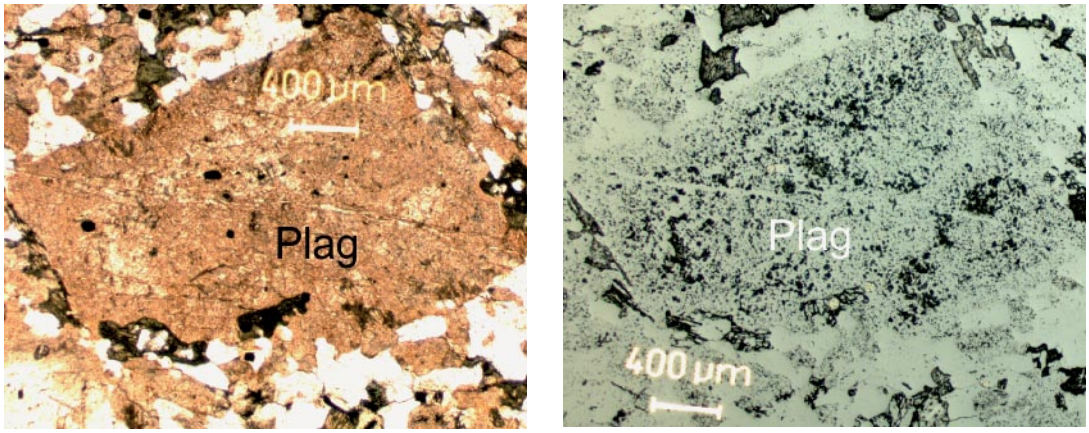

Figure 7-12. *Microphotographs of albite and K-feldspar rich pseudomorph after plagioclase, from sample 128R. Plain polarized light (left) and reflective light (right). Note the high porosity in the plagioclase pseudomorph (right) compared to surrounding quartz crystals*

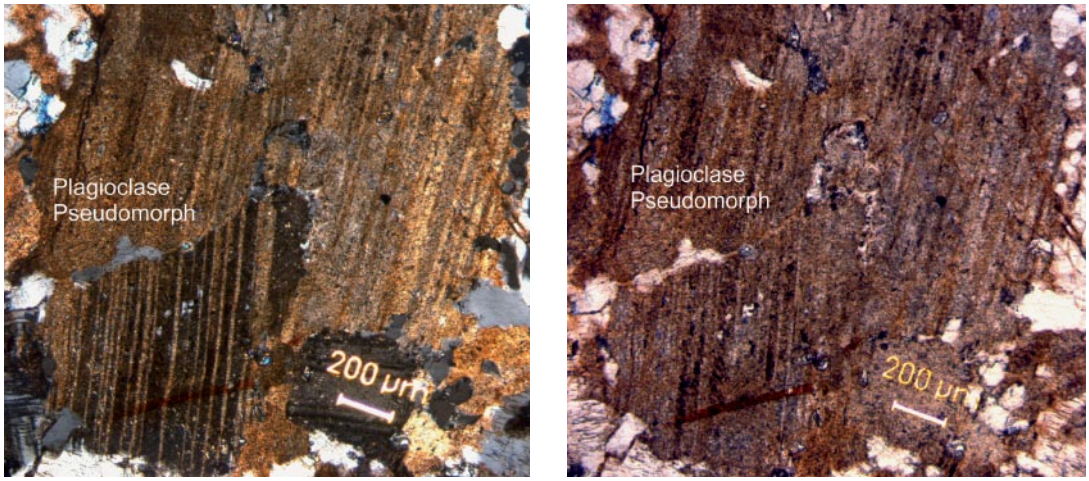

Figure 7-13. *Microphotographs of albite- and K-feldspar-rich pseudomorph after plagioclase, from sample 128R, +nic(left) and plain polarized light(right). Note the albite-twinning, inherited from the primary plagioclase. Note also the relatively high intra grain porosity, visible as dark blue coloured spots.*

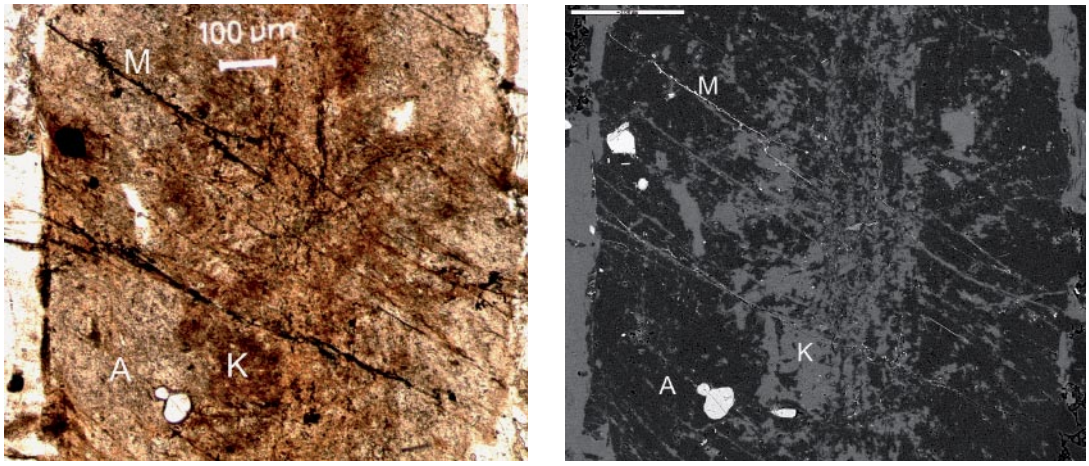

Figure 7-14. *Microphotograph (left) and back-scattered SEM-image (right) of red-stained pseudomorph after plagioclase, from sample 128R. "A" = albite, "K" = K-feldspar, "M" = micro-fractures filled with Fe-oxides/Fe-oxyhydroxides(?).*

The red-staining of albite and K-feldspar is caused by minute inclusions of Fe-oxides in the micro-pores, formed during the alteration and replacement of primary plagioclase. The secondary albite and K-feldspar are fairly equally porous, Fe-oxides are more commonly found in pores in K-feldspar than in albite (Figure 7-15a and Figure 7-17a–b) explaining why K-feldspar is more intensively red-stained than the albite. The high amount of micro-pores makes the crystals look clouded. Figure 7-15a, shows a close-up of highly porous secondary K-feldspar with numerous inclusions of Fe-oxides. Figure 7-15b shows a close-up of the Fe-oxides (or possibly Fe-oxyhydroxides) that fill the micro-fractures in the altered plagioclase.

SEM-investigations show that the inherited albite-twinning and optical orientations in the plagioclase pseudomorphs are made up of an intergrowth of albite and K-feldspar (Figure 7-16). The red-staining is more intense in the inherited twins occupied by K-feldspar (K), while albite-rich parts (A) are less red-stained. The inherited twins are somewhat distorted, which results in a patchy extinction of the twin-lamellae.

Figures 7-17a and 7-17b show that the twin-lamellae made up of K-feldspar (K), have more Fe-oxide inclusions in the micro-pores, than albite (A).

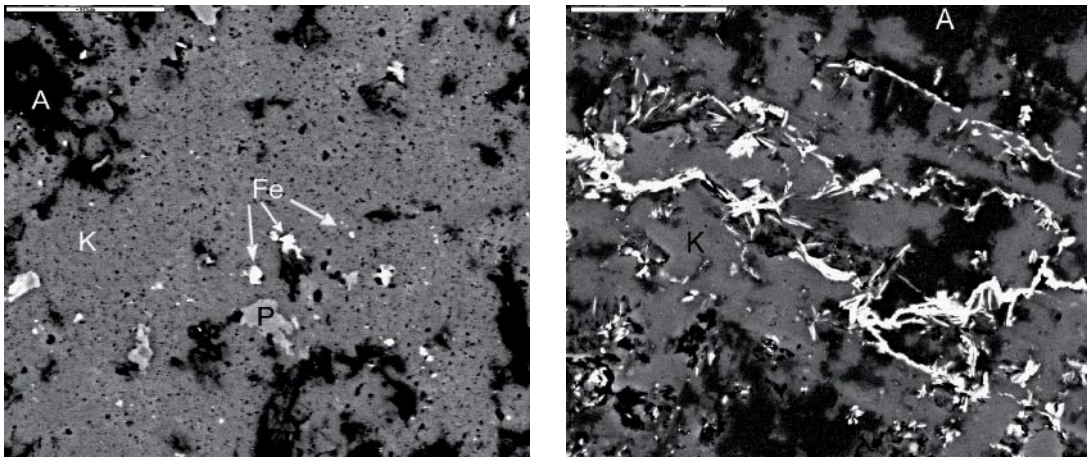

Figure 7-15a–b. *Back-scattered SEM-images of highly porous K-feldspar (K) with Fe-oxide (Fe) inclusions (left, sample 82R), and fine-grained Fe-oxides (or possibly Fe-oxyhydroxides) filling micro-fractures cutting through albite (A) and K-feldspar(K) in plagioclase pseudomorph (right, sample 128R). Scale marker bars are 50 µm. P = prehnite.*

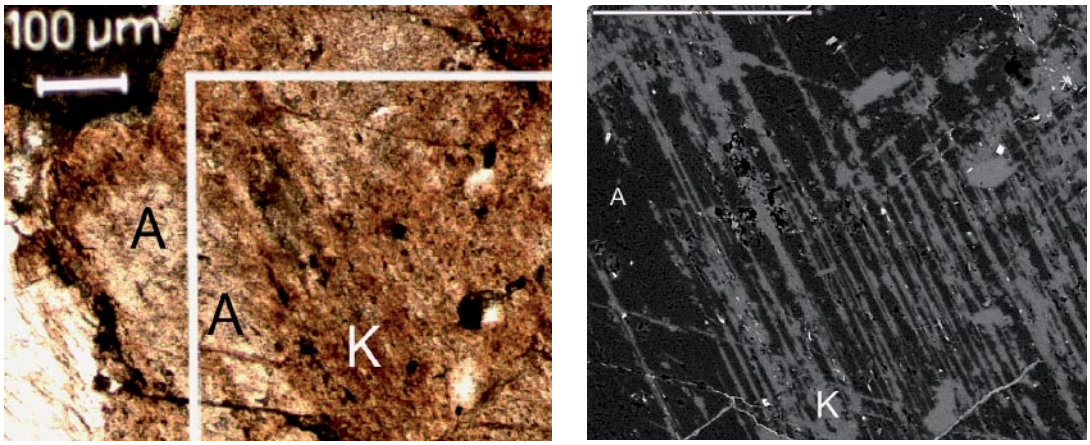

Figure 7-16. *Microphotograph (left, square shows the SEM-image view) and back-scattered SEM-image (right) of red-stained pseudomorph after plagioclase with inherited twinning, from sample 128R. "A" = albite, "K" = K-feldspar. Some later filled micro-fractures are also present. Scale bar (right) is 200 µm.*

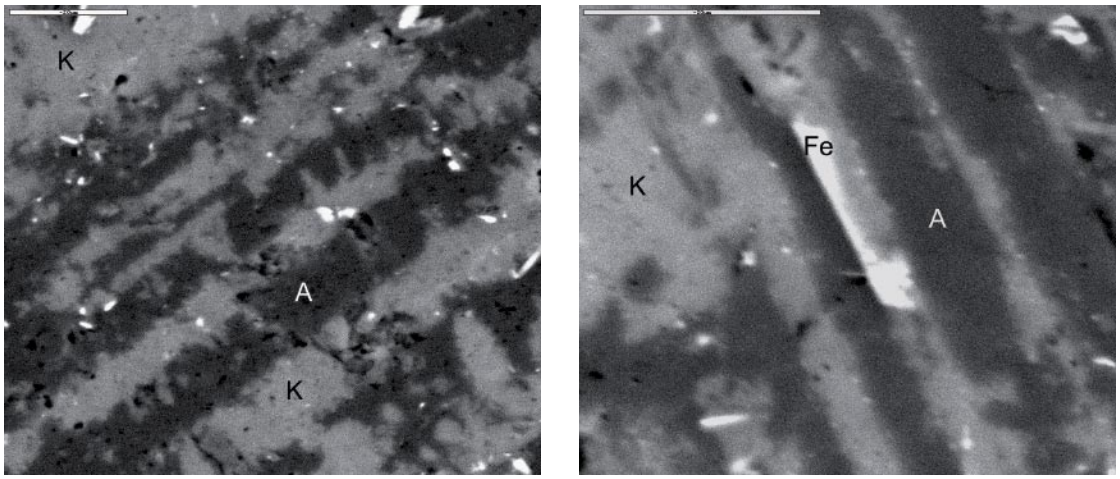

Figure 7-17(a–b). *Back-scattered SEM-images of twin-lamellae inherited from primary plagioclase, occupied by porous K-feldspar (K) with Fe-oxide (Fe) inclusions, and albite (A) with less Fe-oxide inclusions. Scale marker bars are 20 µm. Sample 128R.*

SEM-EDS analyses of pure secondary albite and K-feldspar in altered plagioclase from the red-stained samples show that the albite has no detectable amount of FeO (< 0.1%, Table 7-7), while the K-feldspar in altered plagioclase have higher amounts of FeO than the primary microcline and perthite have (Tables 7-3 and 7-8). When only considering the Fe contained in the entire feldspar crystal lattice it is observed that the secondary K-feldspar contains somewhat more FeO than the primary plagioclase while the albite contains less FeO than the primary plagioclase. The secondary K-feldspar also contain relatively high amounts of BaO, although not as high as in the perthite.

Selected whole crystal analyses (SEM-EDS) of the whole plagioclase pseudomorphs are shown in Table 7-8. These analyses show that the K_2O-content is very high, with an average of ~7%, caused by increased K-feldspar and sericite contents. The average FeO- and MgO-contents are slightly higher than in the unaltered samples, which may be explained by slightly higher sericite and Fe-inclusion contents, and probably Fe-rich minerals in micro-fractures.

Comparisons between the whole crystal-analyses (plagioclase) in the reference samples (Table 7-5) and pseudomorphs (after plagioclase) in the red-stained samples are shown in Figures 7-18, 7-19, and 7-20.

Figure 7-18 shows that the $K_2O/(K_2O+CaO)$-ratio is higher in the red-stained samples compared to reference samples. There is a trend of higher FeO-contents with higher $K_2O/(K_2O+CaO)$-ratio in the reference samples, which is coupled to higher sericite-contents, and higher grade of alteration.

Figure 7-19 shows the CaO versus Na_2O-content in the red-stained samples compared to reference samples. The CaO-content is consistently higher in the reference samples.

Table 7-7. Selected SEM-EDS analyses of albite in plagioclase pseudomorphs from red-stained samples.

	Na_2O	Al_2O_3	SiO_2	K_2O	CaO	Total
82R	10.79	20.05	68.97	*	0.20	100.01
128R(1)	11.10	20.34	68.46	*	0.47	100.37
128R(2)	11.06	20.04	67.56	0.06	0.42	99.15
536-2R	10.23	20.90	67.76	0.84	0.17	99.90

* = Below detection limit.

Table 7-8. Selected SEM-EDS analyses of whole plagioclase pseudomorphs from red-stained samples.

	Na_2O	MgO	Al_2O_3	SiO_2	K_2O	CaO	FeO	BaO	Total
62R-4	5.57	0.24	21.81	62.52	7.46	0.89	0.73	0.23	99.45
100R-4	4.08	0.51	24.25	59.00	8.70	0.62	1.49	0.53	99.18
100R-1	8.12	*	23.15	63.48	3.40	0.89	0.67	*	99.72
128R-2	4.95	0.30	20.65	63.09	8.48	0.55	1.25	*	99.27
128R-6	6.16	0.28	24.08	61.83	6.07	0.90	1.02	*	100.34
372R-2	5.41	0.40	21.30	62.36	7.39	1.22	0.65	*	98.73
394R-4	6.01	0.33	23.26	62.03	5.77	1.75	0.34	0.26	99.74
661R-4	5.44	0.26	20.59	63.76	8.23	0.62	0.46	*	99.36
Av.(n=62)	5.55	0.19	22.15	62.82	6.99	1.23	0.82	0.08	99.85

Av.(n=62) = Average value from 62 samples of whole plagioclase pseudomorphs. * = Below detection limit.

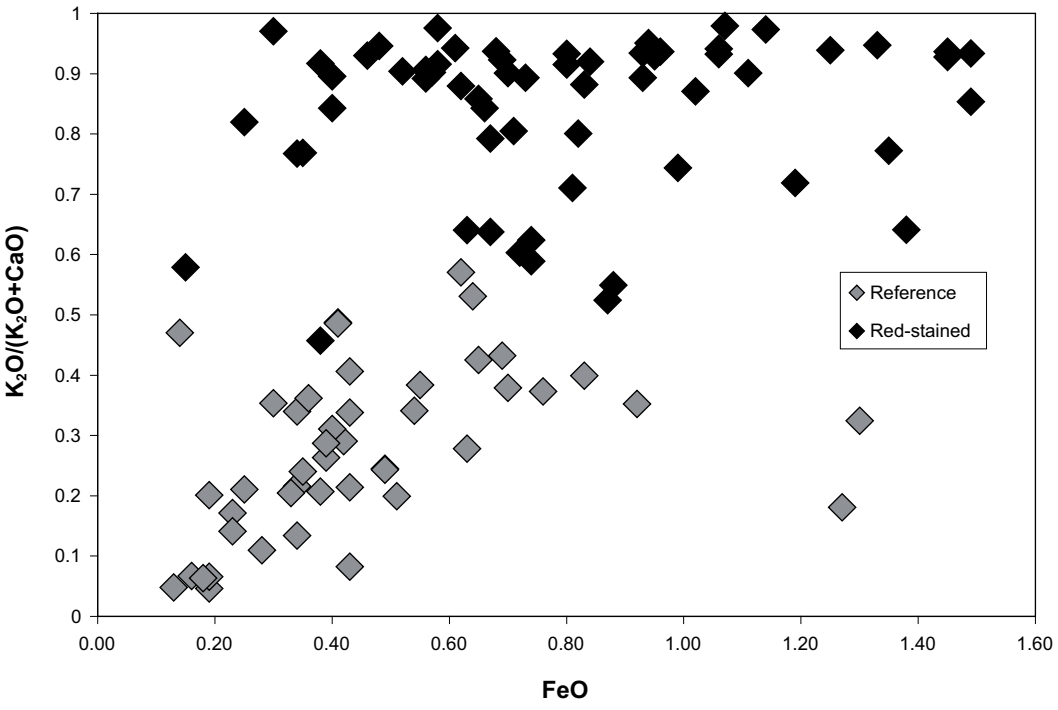

Figure 7-18. *Plot of $K_2O/(K_2O+CaO)$ vs. FeO from SEM-EDS analyses of whole plagioclase crystals/pseudomorphs from reference samples and red-stained samples, respectively.*

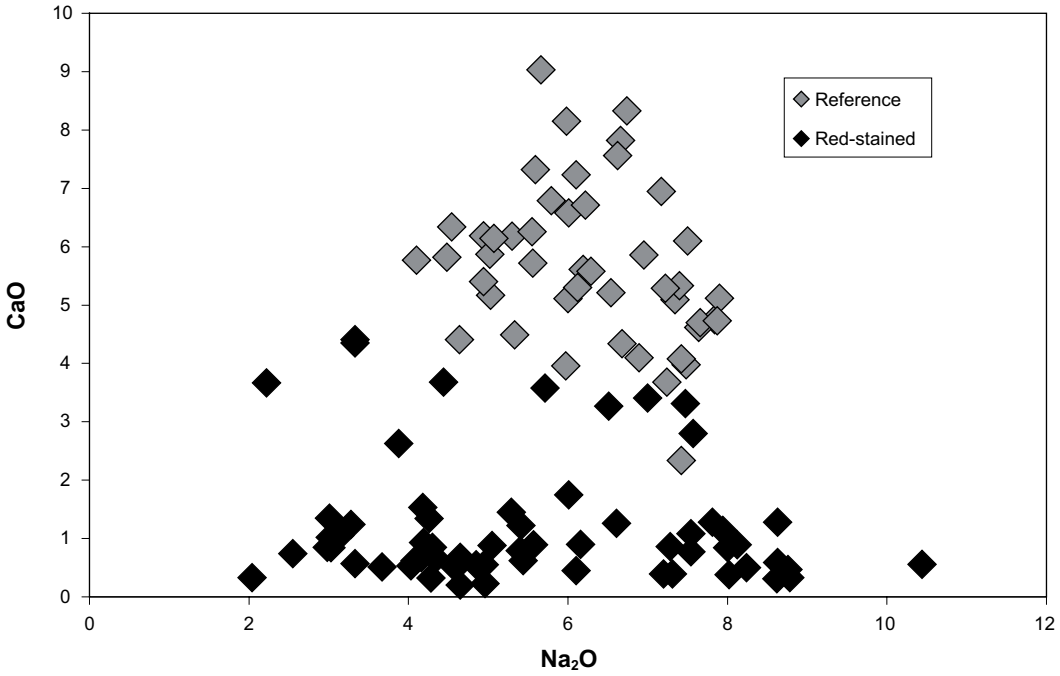

Figure 7-19. *Plot of CaO vs. Na_2O from SEM-EDS analyses of whole plagioclase crystals/pseudomorphs from reference samples and red-stained samples.*

Figure 7-20 shows Al_2O_3-contents versus SiO_2-contents in the red-stained samples compared to the reference samples. The Al_2O_3-content is generally lower and the SiO_2-content is generally higher in the red-stained rock. This is mainly dependent of the removal of the anorthite content in plagioclase ($CaAl_2Si_2O_8$) and the increase in albite ($NaAlSi_3O_8$) and K-feldspar ($KAlSi_3O_8$) in the red-stained samples. The low Al_2O_3-content and high SiO_2-content indicates that albite and K-feldspar is dominant over sericite (high in Al_2O_3, low in SiO_2, see Table 7-6) in the plagioclase. The stabilization of K-feldspar before muscovite in the red-stained granite was also noted by /Eliasson 1993/. This indicates a rather high activity of K^+ in the hydrothermal solution /Beane and Titley 1981/, as shown by whole rock chemistry analyses (Section 7.3).

Replacement processes

The replacement of primary plagioclase by albite (and K-feldspar) is rather complex and have been described or briefly reported in many earlier studies e.g. /O'Neil 1977, Kastner and Siever 1979, Saigal et al. 1988, Morad et al. 1990, Slaby et al. 1990, Slaby 1992, Lee and Parsons 1997, Petersson and Eliasson 1997, Lee and Parsons 1998, Ennis et al. 2000, Larsson et al. 2002, Putnis 2002, Holness 2003/. Inherited twins and inherited optical orientation in plagioclase pseudomorphs have been reported by /Morad et al. 1990, Slaby et al. 1990, Petersson and Eliasson 1997, Taboada and Garcia 1999, Holness 2003/. /Putnis 2002/ describes that the parent crystal will have crystallographic control over the product, even when all bonds may have been broken in the dissolution process.

Plagioclase alteration and replacement are dependent on a large number of parameters like temperature, pressure, pH, dissolution rates, time, solution composition, mineral (solid) composition, closeness to equilibrium, mineral surface area etc. One of these processes, where the primary plagioclase is replaced by secondary minerals, is the dissolution-reprecipitaion process, described by e.g. /Slaby 1992, Ennis et al. 2000, Larsson et al. 2002,

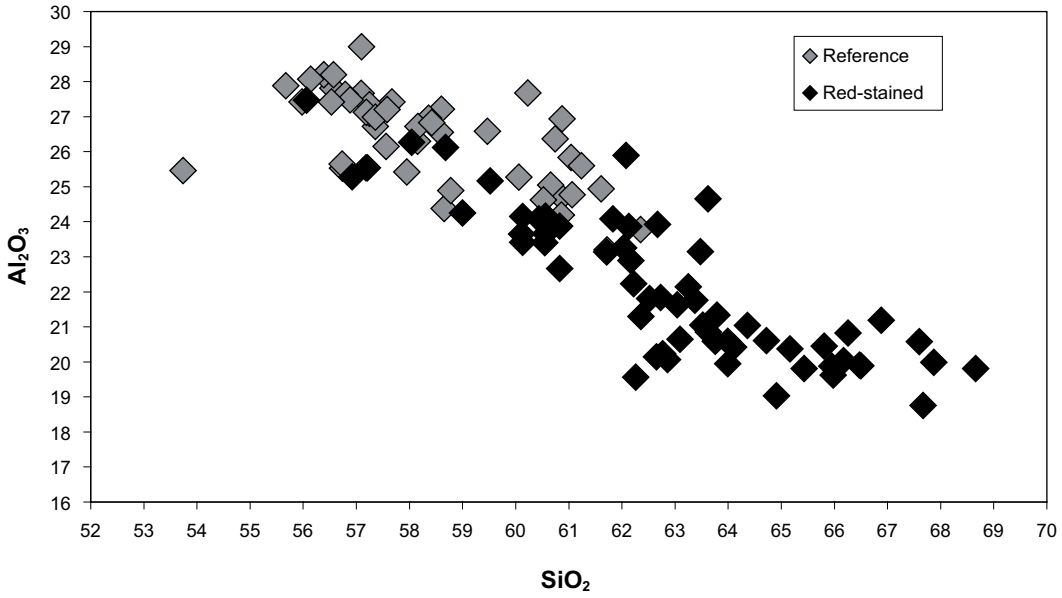

Figure 7-20. *Plot of Al_2O_3 vs. SiO_2 from SEM-EDS analyses of whole plagioclase crystals/pseudomorphs from reference samples and red-stained samples.*

Putnis 2002, Holness 2003/. This process (albitization and/or "microclinization") results in a sharp compositional gradient between the host and the secondary mineral /Putnis 2002/ and often feature micro-porosity in the secondary mineral /Morad et al. 1990, Lee and Parsons 1997, Putnis 2002/. This occurs whenever the amount precipitated is less than the amount dissolved and depends on solubility and composition of the solid and the fluid phases. In the presence of a fluid phase, comparatively small differences in free energy are sufficient to drive the re-crystallization by the dissolution re-precipitation process /Putnis 2002/. Exchanging cations through a "passive" aluminosilicate structural framework often, if not always involves the re-crystallization of the whole structure /O'Neil 1977/. However, /Krauskopf and Bird 1995/ using data from /Busenberg and Clemency 1976, Helgeson et al. 1984, Wollast and Chou 1985/ describe alteration of plagioclase that is mainly caused by formation of a surface layer of the feldspar that has been altered by partial loss of the alkali metals. The dissolution rate is controlled by reactions at the solution-mineral interface and not by the rate of ion diffusion away from the mineral into solution. This would involve a passive Al-Si network while the cations are exchanged. /Orville 1963, Lagache and Weisbrod 1977/ showed that fluid flow in combination with a temperature gradient in a rock containing two alkali feldspar phases, will result in redistribution of alkalis, which is suggested in this study.

In conclusion; the presence of elevated micro-porosity in the secondary minerals of the plagioclase pseudomorphs as well as the local sharp compositional contrasts between K-feldspar and albite, may suggest a dissolution-reprecipitation process. It is however difficult to discern whether the plagioclase crystals have been completely dissolved or if a Al-Si structural network remained in the host crystal and exchange mainly progressed as cation exchange. The plagioclase crystals are sometimes replaced in a well structured manner with inherited twinning and sometimes in an unstructured manner. This suggests that the replacement of plagioclase have involved different replacement processes. The order-disorder in the secondary albite, and presence or absence of twins may be controlled by the composition of the solution affecting the speed of albite growth /Slaby 1992/.

Feldspar thermometry

Two-feldspar thermometry has been used in many studies to interpret at which temperature the feldspars in the rock were in equilibrium. Thermometers have been developed by e.g. /Nekvasil and Burnham 1987, Fuhrman and Lindsley 1988, Elkins and Grove 1990, Benisek et al. 2004/. Applications of feldspar geothermometry is generally applied on high temperature processes and results from amphibolite and greenschist facies and lower are often yielding unreasonable low temperature values /Bucher and Frey 2002/. Analyses of secondary feldspars from this study was tested using the two-feldspar thermometers from /Nekvasil and Burnham 1987, Fuhrman and Lindsley 1988, Elkins and Grove 1990, Benisek et al. 2004/. The analyses come from close to end member K-feldspar and albite intergrowth in two plagioclase pseudomorphs with inherited albite-twinning from sample 128R. It is however uncertain if the feldspars were formed close to equilibrium, which is a criterion that must be fulfilled for the thermometers to be valid. The results from /Nekvasil and Burnham 1987/ and /Benisek et al. 2004/ gave temperatures of 296–341°C and 269–326°C, respectively, at chosen pressures of 2–5 kbars. These pressures were used because of the stability limit of associated prehnite. These temperatures are reasonable for the hydrothermal alteration, while the results from /Fuhrman and Lindsley 1988/ and /Elkins and Grove 1990/ gave values that most certainly are too low, 200–246°C and 202–253°C, respectively, for the secondary paragenesis of this alteration. Once again, the temperatures yielded from these thermometers are only very vague indications but are in accordance with temperatures of chloritization and prehnite formation (see the "Chlorite" and "Prehnite" sections in this chapter). The results from the present study are also somewhat uncertain since the end-member compositions of the feldspars are used in the thermometry-modeling, knowing that the SEM-EDS accuracy and precision for Na_2O is quite poor. Results from two-feldspar thermometry have however been found to be valid in some other studies of low-temperature paragenesis /Lee and Parsons 1997/. /Eliasson 1993/ argued that the alteration of plagioclase to albite took place at temperatures of 300–400°C. Similar formation of clouded secondary albite has been interpreted to be formed at temperatures lower than 370°C /Slaby 1992/.

7.2.4 Magnetite and hematite

Magnetite is the most common opaque mineral in the reference samples and it is extensively replaced by hematite in the red-stained samples. Magnetite in the reference samples is often unaltered and euhedral (Figure 7-21). Euhedral magnetite crystals commonly occur in close relationship with amphibole, pyroxene, chloritized or unaltered biotite and to some extent, titanite. Primary and unaltered magnetite crystals are also found as swarms of fine-grained crystals in clusters of pyroxene and amphibole, e.g. in sample 82G. The replacement of magnetite by hematite is commonly incomplete and remnants of magnetite are commonly visible in the pseudomorphs (Figure 7-22).

Fine-grained Fe-oxides are also present in plagioclase pseudomorphs. These Fe-oxides are often too small to be analysed by SEM-EDS, but the few analyses that have been performed indicate that it is hematite. Fine-grained Fe-oxide (or possibly Fe-oxyhydroxide) is present in micro-fractures cutting through crystals of plagioclase, quartz etc. These crystals are also too small to be analysed properly with SEM-EDS.

Ilmenite and pyrite are present in some samples. Sometimes ilmenite is partially altered to titanite and Ti-oxide. Euhedral pyrite is more common in the reference samples than in the red-stained samples. This might be caused by oxidation of the pyrite although no pseudomorphs have been observed. Rarely, pyrite is increased in the red-stained samples, as pyrite crystals have precipitated in voids of the porous rock, probably during reducing conditions subsequently to the major red-staining event.

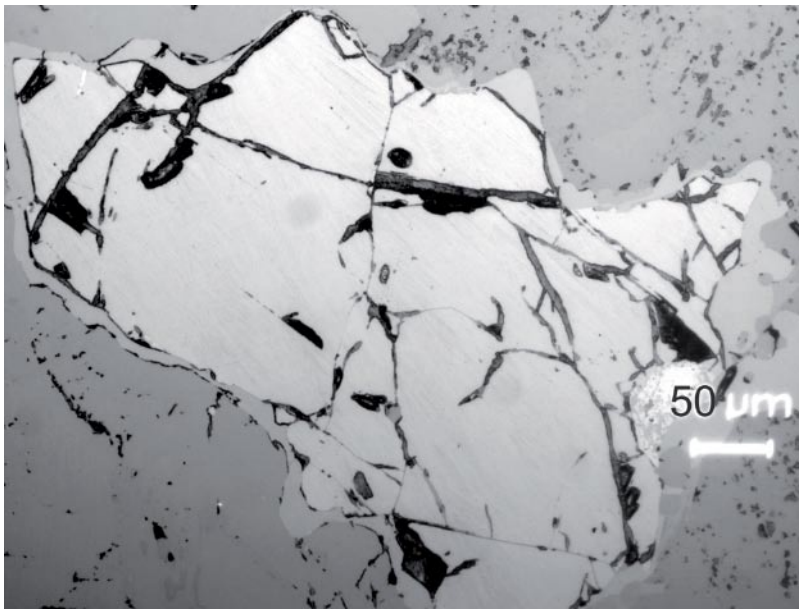

Figure 7-21. *Microphotograph of magnetite from sample 62G, reflective light.*

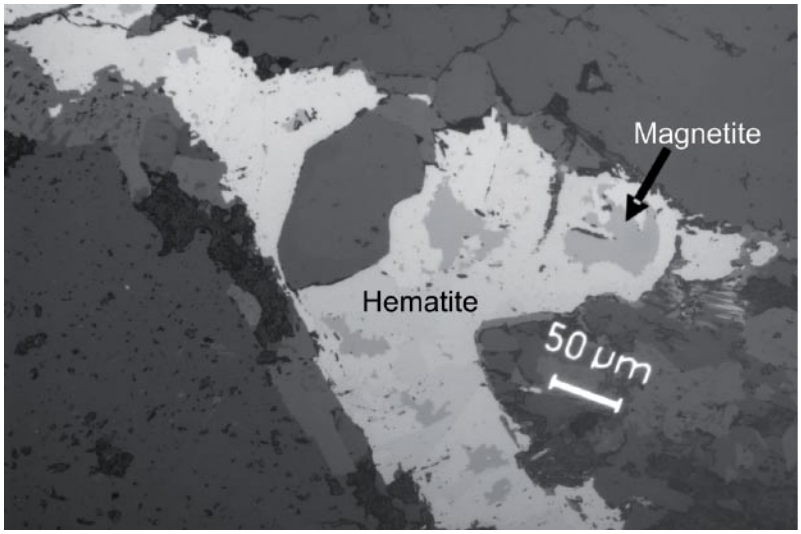

Figure 7-22. *Microphotograph of hematite partially replacing magnetite in a pseudomorphic manner, from sample 372R, reflective light.*

7.2.5 Biotite

Biotite is partially or completely replaced by chlorite in most of the reference samples and all of the red-stained samples. The replacement is pseudomorphic and titanite and possibly Ti-oxides are present together with chlorite in the pseudomorphs.

The suggested simplified reaction is:

Biotite + H_2O ($+Ca^{2+}$) → Chlorite ± Titanite ± Ti-oxide + K^+

These new crystals are formed along the (001)-cleavages of biotite. The Ti-content in biotite is sometimes quite high (e.g. in 536-2G cf. Table 7-9). The Ti-content has been found to range from 2 to 5%. The released K^+ has formed K-feldspar and sericite in the

Table 7-9. Selected SEM-EDS analyses of biotite.

	MgO	Al_2O_3	SiO_2	K_2O	TiO_2	MnO	FeO	Total
144G	13.50	15.58	37.85	8.65	2.53	0.44	18.93	97.47
144G	13.50	15.58	37.85	8.65	2.53	0.44	18.93	97.47

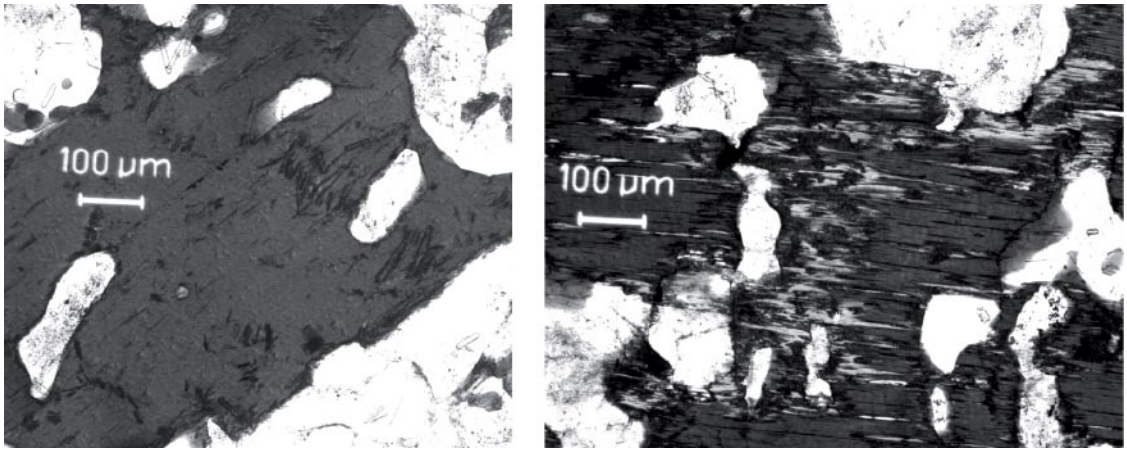

Figure 7-23. *Microphotographs of fresh biotite (left) and partly chloritized biotite (right), from sample 536-2G, plain polarized light.*

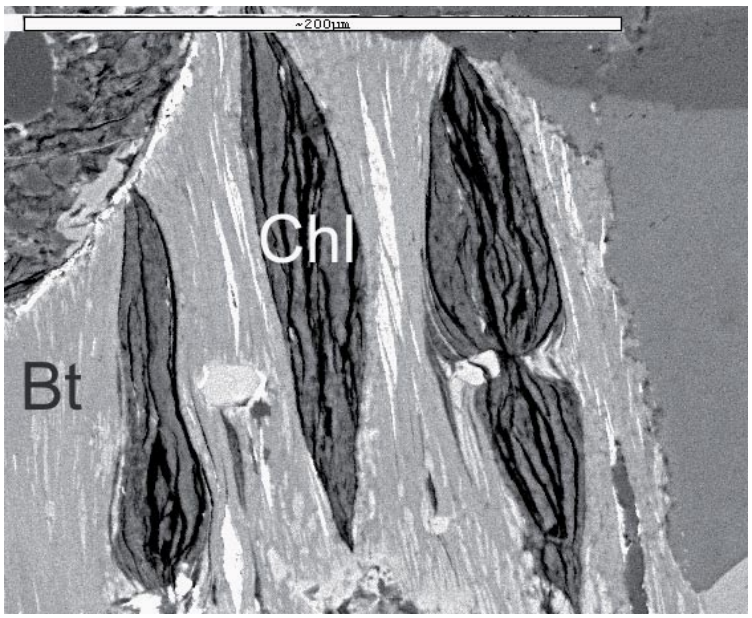

Figure 7-24. *Back-scattered SEM-image of partly chloritized (Chl) biotite (Bt) from sample 128G.*

surrounding rock. Even a small degree of chloritization gives intense potassium removal, as suggested by /Wilamowski 2002/. In some samples prehnite is formed along with chlorite in biotite-pseudomorphs. This prehnite and the titanite are formed by Ca^{2+}, mainly released during plagioclase breakdown. Although some Ca^{2+} may be contributed from alteration of pyroxenes and hornblende as well. /Ferry 1979/ suggested that Al- and Ti-contents remained unchanged during chloritization of biotite. /Parneix et al. 1985/ suggested that the Ti-content

was unchanged but that the Al-content was more variable at chloritization, although Al can not be transported for long distances since Al activity in hydrothermal fluids is very weak /Ellis and Mahon 1977/.

/Spear 1993/ proposes that the reaction biotite + H_2O = chlorite + K-feldspar, takes place below approximately 400°C, at conditions close to equilibrium, normally at maximum depth of 16 km. /Wilamowski 2002/ describes chloritization of biotite at temperatures of approximately 300°C.

7.2.6 Amphibole and pyroxene

Amphibole and pyroxene are quite common in the investigated samples, especially in the quartz monzodiorite to diorite samples. Amphibole and pyroxene are commonly found in clusters together with completely or partially chloritized biotite, magnetite and sometimes titanite. The highest amount amphibole and pyroxene is from sample 62G, where they constitute 18.8% of the modal composition. These minerals are often partially replaced by chlorite, especially in the red-stained samples (Figure 7-25). This replacement is however not as extensive as the chloritization of biotite. Amphiboles are commonly hornblende but actinolite may also be present (Table 7-10). All of the analysed pyroxene crystals are identified as augite (Table 7-10). The pyroxene/amphibole-ratio is lower in the Ävrö granites than in the other rock types. Chloritization of amphibole and pyroxene results in mobilisation of Ca^{2+}. Chloritization of hornblende results in mobilisation of small amounts of Na^{+} and K^{+}. The other major and minor elements are fixed in chlorite and titanite, which is sometimes formed together with chlorite. Some Ca^{2+} may also be fixed in the secondary titanite.

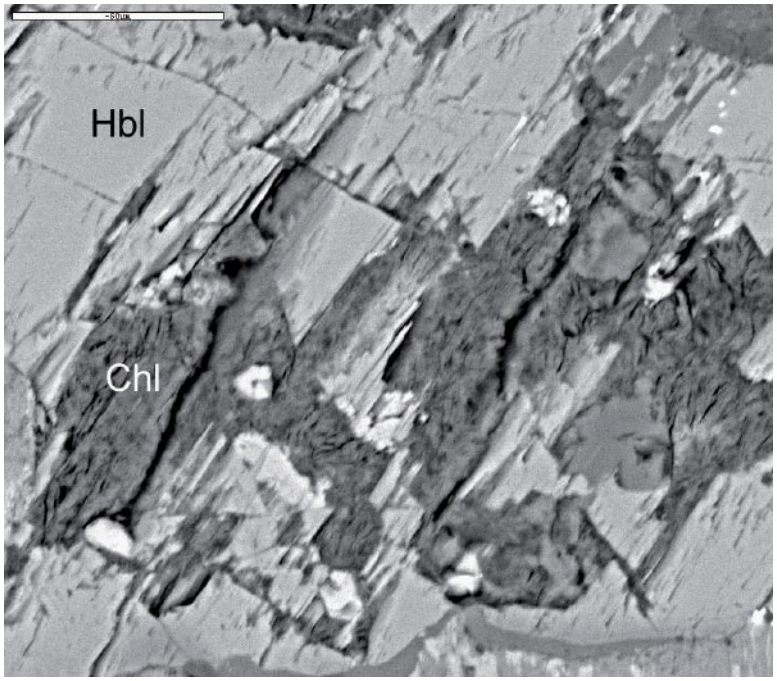

Figure 7-25. *Back-scattered SEM-image of partly chloritized (Chl) hornblende (Hbl) from sample 128G.*

Table 7-10. Selected SEM-EDS analyses of amphibole and pyroxene.

	Na_2O	MgO	Al_2O_3	SiO_2	K_2O	CaO	TiO_2	MnO	FeO	Total
Hornblende										
62G	1.24	11.78	8.51	45.69	0.88	11.68	1.18	0.42	16.87	98.27
536-1G	1.36	9.29	9.35	43.78	1.38	11.21	1.50	0.56	19.90	98.33
536-2G(1)	1.25	10.29	9.27	45.36	1.19	11.57	1.44	0.51	18.97	99.84
536-2G(2)	1.20	9.54	9.17	44.06	1.15	11.27	1.61	0.56	19.43	98.01
Actinolite										
100R	*	16.31	2.75	55.77	*	12.61	*	*	11.81	99.79
Augite										
81G	*	12.62	0.95	52.61	*	23.81	*	0.75	9.21	99.95
128G	0.77	12.00	3.37	51.31	0.32	18.59	0.51	0.73	12.80	100.40
172R	0.66	12.66	2.31	52.55	0.12	19.70	0.35	0.61	11.42	100.38

* = Below detection limit.

7.2.7 Chlorite

Chlorite is one of the most common secondary minerals in the studied samples. Chlorite replaces biotite and to a smaller degree amphibole and pyroxene. Crystallisation of fine-grained titanite accompanies the chloritization. Impregnation by ink shows that chlorite is highly porous. SEM-EDS analyses show that the chlorite has a homogenous composition in all of the analysed red-stained and reference samples (Table 7-11), in contrast to chlorite formed in fractures.

Comparison with SEM-EDS-analyses of fracture filling chlorites, from KSH01, KSH03, KLX02, KAS04 and KA1755A (Figure 7-26 and Figure 7-27) /Drake and Tullborg 2004, 2005, 2006a/ shows that chlorite in the wall rock shows similar composition as fracture filling chlorites of generation 1 to 4 (Table 3-1). This means that the chloritization in the wall rock coincide chronologically with these fracture filling generations and that they are formed at similar hydrothermal conditions.

Chlorite is generally formed at temperatures up to about 400°C and pressures of a few kilobars /Deer et al. 1992/.

Table 7-11. Selected SEM-EDS analyses of chlorite.

	MgO	Al_2O_3	SiO_2	K_2O	TiO_2	MnO	FeO	Total
62G	16.18	16.87	29.01	0.10	0.19	0.35	24.84	87.54
100R	16.90	18.83	29.14	*	0.14	0.39	23.94	89.33
172G	16.29	17.02	28.83	*	0.24	0.52	25.40	88.31
172R	16.33	16.64	29.59	0.15	0.20	0.45	24.98	88.34

* = Below detection limit.

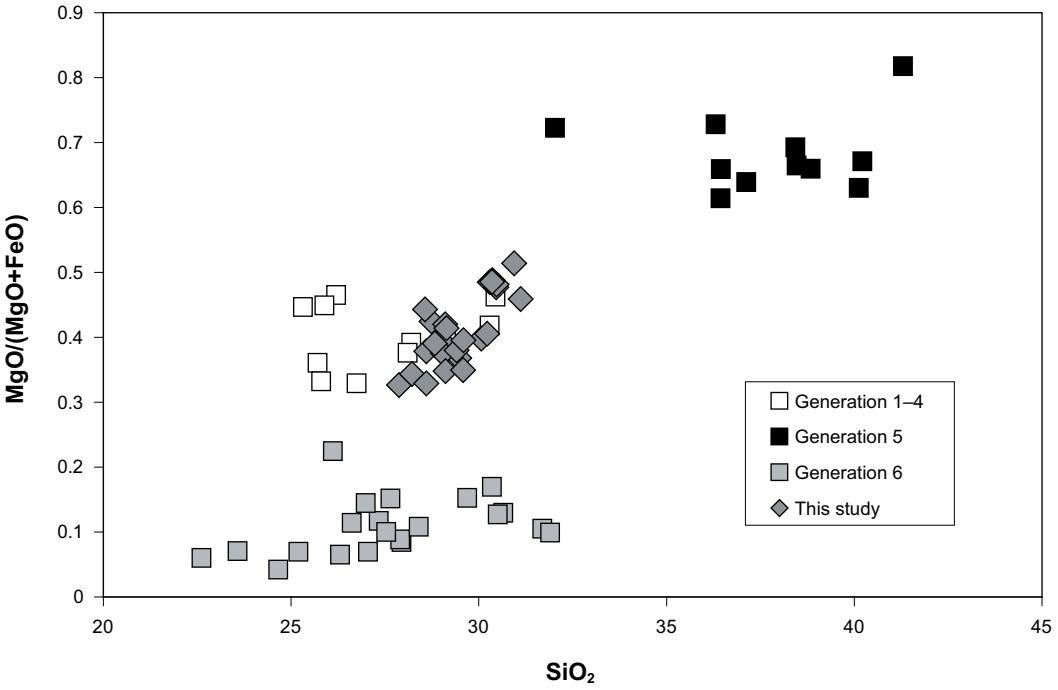

Figure 7-26. *Plot of MgO/(MgO+FeO) vs. SiO_2 from SEM-EDS-analyses of the wall-rock chlorites from this study and chlorites from fracture fillings from drill cores KSH01,KSH03, KLX02, KAS04 and KA1755A /Drake and Tullborg 2004, 2005, 2006a/.*

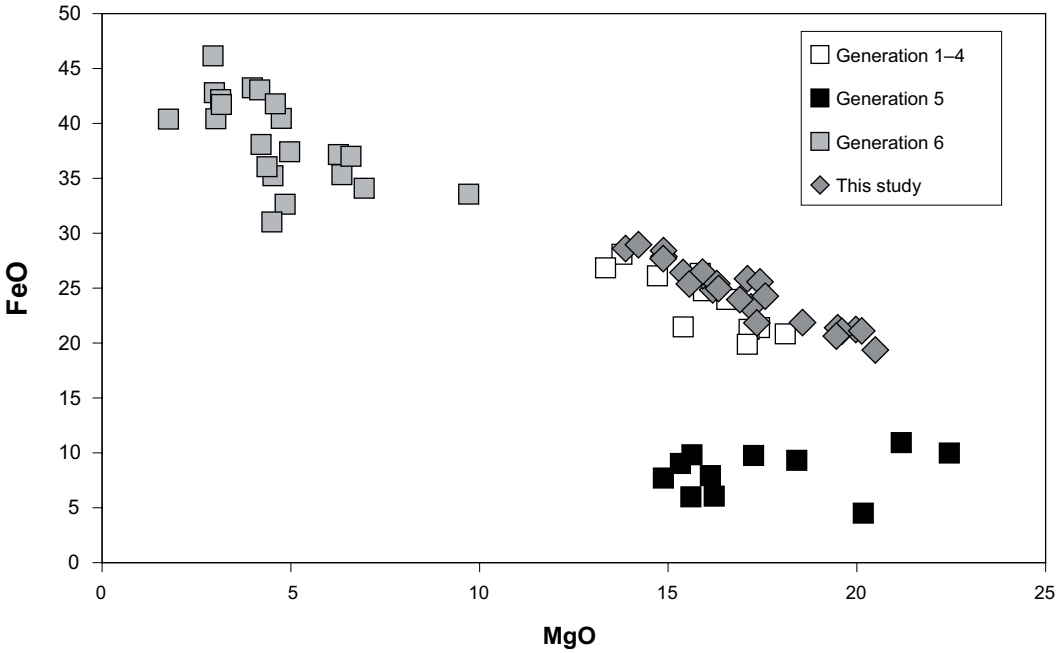

Figure 7-27. *Plot of FeO vs. MgO from SEM-EDS-analysis of the wall-rock chlorites from this study and chlorites from fracture fillings from drill cores KSH01, KSH03, KLX02, KAS04 and KA1755A /Drake and Tullborg 2004, 2005, 2006a/.*

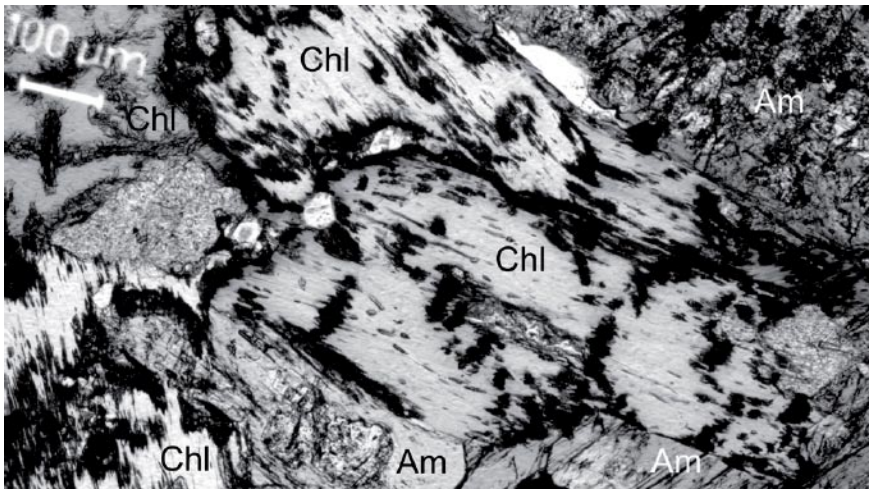

Figure 7-28. *Microphotograph of chlorite (Chl) and amphibole (Am), from sample 100G, plain polarized light.*

7.2.8 Titanite

Euhedral titanite is found in most of the samples except for in the dioritoid samples and some of the quartz monzodiorite samples. The Ävrö granite samples have the highest amount of titanite and the crystals are bigger in the Ävrö granite samples compared with the other samples. The crystals often have a primary interior and a secondary rim (Figure 7-29). Titanite crystals with rims are found in red-stained samples as well as in reference samples. SEM-EDS analyses (Table 7-12) show that there is no distinct compositional difference between the primary euhedral crystal, 372G(1) and the secondary rim, 372G(2). /Eliasson 1993/ found changes in the REE-content between rims and core of titanite crystals from Äspö, which along with presumed low mobility of Ti in the altered zone made him suggest that the Ti originates from biotite decomposition. Only trace amounts of titanite are found in the reference samples in which no chloritization of the biotite has occurred. Coexisting titanite and biotite have been described earlier from Simpevarp and Äspö e.g. /Kornfält and Wikman 1987/. Five thin sections of roughly unaltered granite to quartz monzodiorite from Äspö HRL, of coexisting titanite and biotite were briefly examined in this study. Titanite with rims occurs in co-existence with virtually unaltered biotite in at least three of the samples. In one of the samples the titanite crystals have no rims. In another sample there are indications of rim formation on titanite and in a third sample the rimmed titanite crystals are subordinate to the crystals without rims. The rims in the Äspö HRL thin sections are however less distinct than in the samples of this study. The rims are also more frequent in the more deformed samples from Äspö HRL. Since titanite crystals with rims occur in co-existence with fresh biotite it is suggested that the initial rims are formed prior to biotite decomposition but the fact that the rims seem to be more distinct close to the fractures and that some samples lack rims might infer that the distinct rims are associated to biotite decomposition and hydrothermal alteration.

Some titanite may alternatively be formed from breakdown of primary ilmenite, as seen in e.g. drill core KA1755A from Äspö /Drake and Tullborg 2005/.

Titanite also occurs as fine-grained crystals, along with chlorite in biotite-pseudomorphs. These fine-grained crystals have high Al-content, low Ti-content and somewhat higher Fe (Table 7-12, sample 82R). It is thus presumed that these crystals are grothite, a titanite variety high in Al and Fe^{3+}.

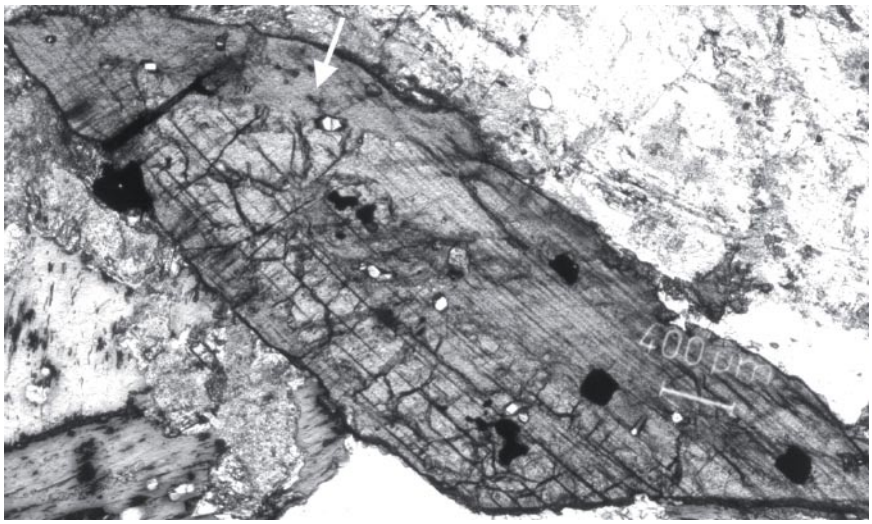

Figure 7-29. *Microphotograph of extraordinary big euhedral titanite with a secondary rim (arrow), from sample 372G, plain polarized light.*

Table 7-12. Selected SEM-EDS analyses of titanite.

Titanite	MgO	Al_2O_3	SiO_2	CaO	TiO_2	FeO	Total
82R	0.41	8.00	32.29	27.33	27.08	2.25	97.36
372G(1)	*	1.46	30.60	27.44	37.50	1.46	98.46
372G(2)	*	1.44	30.27	27.07	37.28	1.41	97.47

* = Below detection limit.

7.2.9 Epidote

The epidote-content is commonly higher in the red-stained samples than in the reference samples, although in the Ävrö granite samples the epidote content is very high and similar in both the reference sample and in the red-stained sample (372, 394, 661). In these samples the epidote crystals are euhedral to subhedral and rather Fe-rich (Table 7-13). This might indicate that at least some of the epidote is late-magmatic, as suggested by /Eliasson 1993/ or that the hydrothermal alteration causing formation of epidote reaches further from the fracture than the red-staining does. These epidote crystals are different in grain-size and morphology than the fine-grained crystals, found locally in saussuritic plagioclase. /Eliasson 1993/ identified secondary rims on magmatic epidote crystals, formed during hydrothermal alteration of plagioclase. A major part of the epidote found in the red-stained samples of quartz monzodiorite to diorite in this study are thought to be secondary and formed by Ca^{2+} (and Al^{3+}) removal from altered plagioclase.

Epidote is common as a fracture filling in fractures with adjacent red-staining of the host rock. Epidote does however not commonly occur in the major or micro-fractures in this study, except for in the most deformed Ävrö granite samples.

Table 7-13. Selected SEM-EDS analyses of epidote.

	Al_2O_3	SiO_2	CaO	MnO	FeO	Total
394G	22.51	38.11	22.61	0.29	13.38	96.89
394R	22.80	37.64	22.80	0.35	13.24	96.83
661G	23.07	38.30	23.19	0.44	13.29	98.29

7.2.10 Prehnite

Prehnite is the most common mineral filling in voids and minor fractures in the red-stained samples. Prehnite is also the most common mineral filling in the major fractures that probably worked as conduits for the hydrothermal fluids causing the red-staining. It is commonly present in both the reference samples and the red-stained samples but the modal content is normally higher in the red-stained samples, where prehnite commonly fills voids and is rarely replacing biotite (along the [001]-cleavage) and amphibole/pyroxene. In amphiboles and pyroxenes prehnite is found as irregular rounded inclusions within the crystals, commonly in the middle of the crystals. These observations are similar to those made by /Tulloch 1979/, who studied the alteration of biotite in granitoids and suggested the reaction: "biotite + anorthite (component in plagioclase) + H_2O = prehnite + chlorite + K-feldspar + titanite + muscovite" to take place.

Prehnite is also found as aggregates of big euhedral crystals and most of the prehnite is thought to be secondary and related to hydrothermal alteration. Prehnite is next to sericite the most common mineral in partially altered plagioclase in the reference sample. Prehnite is slightly more common in the completely replaced plagioclase pseudomorphs in the red-stained rock, although still minor compared with the albite-content and K-feldspar-content in the pseudomorphs. The prehnite-content is much higher than the epidote-content in altered plagioclases, which indicates alteration in accordance with prehnite-pumpellyite facies conditions, rather than greenschist facies.

Prehnite is commonly fresh and unaltered in the reference rock and in the red-stained rock, e.g. in the altered plagioclases, where the crystals are commonly not red-stained. Some of the aggregates of euhedral prehnite crystals are slightly altered by fine-grained crystals, possibly clay-minerals. The prehnite crystals are rather porous as shown by ink impregnation.

SEM-EDS analyses (Table 7-14) show quite homogenous compositions in euhedral prehnite crystals (100R, 172R) and fine-grained crystals in red-stained plagioclase pseudomorphs (536-1R(1), 536-1R(2), 536-2R). The most striking difference is the higher FeO-content in analysis 536-1R(2). The K_2O-content detected may be contamination from neighbouring crystals of K-feldspar. The SEM-EDS analyses resemble those from fracture-filing prehnite from KSH01 and KLX02 /Drake and Tullborg 2004, 2005/.

/Liou et al. 1983/ carried out experiments of the stability of prehnite and epidote under certain temperatures and pressures, in which the upper prehnite stability is set to 405°C at 2 kbar. /Deer et al. 1992/ report the upper stability of prehnite to occur at 400°C at 2–4 kbar, and that prehnite-pumpellyite facies in natural environments at 3 kbar has been estimated to about ~250–380°C. /Bucher and Frey 2002/ tell that the upper pressure limit of prehnite is about 5 kbar, but that a more realistic value is around 3 kbar. This temperature and pressure range is thought to be valid for the hydrothermal alteration in this study.

The lack of laumontite, which replaces prehnite at lower temperatures /Tullborg 1997, Drake and Tullborg 2004, 2005/ and has an upper stability of about 260–280°C /Frey et al. 1991/ or 230–260°C /Bucher and Frey 2002/, suggest that the temperature of alteration is higher.

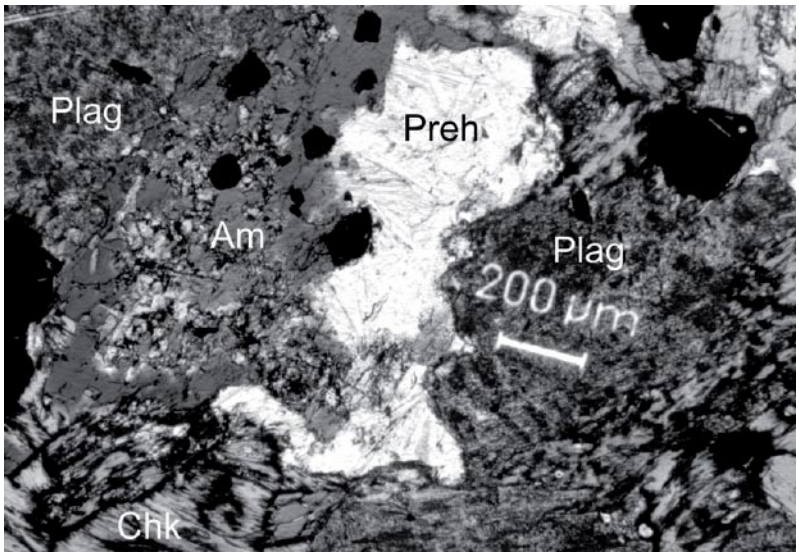

Figure 7-30. *Microphotograph of unaltered, secondary prehnite (Preh) filling space between altered plagioclase (Plag), chlorite (Chl) and altered amphibole (Am). From sample 82R, plain polarized light.*

Table 7-14. Selected SEM-EDS analyses of prehnite.

	Al_2O_3	SiO_2	K_2O	CaO	FeO	Total
100R	24.36	43.75	0.16	26.29	0.99	95.55
172R	23.94	43.97	*	26.89	1.55	96.34
536-1R(1)	23.57	44.33	0.11	26.53	1.65	96.19
536-1R(2)	22.29	43.78	0.17	26.62	3.09	95.95
536-2R	23.71	43.91	*	26.96	1.69	96.27

* = Below detection limit.

7.3 Porosity

The porosity is occasionally seen as macroscopic voids or minor-fractures but the porosity in the examined samples is mainly due to microscopic pores of different geometry and occurrence. According to /Mazurek et al. 1995/ the following porosities are distinguished; grain-boundary porosity, trans-granular porosity, micro-fractures, sheet silicate porosity and solution porosity.

Grain-boundary porosity is made up of planar micro-pores aligned along the grain boundaries of quartz or feldspars. Quite often, this type of pore-space constitutes an interconnected network in the rock matrix. This is characteristic in samples 661 and to a lesser degree sample 144, and is generally more prominent in samples that show signs of mechanical deformation. Trans-granular porosity is made up of planar micro-pores cross-cutting minerals, mostly feldspars, very often along crystallographic cleavage planes of the minerals. This is seen in e.g. partly altered microcline. Micro-fractures cutting through the primary and secondary minerals are numerous in this study and have controlled migration of hydrothermal fluids to a large extent. Sheet silicate porosity is due to planar micro-pores along the basal planes at the rims or within sheet silicates, such as biotite or chlorite. These pores do not form an interconnected network unless they are connected by other types of pores.

This porosity is observed parallel to the basal sheets of chlorite pseudomorphs after biotite. Since these occur in clusters, sheet silicate pores may provide interconnected networks over several millimetres. Solution porosity is formed during metamorphic events with hydrothermal fluids penetrating through the rock matrix. Unstable minerals are partly dissolved and irregular-shaped microscopic pore space is created. These pores become visible when occurring in clusters and are identified as cloudy regions in the crystals that are mostly aligned along grain boundary or trans-granular pores. These pore spaces are quite prominent in plagioclase in this study (cf. Figure 7-12), and maybe also in microcline to some degree. The pores contain variable amounts of inclusions of secondary nature, e.g. hematite.

The above mentioned micro-porosity-features have been found to be more prominent in the red-stained samples than in the reference samples, sometimes high-lightened by ink-impregnation. Sheet silicate porosity is however wide-spread in the in the reference samples where biotite is completely chloritized. Similar pore-space features have been documented in altered granite from Äspö, using the more advanced ^{14}C- and ^{3}H -PMMA-techniques /Kelokaski et al. 2001/, although this was only a test of different techniques and improvements can be made. Porosities of 0.13 to 0.20% (average 0.17%) for unaltered rock and 0.15 to 0.85% (average 0.35%) for red-stained rock have been measured on granitic rock at Äspö /Eliasson 1993/. Porosities of about 0.2 to 1% for unaltered rock and about 1 to 2.5% for altered rock were measured on fine-grained dioritoid in drill core KSH02, Simpevarp /Mattsson and Thunehed 2004/.

7.4 Whole rock chemistry

24 samples were analysed for major elements, minor elements, trace elements and LOI at Analytica AB Sweden. When comparing the absolute values of each element, the values differ quite a lot between the first analysis and the second one. However, the normative change between the red-stained sample and the reference sample for the duplicate analyses gave similar results for most of the elements. This shows that the normative changes between the samples are adequate for most of the elements and gives also indications of which elements that are poorly measured, or unevenly distributed in the samples. The result from analysis of major-, minor- and trace elements from each sample is shown in Table 7-15. Results of REE-analyses are shown in Table 7-16. The analyses made to test reproducibility, 81, 144, 172 did not include measurement of Cs, S, and F.

The normative changes are obtained from the following equation:

$$\Delta C_i = (C_i^A / C_i^0) - 1$$

where ΔC_i is the normative change in concentration of element *i*, C_i^A is the measured concentration of element *i* in the red-stained rock and C_i^0 is the measured concentration of element *i* in the reference sample. The ΔC_i-value is then multiplied by 100 to give the changes in per cent.

Table 7-15. Chemical whole rock analyses.

	62G	62R	81G	81R	81G(2)	81R(2)	82G	82R	100G	100R	128G	128R	144G	144R	144G(2)	144R(2)
SiO_2 (%)	53.6	53	52.4	53.2	51.7	52.1	52.7	51.1	52.5	51.1	60.1	60.7	67.4	66.5	68.2	68
Al_2O_3 (%)	17	15.9	16.8	16.1	16.6	15.9	17	16.1	17.4	16.7	16.5	15	15.3	15.4	15.5	15.7
CaO (%)	6.14	7.33	7.23	6.94	7.24	6.92	6.92	6.23	5.57	4.22	4.66	2.98	3.03	1.51	3.05	1.53
Fe_2O_3 (%)	9.06	8.77	9.9	9	10.1	9.05	10	10.3	9.7	9.98	6.65	6.61	3.91	3.68	4.03	3.84
K_2O (%)	3.29	3.37	1.65	3.18	1.6	3.12	2.18	3.23	1.93	3.7	3.42	4.39	3.35	5.09	3.41	5.22
MgO (%)	3.99	3.78	4.51	3.97	4.52	3.97	4.38	4.25	4.61	5	2.62	2.77	1.5	1.56	1.53	1.61
MnO (%)	0.145	0.152	0.165	0.15	0.168	0.151	0.162	0.161	0.195	0.164	0.122	0.118	0.0673	0.0653	0.0697	0.0675
Na_2O (%)	3.05	4.11	3.26	3.65	3.24	3.59	3.31	4.13	3.76	3.55	3.46	3.88	3.87	4.21	3.9	4.3
P_2O_5 (%)	0.415	0.409	0.483	0.435	0.502	0.453	0.476	0.606	0.451	0.458	0.327	0.321	0.204	0.193	0.208	0.201
TiO_2 (%)	1.13	1.12	1.27	1.16	1.28	1.17	1.27	1.4	1.16	1.21	0.984	0.978	0.543	0.508	0.559	0.523
LOI (%)	2	1.9	1.8	2.1	1.8	2	1.3	2.2	2.5	3.3	1	1.7	0.9	1.4	0.8	1.2
Total (%)	**97.8**	**97.9**	**97.7**	**97.8**	**97**	**96.4**	**98.4**	**97.5**	**97.3**	**96.1**	**98.8**	**97.7**	**99.2**	**98.7**	**100.5**	**101**
Ba (ppm)	1,250	868	780	1,380	826	1,460	1,150	885	846	1,190	986	1,010	916	1,650	988	1,810
Be (ppm)	1.96	1.67	1.9	1.63	1.8	1.78	1.79	1.51	2	1.88	2.41	1.83	2.54	1.95	2.73	2.14
Co (ppm)	13.8	14.2	15.7	14.8	25.8	22.7	17.6	17.7	16.6	18.4	10	10.3	6.2	6.51	< 6	6.51
Cr (ppm)	123	95.3	153	136	119	126	175	110	163	112	131	105	227	133	201	142
Cs (ppm)	1.43	0.438	0.993	0.912			2.11	0.562	2.64	2.27	2.55	1.98	1.73	1.26		
Cu (ppm)	28.6	30.2	31.2	29.7	39.6	36.7	30	33.4	32.1	22.7	53.7	12.3	< 2	< 2	10.1	16.6
F (%)	0.12	0.2	0.12	0.13			0.13	0.14	0.12	0.12	0.11	0.11	0.07	0.05		
Ga (ppm)	14.4	13.6	14.1	13.6	23.6	18.1	16.3	12.9	16.3	13.1	15.1	10.9	13	9.74	78.1	122
Hf (ppm)	4.56	4.49	1.99	2.86	1.1	2.22	4.73	4.8	2.58	4.98	5.36	5.32	4.49	4.05	4.5	5.01
Mo (ppm)	< 2	< 2	< 2	< 2	< 2	< 2	< 2	< 2	< 2	< 2	< 2	< 2	< 2	< 2	< 2	< 2
Nb (ppm)	9.47	8.18	9.4	11.5	7.72	10.1	9.67	7.12	9.25	9.87	10.4	9.05	7.67	8.46	11.9	10.4
Ni (ppm)	16.5	17.3	18.7	18.4	32.1	32.4	21.7	18.5	19.7	21	5.69	5.65	8.12	7.92	13.8	< 10
Rb (ppm)	89.1	68.9	39.5	86.2	43.9	76.8	52.4	77.1	76.4	117	80.9	134	53.1	93.8	65.4	109
S (ppm)	887	859	1,040	891			995	1,000	830	35.1	72.4	15.5	24.4	15.9		
Sc (ppm)	21.3	22.3	24.3	21.8	23.8	21.4	24.5	22.8	23.7	23.1	16.4	15.9	8.17	6.37	8.01	6.68

	62G	62R	81G	81R	81G(2)	81R(2)	82G	82R	100G	100R	128G	128R	144G	144R	144G(2)	144R(2)
Sn (ppm)	< 1	< 1	1.65	< 1	1.71	< 1	2.08	< 1	< 1	< 1	2.96	< 1	1.94	< 1	1.83	1.74
Sr (ppm)	924	329	888	496	896	499	876	404	924	448	614	388	786	391	804	407
Ta (ppm)	0.611	0.617	0.641	0.675	0.471	0.482	0.61	0.554	0.52	0.409	0.879	0.84	0.84	0.837	1.07	1.11
Th (ppm)	3.4	2.13	3.25	3.54	2.96	3.77	2.19	2.51	2.06	2.14	4.63	5.13	6.75	4.49	11.6	8.95
U (ppm)	1.42	1.31	1.56	2.39	1.38	1.92	1.54	1.51	1.11	1.52	2.32	2.44	3.09	2.78	3.38	3.24
V (ppm)	157	146	177	155	180	159	175	168	164	165	103	92.3	53.4	47.2	56.4	51.1
W (ppm)	< 0.3	0.554	< 0.3	< 0.4	0.504	0.457	< 0.3	< 0.4	< 0.4	< 0.4	0.444	1.05	< 0.3	0.479	1.04	1.3
Y (ppm)	29.7	29.1	31.6	28.7	30.9	28.1	30.3	32.4	30.2	30.9	33.7	34.3	17.7	16.1	18.1	15.7
Zn (ppm)	59.7	60.1	70.2	67.4	118	108	83.7	89.3	89	108	65.3	72.5	91.7	52.8	62.9	94.6
Zr (ppm)	219	191	78.3	113	63.3	121	203	202	117	260	229	251	195	175	188	206

Table 7-15 cont. Chemical whole rock analyses.

	172G	172R	172G(2)	172R(2)	372G	372R	394G	394R	536-1G	536-1R	536-2G	536-2R	661G	661R
SiO_2 (%)	56.8	56.9	57.8	57.5	60.9	61.8	60.2	59.6	60.4	60.7	58.4	59	59.7	59.8
Al_2O_3 (%)	16.6	15.9	16.8	16.1	17.4	16.9	17.5	16.7	16	15.1	16.5	15.4	17.9	16.7
CaO (%)	4.8	4.62	4.81	4.64	3.94	3.42	4.22	4.02	3.92	3.44	5.56	5.26	4.07	4.29
Fe_2O_3 (%)	7.83	7.87	8.01	8.07	5.1	5.48	4.99	5.27	7.29	7.39	7.9	7.25	5.23	5.42
K_2O (%)	2.93	3.26	2.93	3.44	3.26	3.97	3.19	4.23	3.34	3.25	3.14	3.54	2.86	3.76
MgO (%)	3.61	3.66	3.67	3.72	2.08	2.15	2.21	2.21	2.66	2.78	2.96	2.6	2.44	2.19
MnO (%)	0.15	0.146	0.153	0.15	0.087	0.0844	0.0931	0.0945	0.114	0.103	0.124	0.109	0.0935	0.0891
Na_2O (%)	3.35	3.75	3.38	3.78	4.47	4.44	4.41	3.76	3.17	3.65	3.25	3.47	4.61	4.41
P_2O_5 (%)	0.353	0.361	0.357	0.371	0.305	0.346	0.33	0.339	0.264	0.29	0.293	0.273	0.356	0.343
TiO_2 (%)	1.03	1.02	1.04	1.04	0.736	0.81	0.77	0.813	0.929	0.988	1.01	0.981	0.821	0.827
LOI (%)	2.1	2.1	2	2	1.6	1.8	1.6	1.9	1.9	2.3	0.9	2	1.7	1.7
Total (%)	97.5	97.5	99	98.8	98.3	99.4	97.9	97	98.1	97.7	99.1	97.9	98.1	97.8
Ba (ppm)	1,150	1,180	1,240	1,280	1,350	1,270	2,070	2,460	775	529	775	616	965	1,110
Be (ppm)	2.21	2.05	2.37	2.13	3.26	2.56	2.88	2.05	2.38	1.79	2.2	2.2	2.81	2.31

	172G	172R	172G(2)	172R(2)	372G	372R	394G	394R	536-1G	536-1R	536-2G	536-2R	661G	661R
Co (ppm)	13.5	13.3	18.2	17.9	8.82	9.92	9.57	10.5	11.5	13.6	11.4	11.3	9.99	9.09
Cr (ppm)	178	122	155	121	128	122	159	115	167	118	87.7	133	103	88.1
Cs (ppm)	2.03	1.83			0.927	1.03	0.885	0.793	1.97	0.99	2.09	0.948	0.841	0.914
Cu (ppm)	31	28	27.8	32.2	2.86	2.74	< 2	< 2	27.6	28.4	18	16.2	27.3	22
F (%)	0.09	0.09			0.13	0.17	0.11	0.22	0.12	0.13	0.14	0.13	0.11	0.25
Ga (ppm)	37.8	12.6	95	91.3	42	12.9	40.4	14.8	39.2	10.7	32.2	11.5	40.7	13.9
Hf (ppm)	4.19	4.44	4.75	4.04	4.5	5.53	5.54	5.24	6.4	7.1	5.18	5.56	5.09	5.73
Mo (ppm)	< 2	< 2	< 2	< 2	< 2	< 2	< 2	< 2	< 2	< 2	< 2	< 2	< 2	< 2
Nb (ppm)	9.67	6.69	14	12.5	10.1	13	10.2	6.03	8.97	8.28	6.29	10.1	12.8	11.1
Ni (ppm)	13	12.3	20.5	20.7	11.7	12.7	13.4	14.8	3.34	2.82	2.93	2.84	14	12.9
Rb (ppm)	73.8	77.3	77.6	87.9	91.2	117	71.7	107	111	83.8	90.7	81.5	90	115
S (ppm)	533	189			124	28.2	215	213	88.4	87.6	108	77.4	94.7	86.1
Sc (ppm)	19.1	19	18.8	19.4	8.34	9.58	8.86	8.55	17.6	18.4	19.9	17.5	9.77	9.33
Sn (ppm)	2.67	2.13	1.92	1.62	3.32	3.32	3.15	1.95	3.84	3.92	1.91	< 1	3.85	1.44
Sr (ppm)	770	618	788	635	1,220	1,040	1,360	1,250	624	237	619	234	1,220	1,150
Ta (ppm)	1.08	0.79	1.07	1.12	1.35	1.31	1.17	1.09	1.15	0.966	1.15	0.737	1.35	1.29
Th (ppm)	7.42	3.88	6.26	5.89	15.5	10	9.26	7.03	12.5	7.64	6.78	5.86	15.7	10.8
U (ppm)	1.8	2	2.15	2.16	6.94	7.14	4.66	5.63	4.98	3.42	1.9	2.65	4.02	4.71
V (ppm)	128	127	132	134	78.1	82	76.3	71.4	108	103	131	119	80.8	79.3
W (ppm)	0.587	0.63	1.2	1.38	< 0.3	0.467	0.438	3.36	< 0.3	0.65	0.392	0.888	< 0.3	< 0.3
Y (ppm)	31.2	32.1	30.5	30.9	22.6	26.4	24	25.5	42	40.8	33.2	32.1	25.2	25.8
Zn (ppm)	70.9	76.7	97.2	105	64	73.2	72.7	84.3	62.5	79.8	56.2	59.6	73.8	64.3
Zr (ppm)	227	199	223	204	228	259	261	257	286	296	234	243	255	249

Table 7-16. Chemical whole rock analyses – Rare earth elements (ppm).

	62G	62R	81G	81R	81G(2)	81R(2)	82G	82R	100G	100R	128G	128R	144G	144R	144G(2)	144R(2)
La	34	36.2	35	33.8	33.4	33.3	35.4	40.8	34.5	35.4	38.4	42.8	39.4	38.6	40.8	38.5
Ce	76.1	80.1	79.7	76.7	77.7	72.9	80	89.5	78.9	78.1	85.9	91.6	81.3	77.7	85.7	78.1
Pr	10.1	9.72	10.7	9.17	12.3	9.86	10.9	11.1	10.7	10.1	11.4	10.8	9.81	8.64	9.37	8.41
Nd	39	41	43.4	38.4	42.5	37.6	42	46.1	41.3	40.5	41.7	40.4	33	28.9	34	30.4
Sm	5.88	4.94	6.06	5.47	7.64	5.61	6.39	7.21	5.93	5.05	5.66	4.74	3.77	2.29	5.2	4.92
Eu	1.86	1.61	1.72	1.54	1.63	0.393	2.03	1.86	2.01	1.76	1.58	1.3	1.07	0.872	0.832	0.708
Gd	5.59	5.2	5.42	4.71	3.83	2.77	6.53	6.3	5.59	5.05	6.01	5.87	2.95	2	3.28	4.02
Tb	0.803	0.772	0.921	0.674	0.768	0.691	0.787	0.85	0.869	0.74	0.894	0.77	0.52	0.35	0.688	0.572
Dy	4.44	4.69	4.75	3.78	4.39	3.66	4.97	4.22	4.74	4.27	4.98	4.29	2.62	2.09	3.03	2.34
Ho	0.85	0.814	0.836	0.787	0.89	0.881	0.918	0.879	0.88	0.866	0.986	0.965	0.486	0.354	0.58	0.609
Er	2.29	1.88	2.25	1.95	3.37	2.93	2.46	2.34	2.24	1.94	2.98	2.22	1.5	0.767	1.25	1.21
Tm	0.474	0.305	0.289	0.306	0.471	0.388	0.34	0.355	0.378	0.289	0.4	0.435	0.257	0.16	0.245	0.194
Yb	1.98	2.05	2.37	1.91	2.07	2.16	2.48	1.99	2	1.76	2.47	2.4	1.26	0.934	1.67	1.32
Lu	0.186	0.254	0.29	0.229	0.331	0.307	0.265	0.276	0.266	0.26	0.352	0.329	0.117	0.0643	0.277	0.212

Table 7-16 cont. Chemical whole rock analyses – Rare earth elements (ppm).

	172G	172R	172G(2)	172R(2)	372G	372R	394G	394R	536-1G	536-1R	536-2G	536-2R	661G	661R
La	34.4	36.2	33.4	37.5	60.9	64.4	48.9	50.9	35.3	35.4	34.6	36.3	57.7	56.6
Ce	77.4	81.2	80.5	85.3	122	146	113	119	80.6	85.7	73.9	76.9	132	129
Pr	11.2	10	9.97	9.6	15.3	16.1	15.5	14.8	11	11.3	10.2	9.65	17.2	15.4
Nd	37.2	38.9	37.8	41.9	48.4	58.6	51	54.9	38.2	40.2	34.7	35.5	56.8	57.9
Sm	5.21	5.11	6.84	6.29	6.65	7.04	6.14	6.72	6.28	6.6	6.01	4.45	6.75	7.24
Eu	1.71	1.65	1.47	1.46	1.53	1.56	1.63	1.64	1.28	1.34	1.48	1.36	1.65	1.57
Gd	5.53	4.74	6.4	6.76	3.82	5.61	4.71	4.92	5.72	5.81	5.49	5.28	4.73	4.52
Tb	0.803	0.792	1.02	0.958	0.68	0.683	0.654	0.703	0.965	0.947	0.801	0.853	0.757	0.759
Dy	4.79	4.6	5.25	5.33	3.69	3.58	2.97	3.45	6.06	5.97	5.07	4.21	3.6	3.6
Ho	0.971	0.957	1.13	0.912	0.577	0.774	0.681	0.681	1.16	1.18	0.943	0.893	0.693	0.704
Er	2.58	2.17	2.86	3.61	1.99	2.02	1.88	1.63	3.67	3.2	2.7	2.44	2.26	1.73
Tm	0.477	0.38	0.294	0.407	0.373	0.332	0.335	0.344	0.544	0.476	0.504	0.397	0.368	0.296
Yb	2.2	2.35	2.62	2.88	1.51	1.77	1.54	2.29	3.77	2.77	2.44	2.4	1.68	1.99
Lu	0.341	0.317	0.438	0.461	0.242	0.267	0.237	0.243	0.443	0.405	0.359	0.349	0.248	0.231

7.4.1 Classification of samples

Classification of the reference samples from various classification diagrams based on chemical (and modal) analyses from this study along with classification of the samples from Boremap /Ehrenborg and Stejskal 2004ab/, are shown in Table 7-17. A majority of the reference samples are classified as quartz monzodiorite, quartz diorite or granodiorite and show fairly good correspondence between the different classification methods, except for the TAS classification indicating Monzodiorite instead of Quartz monzodiorite for most of the samples.

A comparison between the principal modal alkali feldspar, plagioclase and quartz contents in a QAP-plot (Figure 7-1) and the normative chemical QAP-classification (Figure 7-32), shows that the alteration of feldspar phases, from plagioclase to albite and K-feldspar, will not influence the classification in Figure 7-32, but will give a serious influence on the classification in Figure 7-1. This is because CaO is partly fixed in secondary epidote and prehnite in the altered rock. The assumption (used in the modal QAP-plot) that all plagioclase is altered to K-feldspar and albite is exaggerated.

Table 7-17.

Sample	Depth	Rock type (mapping)	Rock type (TAS)*	Rock type (QAP) normative* (modal)#	Rock type (QP)**
KSH03					
62	61.94–62.15	Quartz monzodiorite^	Monzodiorite	Quartz monzodiorite (Quartz diorite)	Quartz monzodiorite
81(1+2)	81.46–81.65	Quartz monzodiorite^	Gabbroic diorite	Quartz diorite (Quartz diorite)[1]	Quartz diorite
82	82.05–82.25	Quartz monzodiorite^	Monzodiorite	Quartz diorite (Granodiorite)	Quartz monzodiorite
100	100.41–100.56	Quartz monzodiorite^	Monzodiorite	Quartz diorite (Quartz diorite)	Quartz monzodiorite
128	128.08–128.23	Quartz monzodiorite^	Monzonite	Granodiorite (Granodiorite)	Quartz monzodiorite
144(1+2)	144.49–144.89	Ävrö Granite^^	Granodiorite	Granodiorite (Granodiorite)	Granodiorite
172(1+2)	171.85–172.05	Quartz monzodiorite^	Monzonite	Tonalite (Granodiorite)[2]	Quartz monzodiorite
372	372.52–372.50	Ävrö Granite^^	Monzonite	Quartz monzodiorite (Granodiorite)	Quartz monzodiorite
394	394.34–394.45	Ävrö Granite^^	Monzonite	Quartz monzodiorite (Granodiorite)	Quartz monzodiorite
661	661.29–661.34	Ävrö Granite^^	Monzonite	Quartz monzodiorite” (Quartz diorite)	Quartz monzodiorite
KSH01					
536-1	536.65–537.52	Dioritoid	Monzonite	Granodiorite (Granodiorite)	Granodiorite
536-2	536.65–537.52	Dioritoid	Monzonite	Quartz monzodiorite“” (Granodiorite)	Quartz monzodiorite

* /Le Maitre 1989/ – normative

** /Debon and Le 1982/

/Streckeisen 1976/ – modal

^^ Granite to quartz monzodiorite

^ Incl. quartz monzonite to monzodiorite

“” Borders to granodiorite

“ Borders to quartz diorite

[2] Borders to quartz monzodiorite

[1] Borders to tonalite

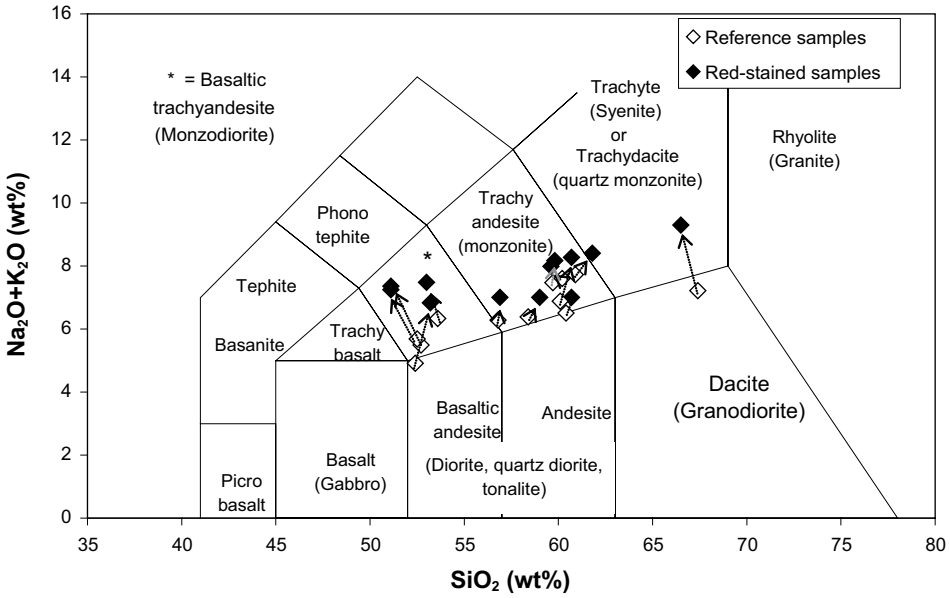

***Figure 7-31**. TAS-diagram from /Le Maitre 1989/. Arrows show related samples, reference samples (white) and red-stained samples (black). Note that all of the red-stained samples have higher Na_2O+K_2O-contents than the reference samples.*

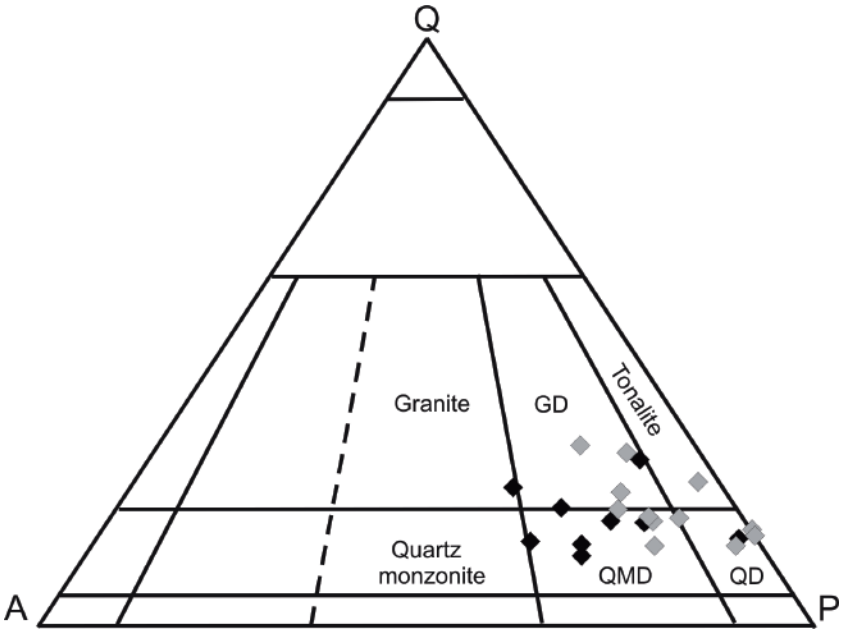

***Figure 7-32**. Normative QAP-diagram of whole rock analyses /Le Maitre 1989/, constructed from whole rock chemical analyses using Newpet software. Q = Quartz, P = Plagioclase, A = Alkali. Reference samples are shown in grey and red-stained samples in black. All of the red-stained samples have higher alkali-contents than the corresponding reference samples have. The samples 62R, 81R and 82R are not shown in the Newpet-software QAP-diagram that is used here. Abbreviations: GD = Granodiorite, QMD = Quartz monzodiorite, QD = Quartz diorite.*

Indications of K-alteration and Na-alteration are visualized in Figure 7-33. The increase in K is generally higher than the increase in Na. Despite the fact that the "Na_2O+K_2O"-contents are higher in all of the red-stained samples compared to the respective reference

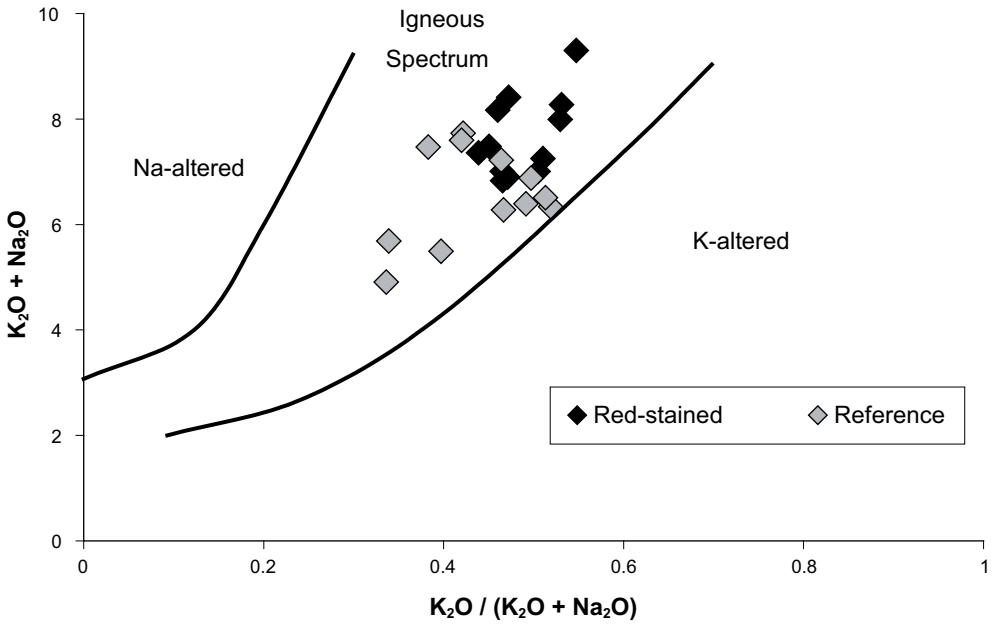

***Figure 7-33**. Igneous spectrum diagram /Hughes 1973/ with plots of reference samples (grey) and red-stained samples (black).*

sample all samples are still hosted within the "igneous spectrum" field. This indicates that element redistribution between minerals in small scale plays a more important role than large scale mobilisation of elements.

7.4.2 Immobile elements

There exist many methods for evaluating the most representative change in chemical composition of an altered rock compared to a reference rock. One of these methods is to assume that some elements, e.g. Zr, Hf, Ti, Ta, Nb, Al, Y, P and REE are immobile during low-grade metamorphic and hydrothermal alteration. The changes of the other analysed elements are then correlated to the change of the immobile elements. Table 7-18 shows elements that have been considered immobile or constant during alteration (or weathering) in a selection of earlier studies. Some elements that have been considered as immobile in some studies have however been shown to be clearly mobile under certain, often extreme conditions /Kerrich and Fryer 1979, Ludden et al. 1982, Van Baalen 1993, van Gaans et al. 1995/.

/Gresens 1967/ presented a method of analysis of changes in volume and concentrations during metasomatism that was applied by e.g. /Eliasson 1993/. This method requires measurements of the density of the samples, which was not carried out in this study. /Grant 1986/ used Gresens' methodology and presented a simplified graphical method, the "isocon"-method, to evaluate chemical mobility during rock alteration. In his method, element concentrations in the altered rock are plotted versus their concentrations in the reference rock and enrichment or depletion of the elements is evaluated from comparison with "immobile" elements.

From the above given compilation it obvious that the choice of elements to be used as references (immobile) needs to fulfil certain criteria:

1. The elements used need to be analysed with high accuracy.
2. The elements need to be distributed relatively homogenously in the samples.
3. The elements need to be immobile on the samples scale. However, redistribution between mineral phases can be accepted.

Table 7-18. Immobile or constant elements used in earlier studies.

Immobile/constant elements	Al	Ti	P	Ta	Hf	V	Y	Zr	Fe(t)
/Nesbitt 1979/		x						x	
/Nesbitt and Markovics 1997/		x						x	x
/Alderton et al. 1980/		x					x	x	
/Ludden et al. 1982/		x					x	x	
/Baker 1985/	x	x	x		(x)		x		
/Grant 1986/	x	x	x					x	
/Middelburg et al. 1988/		x							
/Dipple et al. 1990/		x	x			x			
/Marquer and Burkhard 1992/	x	x	x			x	x	x	x
/Eliasson 1993/	x	x							
/Mongelli 1993/	x								
/van der Weijden and van der Weijden 1995/		x						x	
/Petersson and Eliasson 1997/		x	x						
/Raimbault and Burnol 1998/				x					
/Maghraoui et al. 2002/				x					
/Essaifi et al. 2004/		x	x			x			
/Barnes et al. 2004/	x	x					x		

The changes in element concentration between the reference samples and the red-stained samples in this study is compared by the “isocon”-method /Grant 1986/, generally using Ti, P and Y as “immobile” elements (see below). Comparisons of the changes in concentrations of the absolute concentrations from the whole rock chemical analyses are also used since these are very similar to the “isocon”-results. Comparisons of the “isocon”-results and the normative comparisons show trends in element concentrations that are considered to be valid for a large number of elements. As for the normative changes of element concentrations, the “isocon”-results may yield poor values when the concentrations of the elements are low, when the reproducibility is bad or when the minerals (mostly titanite) hosting the “immobile” elements are heterogeneously distributed in the samples.

In order to evaluate the reproducibility of the analyses 6 samples, 3 reference samples and 3 red-stained samples, were re-analysed (see details below).

The whole rock analyses show that Al is depleted in almost all of the red-stained samples compared to the reference samples. This makes this element unsuitable as an immobile reference element. Results from re-analysed samples show that the changes of “immobile” elements Hf, Nb and to a lesser degree Ta and Zr are not reproducible, and should therefore not be used as immobile reference elements. In contrast, Ti, P and Y show quite good correlation of the normative changes and are thus suggested as reference elements using the isocon method by /Grant 1986/. Ti has evidently been mobile within a limited rock volume since secondary titanite is formed from break down of biotite. Chemical analyses show however that the mobility of Ti is relatively small and that the Ti is mainly fixed within pseudomorphs after biotite.

An isocon plot of sample 128 is shown in Figure 7-34. Element from the reference sample are plotted on the x-axis and elements from red-stained sample are plotted on the y-axis. The elements are normally multiplied with a number in order to fit them all into the same diagram. The multiplied numbers are the same for every sample set. A line is then drawn

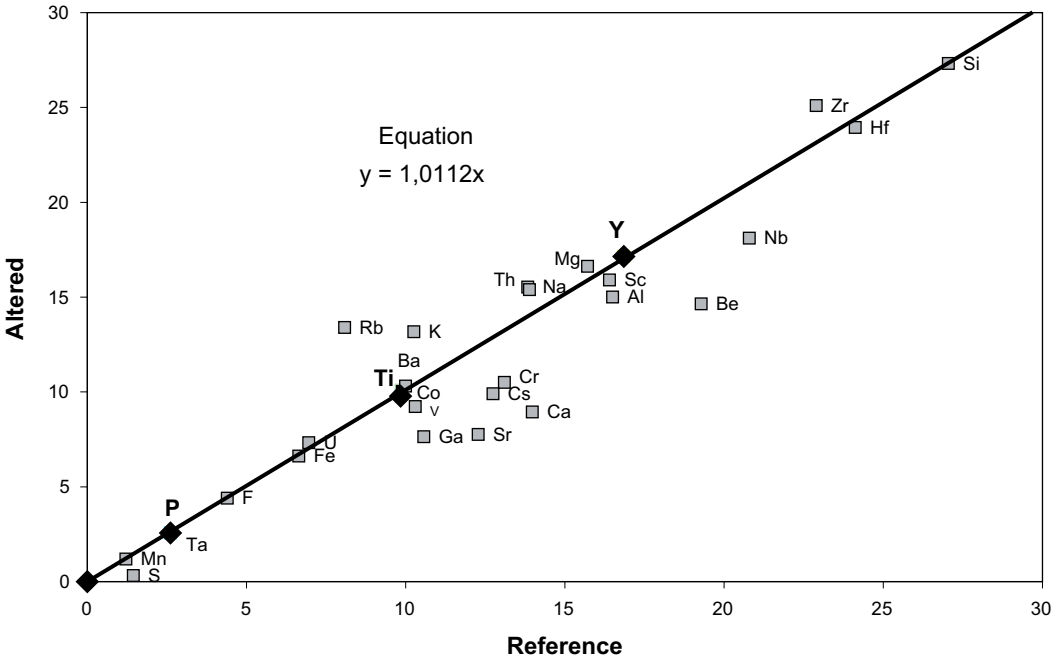

Figure 7-34. *Isocon plot of sample 128, after /Grant 1986/. P, Ti and Y, in bold letters, are considered to be more or less constant during alteration. Elements above the line, e.g. K, Rb and Na are enriched while e.g. Ca, Cs, S and Al below the line are depleted. Elements are generally multiplied with a number to fit into the diagram.*

from the origin of the plot through the "immobile" elements (Ti, P and Y). The slope of the line is then multiplied with the value of each element in the reference sample, and this new value for each element is then compared normatively with the same element in the red-stained sample. The slope of the line (M^A/M^0) indicates mass loss or gain of the "immobile elements" and elements that plot above the line are enriched during alteration while elements that plot below the line are depleted. This gives the equation,

$$\Delta C_i = (C_i^A / C_i^0)(M^A/M^0)_{isocon} - 1$$

where ΔC_i is the normative change in concentration of element *i*, C_i^A is the measured concentration of element *i* in the red-stained rock, C_i^0 is the measured concentration of element *i* in the reference sample and $(M^A/M^0)_{isocon}$ is the slope of the best fit isocon through the "immobile" elements. The ΔC_i-value is then multiplied by 100 to give the changes in per cent.

7.4.3 Changes in element concentrations

In this section changes of each element in the red-stained samples compared to the reference samples are discussed, as well as the general abundance of most elements. Comparisons of absolute values and values obtained from the isocon method have been used for illustration of the changes. Elements that are related, e.g. major element K and trace elements Rb, Ba and Cs may replace one another in the crystal lattice for instance, are described collectively. Reproducibility of e.g. Zr, Hf, Cu, Th and U is less good and therefore these elements are discussed briefly. Elements Nb, Ni, Ta, W, Mo, Zn and Sn are not discussed in detail since the analyses show too low values or the reproducibility was too bad.

SiO_2

The SiO_2-content in quartz monzodiorite reference samples is about 51–60%, in fine-grained dioritoid samples about 58–60%, and in Ävrö granite samples about 60–67%.

SiO_2 can be considered as more or less constant during alteration, although re-distribution in situ is proposed. The normative absolute changes (–2 to +3%) show more consistency than the isocon-values (–12 to +12%) and the changes in concentrations are inconclusive. No trend of enrichment or depletion is found. Some silicon might be leached from the rock and is incorporated in prehnite, chlorite, quartz and epidote in fractures.

Al_2O_3, Be and Ga

Al_2O_3 is depleted in all but one (144R) of the red-stained samples compared to the reference samples, using normative change from absolute values (Figure 7-35). The depletion is generally 3–10%. The isocon plot suggests that Al_2O_3 is also increased in 81R. The re-analyses give similar values of the changes, which indicate good reproducibility. The depletion of Al_2O_3 is thought to reflect break-down of the anorthite-content in plagioclase, which is replaced by albite and K-feldspar mainly. The crystallization of secondary prehnite and epidote is insufficient to fix all of the excess Al_2O_3 and excess Al may also be included in formation of prehnite, chlorite and epidote in fractures. The Al_2O_3-ratio in the alteration of biotite to chlorite is more or less 1:1, based on SEM-EDS analyses (see appendix) and works of e.g. /Ferry 1979, Parry and Downey 1982/. Al activities is very weak in hydrothermal fluids /Ellis and Mahon, 1977/. /Eliasson 1993, Stosnach and Mengel 1998/ were not able to detect changes in Al_2O_3 in their studies.

Depletion of Be and Ga is apparently related to the depletion of Al_2O_3 (Figure 7-36). Depletion of Ga may be related to albitization of plagioclase as proposed by e.g. /Bailey 1971/. Be may possibly be correlated with Al since they both are ions of similar size /Bailey 1971/. This depletion is evidenced in all comparisons of absolute values but the re-analyses and isocon values show some enrichment, which reveal low reproducibility, although there exist a consistent trend overall.

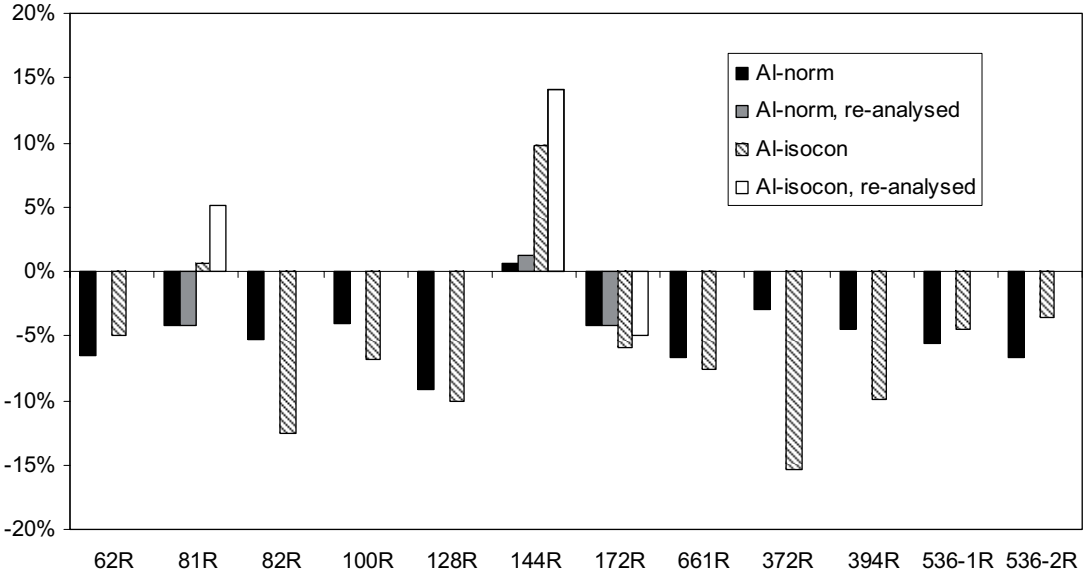

***Figure 7-35**. Plot of normative changes for Al_2O_3 between red-stained samples and reference samples, using absolute values, with re-analyses and isocon-plot values, with re-analyses.*

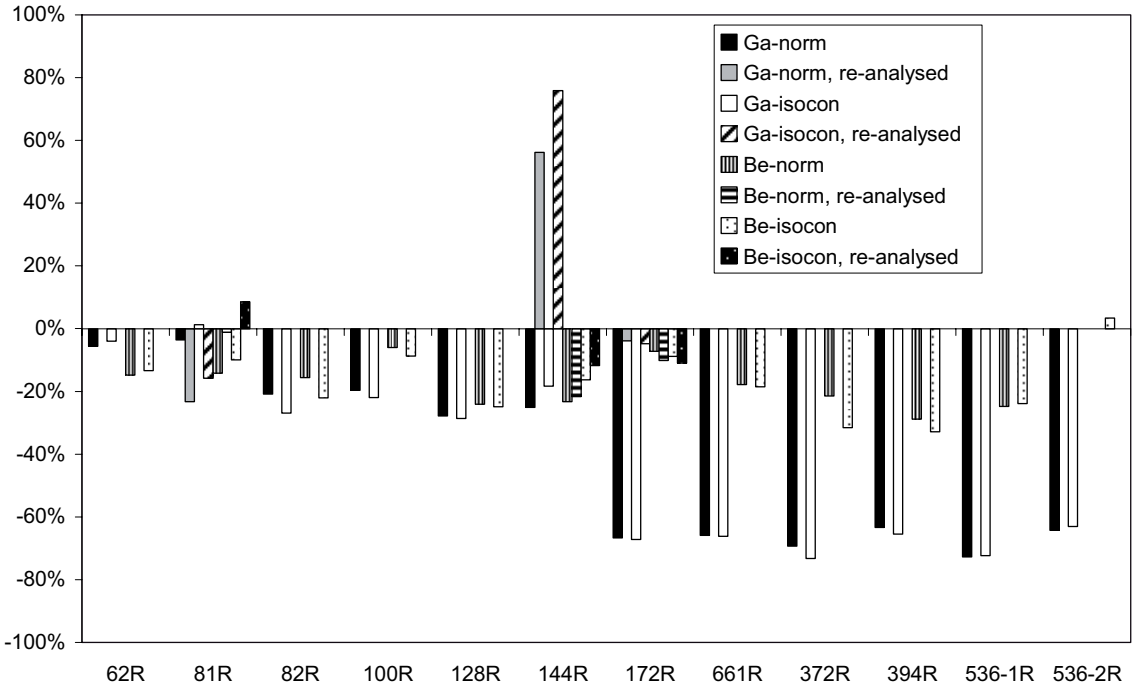

Figure 7-36. *Plot of normative changes for Ga and Be between red-stained samples and reference samples, using absolute values, with re-analyses and isocon-plot values, with re-analyses.*

CaO and Sr

CaO is mainly depleted in the red-stained rock compared to the reference rock (Figure 7-37). This is evidently caused by alteration of plagioclase and removal of the anorthite-content, which is replaced by albite and K-feldspar mainly. The excess CaO is involved in growth of secondary prehnite and smaller amounts of epidote in altered plagioclase pseudomorphs. Occasionally, prehnite is also found in pseudomorphs after biotite in association with chlorite. Secondary prehnite and additional calcite is also found in voids and in micro-fractures in the red-stained rock. This growth of Ca-rich secondary minerals is commonly not enough to make up for the break-down of primary Ca-rich minerals. A large part of the CaO content is removed from the rock and is involved in formation of fracture minerals like prehnite, epidote and calcite. Higher value of CaO in fracture coatings compared to the wall rock is a common feature in the area /Landström and Tullborg 1995, Tullborg 1995, Landström et al. 2001/.

The CaO-contents are higher in the SiO_2-poor quartz monzodiorite and fine-grained dioritoid than in the Ävrö granite samples because of higher anorthite-contents in plagioclase and higher amounts of Ca-bearing amphibole and pyroxene, than in the more SiO_2-rich Ävrö granite samples. Sample 62 and 661 are the only samples that have higher values of CaO in the red-stained rock. Explanations for these two extremes may be that sample 62R is cross-cut by a net of numerous minor fractures, filled with prehnite and calcite that may be included in the whole rock analyses but are absent in the thin section, and that sample 661 is highly heterogeneous because of its coarse-grained nature with a high amount of phenocrysts. The high amount of fine-grained material between the phenocrysts in 661R may also contain considerable amounts of Ca-rich minerals that were not possible to point-count.

Changes in Sr are closely related to the changes in CaO (Figure 7-38). Sr is mainly hosted in Ca-bearing minerals since the ions Sr^{2+} and Ca^{2+} have similar properties and exchange easily. However, the Sr/Ca-ratios in Ca-minerals are quite different for different minerals, e.g. calcite has a much lower Sr/Ca ratio than for example plagioclase. Epidote, in con-

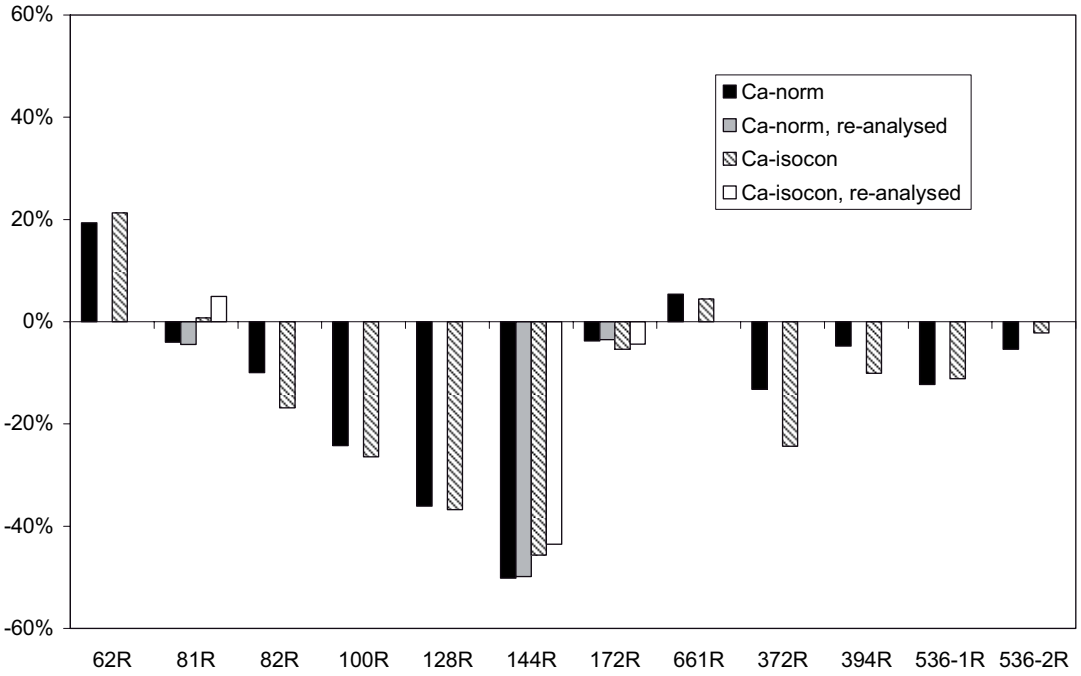

Figure 7-37*. Plot of normative changes for CaO between red-stained samples and reference samples, using absolute values, with re-analyses and isocon-plot values, with re-analyses.*

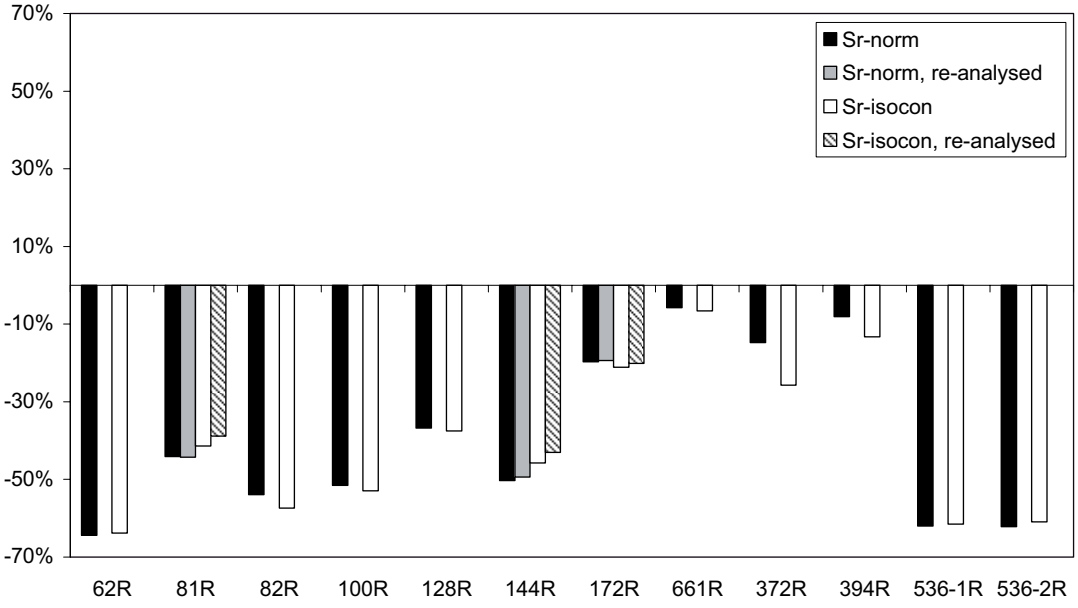

Figure 7-38*. Plot of normative changes for Sr between red-stained samples and reference samples, using absolute values, with re-analyses and isocon-plot values, with re-analyses.*

trast, have shown preferential uptake of Sr (cf. earlier studies from Äspö /Landström and Tullborg 1991, Stosnach and Mengel 1998/). The wide-spread depletion of Sr is related to the alteration of primary plagioclase. Some Sr may be incorporated in secondary prehnite, epidote and possibly also calcite in plagioclase pseudomorphs, in voids, in micro-fractures in the altered rock and as fracture minerals in major fractures. However, the uptake of Sr in secondary minerals within the studied rock volume is insufficient to fix all the excess Sr. However, Sr content in prehnite has not been studied in detail.

The reproducibility of the changes in CaO and Sr was very good and isocon plots of the element changes are very similar to those using absolute values for normative changes.

Fe_2O_3, MgO, MnO, TiO_2, Co, Cr, Sc, V and Y

The iron content measured in the whole rock analyses is expressed as Fe_2O_3. The variation in iron-contents is very small, and both small enrichments and small depletions are visible in the red-stained samples compared to the reference samples. The Fe_2O_3-content in quartz monzodiorite and fine-grained dioritoid samples is higher than in the Ävrö granite samples. All of the elements Fe_2O_3, MgO, MnO, TiO_2, Co, Cr, Sc, V and Y have higher concentrations in quartz monzodiorite and fine-grained dioritoid compared to Ävrö granite, because of the higher amounts of ferromagnesian minerals in these rocks. No major trends of depletion or enrichment could however be discerned in total Fe-content and it appears to be fairly constant during alteration (Figure 7-39). The red-stained Ävrö granite samples (372R, 394R and 661R) are however weakly enriched in Fe compared to the reference rock, which might be caused by enrichment in the epidote-content in the red-stained samples. The reproducibility of the changes in Fe-content was quite good and differs by less than 1% from the first analyses.

The Fe-content shows a positive correlation to contents of MgO, TiO_2, MnO, Sc Co, V and to a smaller degree Y indicating potential coexistence of these elements in iron-bearing minerals. The correlation between Fe and Mg and Ti is exemplified in Figure 7-40 and Fe and Mn and Sc is exemplified in Figure 7-41. Cr, in contrast, is depleted in all but one of the red-stained samples which is probably the result of hematitization of magnetite.

MnO is also depleted to a very small extent in most of the samples. MnO and Co are mainly found in biotite /Gebel et al. 1999/ All the MnO might however, not be entirely fixed in secondary chlorite during the chloritization of biotite. The depletion in Mn is however very small and the slightly different changes of Mn compared to Fe may depend on the different redox properties of the elements. Co may however be fixed in chlorite and opaque minerals since there exist no obvious trend of depletion in Co. The reproducibility of changes in Co-concentrations is poor, though.

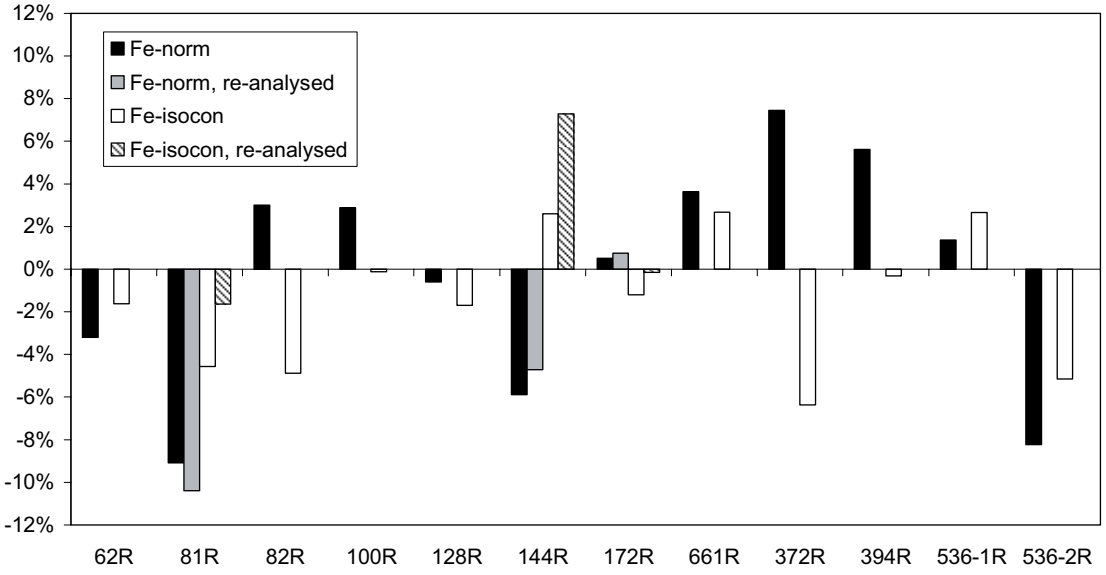

Figure 7-39. *Plot of normative changes for Fe_2O_3 between red-stained samples and reference samples, using absolute values, with re-analyses and isocon-plot values, with re-analyses.*

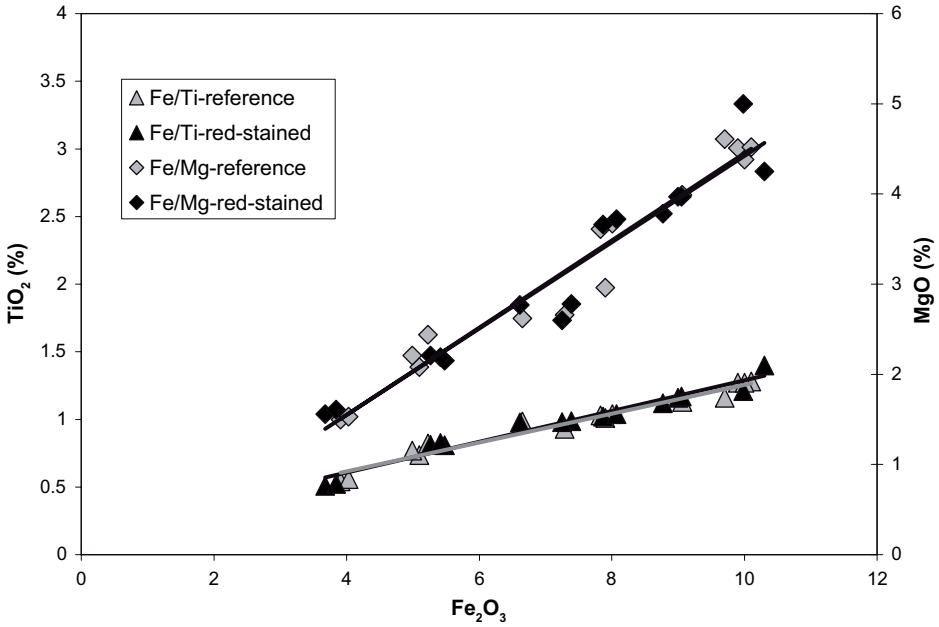

Figure 7-40. *Plot of Fe_2O_3 content vs.TiO_2 (left y-axis) and MgO (right y-axis) which shows a close correlation. Black and grey lines are trend-lines for the red-stained samples and reference samples, respectively.*

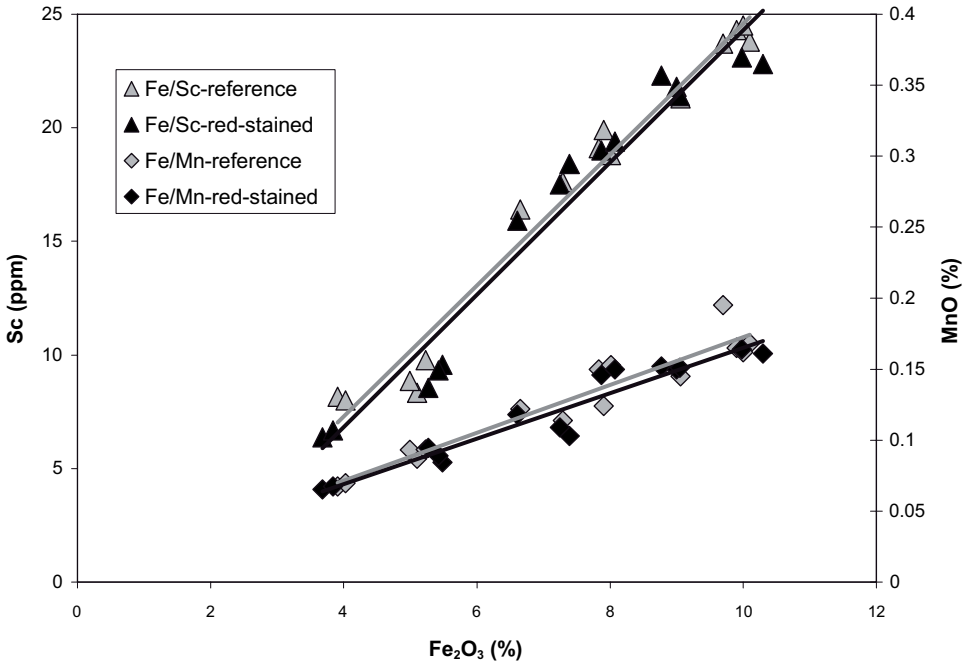

Figure 7-41. *Plot of Fe_2O_3 content vs. Sc (left y-axis) and MnO (right y-axis) which shows a close correlation. Black and grey lines are trend-lines for the red-stained samples and reference samples, respectively.*

V is commonly found as a trace element in Fe-bearing minerals and V and Fe are often correlated during weathering/alteration e.g. /van der Weijden and van der Weijden 1995/. /Landström et al. 2001/ proposed that similar correlation of V, Ni and Sc with Fe in fracture coatings indicates that iron has not been selectively added to the coating by precipitation of groundwater, a suggestion that may be valid for Fe in the red-stained rock in this study as well.

TiO_2 is mainly contained in titanite, biotite (which is more frequent than titanite) and subordinately in hornblende. Small amounts of TiO_2 are also found in augite. Secondary titanite (grothite) is formed during chloritization of biotite and reveals that Ti is mobilised and redistributed during alteration. The quite constant values of TiO_2-show however that the large scale mobility of Ti is very low and that it mostly stay fixed in primary titanite and in grothite in the pseudomorphs after biotite (plus hornblende and augite), or may at most form secondary rims on titanite within a limited rock volume. These rims may however be late magmatic (see "Mineralogy" section). Earlier studies in the area have shown significantly lower Ti values in fracture coatings than in the host rock which indicate very low mobility of Ti /Tullborg 2002/. TiO_2-contents are generally higher in quartz monzodiorite and fine-grained dioritoid than in Ävrö granite, depending on higher amount of biotite and/or chlorite with secondary titanite and hornblende (and augite), although the amount of primary titanite is generally higher in Ävrö granite samples. Y is mainly fixed in titanite /Stosnach and Mengel 1998/ and is thus in close relation to the TiO_2–content and remained fairly constant during alteration. Some Y may however be incorporated in epidote, which might be the reason why Y is somewhat enriched in the only epidote-rich samples, 372R, 394R and subordinately in 661R.

The reproducibility of the changes in contents of MnO, MgO, TiO_2 and Y were good or very good, Sc and V were quite good, whereas the reproducibility of change in Co was poor.

K_2O, Ba, Cs and Rb

The K_2O-content is commonly lower in quartz monzodiorite samples than in Ävrö granite samples, and fine-grained dioritoid samples, although the fine-grained dioritoid samples show lower enrichment in K_2O than the quartz monzodiorite.

The elements K, Rb and Ba are commonly highly enriched in the red-stained samples, while Cs is depleted. The normative enrichment in K_2O is commonly about 20–100%, in Rb about 20–120%, in Ba 10–80%, while the depletion in Cs commonly is 10–70%, although exceptions are found in some samples (Figure 7-42 and 7-43). The ions Ba^{2+}, Rb^{+} and Cs^{+} have similar properties as K^{+} (size and/or charge) and may replace K^{+} in the structure of K-bearing minerals such as K-feldspar (preferably Ba) , biotite and sericite (preferably Rb and even more so Cs) and subordinately hornblende. The enrichment of K_2O in the red-stained rock is related to extensive growth of secondary K-feldspar (adularia) and subordinately sericite in altered plagioclase crystals and depletion of mainly biotite but also hornblende to a smaller degree. Since biotite often is chloritized to some degree in the hydrothermally altered reference rock, the K_2O-content in the reference samples may already be depleted, since the K-content of biotite is intensively depleted in the initial stage of the chloritization /Wilamowski 2002/. In the samples with low increase in K_2O or K_2O-depletion, the Na_2O-content is increased. This reflects the varying contents of albite and K-feldspar in the pseudomorphs after primary plagioclase (Figure 7-45; compare to Na_2O-contents in Figure 7-19).

The Ba-content is dependent on the amount of K-feldspar in the rock and is generally higher in the Ävrö granite samples than in the quartz monzodiorite samples. The lowest BaO values are however found in the fine-grained dioritoid which generally has higher K_2O-values than the Ävrö granite. BaO content is up to 2% in the microperthitic K-feldspar phenocrysts but groundmass K-feldspars and secondary K-feldspar in altered plagioclase have lower content of BaO. Sericite and biotite contain some BaO as well, but the content is usually lower than the content in groundmass K-feldspar and K-feldspar in plagioclase pseudomorphs. The Ba-content is, with a few exceptions enriched in the altered samples, because the K_2O-content and secondary K-feldspar content is higher.

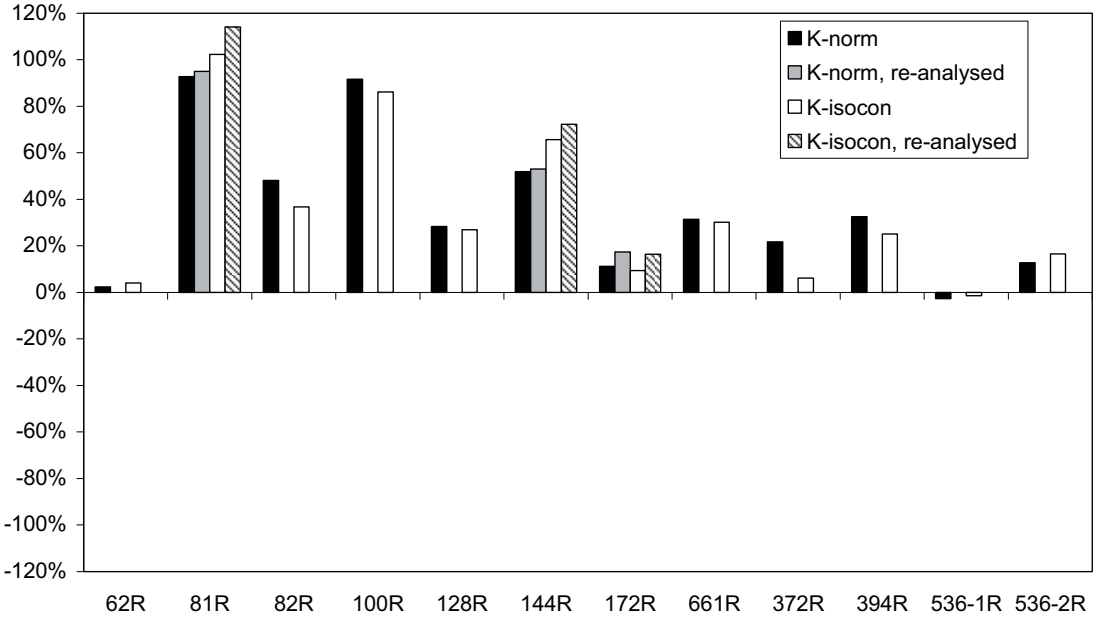

***Figure 7-42**. Plot of normative changes for K_2O between red-stained samples and reference samples, using absolute values, with re-analyses and isocon-plot values, with re-analyses.*

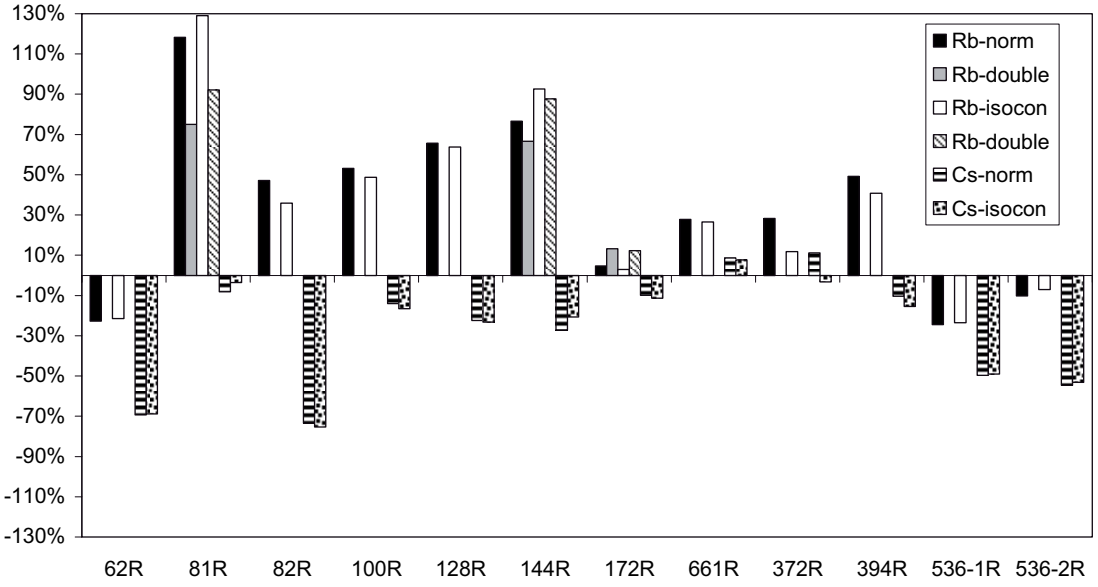

***Figure 7-43**. Plot of normative changes for Rb and Cs between red-stained samples and reference samples, using absolute values, with re-analyses for Rb and isocon-plot values, with re-analyses for Rb.*

The depletion of Cs is related to the chloritization of biotite. Since Cs concentrations are higher in biotite than in K-feldspar /De Albuquerque 1975/ break down of biotite will result in excess Cs that is not entirely incorporated in secondary K-feldspar. Rb is mainly hosted in biotite /Stosnach and Mengel 1998/ but Rb is not as compatible in biotite as Cs and Rb is only slightly enriched in biotite compared to K-feldspar /De Albuquerque 1975/. The large enrichment in Rb-contents in the red-stained samples in this study show however that excess Rb to large extent is fixed in secondary K-feldspar, with a few exceptions. /Gebel et al. 1999/ reports significantly lower concentrations of Cs and Rb in secondary chlorite

than in primary biotite, which is in accordance to the results from this study. Enrichment of Rb and depletion of Cs (Figure 7-43) may also support the observations from e.g. microscopy and SEM-EDS where secondary K-feldspar dominates over secondary sericite.

The reproducibility of the changes of K_2O and Ba is good, while the reproducibility of Rb is quite good. Cs was only analysed once for each sample.

Na_2O

Na_2O is commonly enriched in the red-stained rock as a result of albitization of plagioclase. The enrichment is normally 10–15% but it can be as high as about 35% (Figure 7-44). In a few red-stained samples (mostly Ävrö granite) the Na_2O-content is depleted compared to the reference rock. The Na_2O-content in the reference samples is generally higher in the Ävrö granite samples than in the quartz monzodiorite samples and in the fine-grained dioritoid samples, generally depending on the higher Na_2O-content in plagioclase in more differentiated SiO_2-rich rocks.

In the red-stained samples where the Na_2O-content is depleted in comparison to the reference rock, the enrichment in K_2O-content is larger than the depletion in Na_2O and vice versa (Figure 7-45). This is a strong indication of how extensive replacement of primary plagioclase by secondary albite and K-feldspar during the hydrothermal alteration was.

P_2O_5

P_2O_5 is considered to be fixed in apatite during alteration, which is in agreement with studies of e.g. /Stosnach and Mengel 1998, Tullborg 2002/. P_2O_5 is used as an immobile reference element in the isocon-plot, except for in sample 82 where the normative change of P_2O_5 is anomalously high in comparison to other immobile elements in that sample. Changes in P_2O_5 generally correlate well to changes in TiO_2 and Y. Apatite has been found in studies of the fracture fillings in the area /Drake and Tullborg 2004, 2005, 2006a/. No secondary apatite has however been identified in the present study.

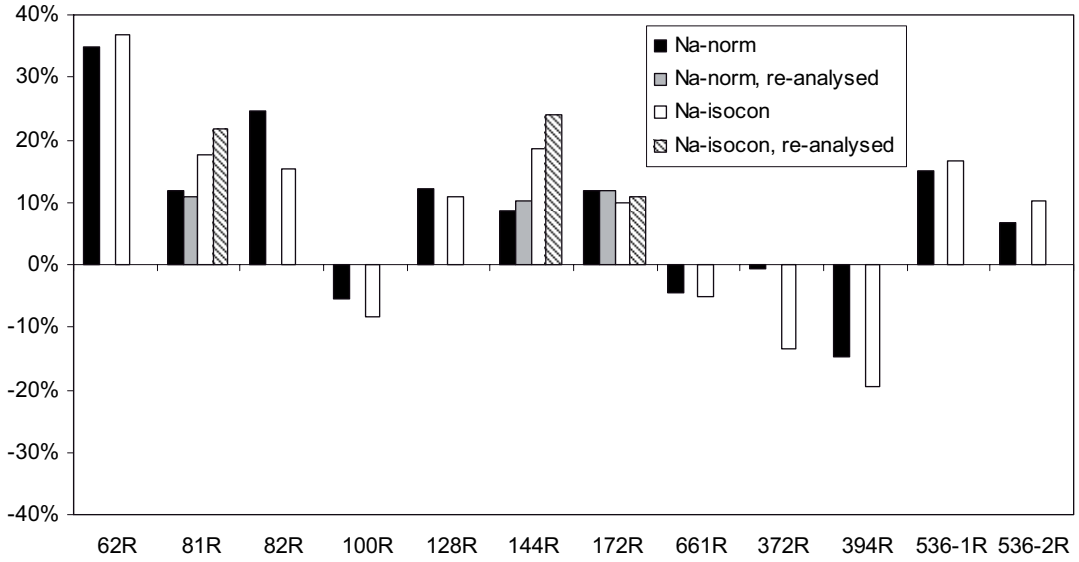

Figure 7-44. *Plot of normative changes for Na_2O between red-stained samples and reference samples, using absolute values, with re-analyses and isocon-plot values, with re-analyses.*

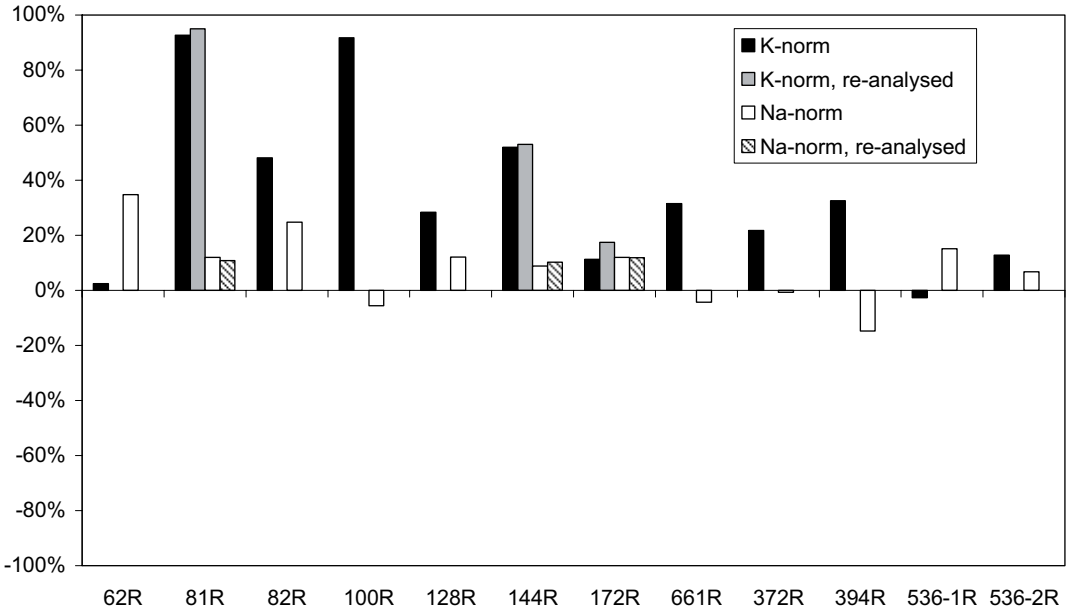

Figure 7-45. *Plot of normative changes for K_2O and Na_2O between red-stained samples and reference samples, using absolute values with re-analyses.*

The total chemical content and the Loss on Ignition (LOI)

The sum of the analysed elements is lower and LOI is higher in the whole rock analyses of the red-stained rock compared to the reference rock. The LOI and total values reflect the amount of "crystal-bound" water and indicate presence of secondary mineral phases (e.g. chlorite, sericite and prehnite). In most of the samples the LOI values are enriched (Figure 7-46), which reflects higher amount of these secondary minerals. In the samples where the LOI-values are higher or similar in the reference rock as in the red-stained rock the chlorite contents are higher or similar in the red-stained rock as in the reference rock. The chlorite content and the LOI-value are for instance higher in 62G than in sample 62R. The isocon-values resemble the normative changes of the absolute values very well.

Zr and Hf

Zircon and hafnium are predominantly contained in zircon. Hf and especially Zr are often used as "immobile" reference minerals in mass balance calculations and in isocon-plots. Since the sample volumes occasionally are quite small and the amounts of zircon varies widely within the rock Zr and Hf are occasionally highly enriched (up to 120% enrichment) or depleted in the red-stained samples, therefore these elements was not used as "immobile" reference elements. However, in some of the samples the changes in Zr and Hf contents are very small and the "best fit" isocon of Ti-P-Y for these samples often intersect Zr and Hf as well. They are however not included in any of the "best fit" isocons.

Cu and S

Sulphur and copper is dominantly found in accessory sulphides, mainly pyrite (S) and subordinately chalcopyrite (S and Cu). The depletion in Cu and S in the red-stained samples reflects corrosion and break-down of the sulphide due to oxidation. The normative depletion in S is also much larger than that of Cu (Figure 7-47). The reproducibility of the changes in Cu is however very poor and because of this no isocon-plot was made that include Cu. S was not re-analysed and it is thus impossible to say anything about the reproducibility of the analyses.

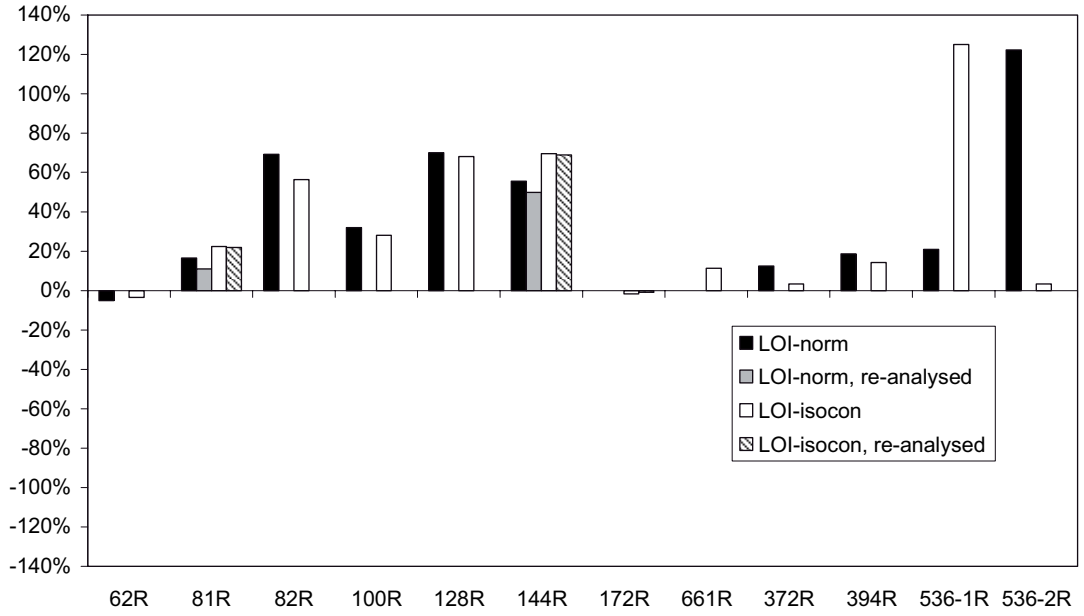

Figure 7-46*. Plot of normative changes for LOI between red-stained samples and reference samples, using absolute values, with re-analyses and isocon-plot values, with re-analyses. Note that both of the changes in absolute values "LOI" and "LOI-double" of sample 172 are "0".*

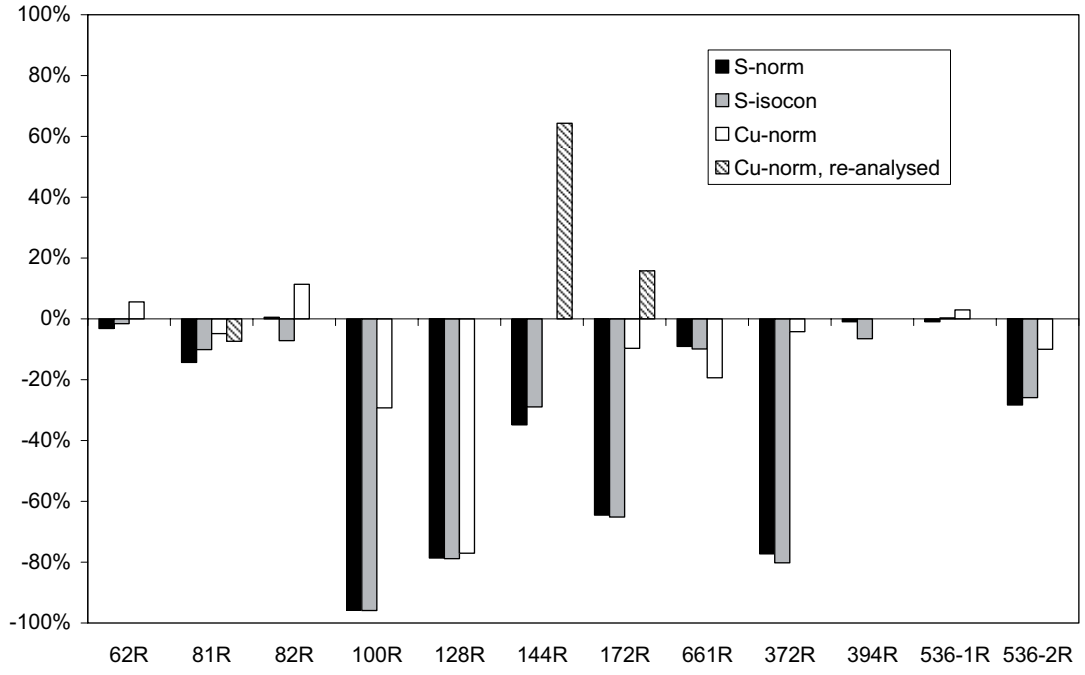

Figure 7-47. *Plot of normative changes for S and Cu between red-stained samples and reference samples, using absolute values, wither-analyses for Cu and isocon-plot values for S. Note that some analyses of Cu are absent because they are below detection limit.*

Th and U

The U-concentrations are generally higher in the Ävrö granite samples than in the quartz monzodiorite and fine-grained dioritoid, in both red-stained and reference samples. A very weak trend of U enrichment in a majority (7–8 of 12 samples) of the red-stained samples is visible (Figure 7-48). Th, in contrast, is generally depleted in the red-stained rock (8 of

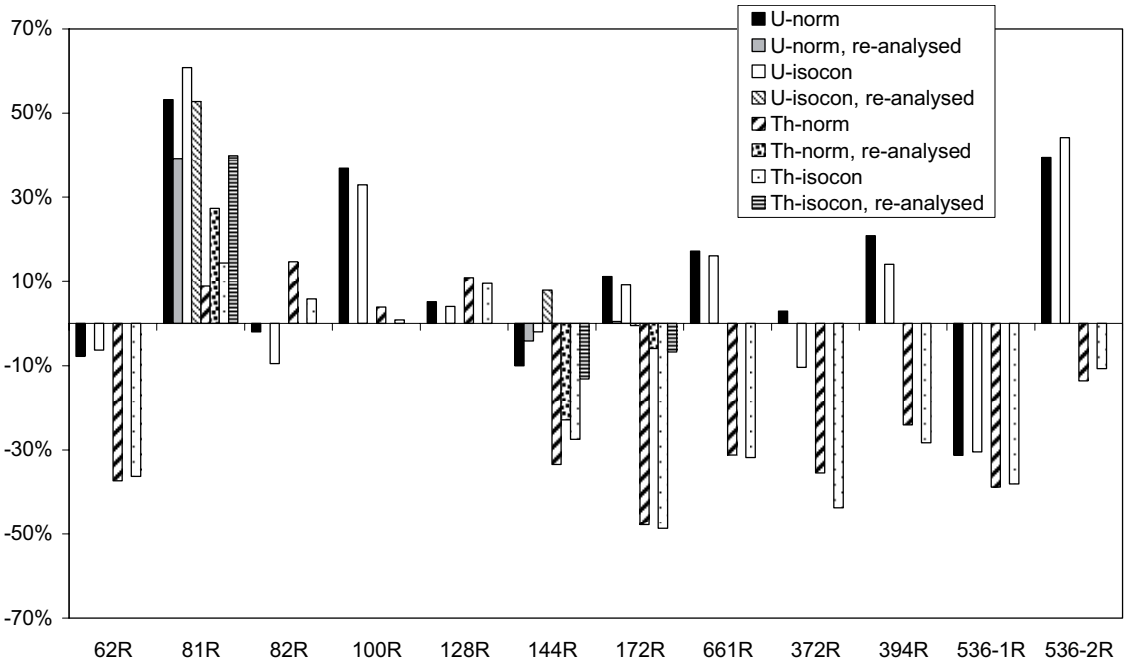

***Figure 7-48**. Plot of normative changes for U and Th between red-stained samples and reference samples, using absolute values, with re-analyses and isocon-plot values, with re-analyses.*

12 samples) and concentrations from all of the samples (reference and red-stained) are generally higher in Ävrö granite and fine-grained dioritoid than in quartz monzodiorite The higher amounts of U and Th in Ävrö granite can be correlated with the higher amount of euhedral titanite and possibly also epidote in these samples. This is in agreement with studies of /Stosnach and Mengel 1998/ who, report that Th and U are predominantly fixed in titanite. U may however also be present in sub-microscopic U-rich phases along grain boundaries. The U in these phases may be mobilised as U(VI) during oxidizing conditions, by diffusion in pores and micro-fractures, as proposed by /Landström et al. 2001/ enriching the U-concentrations in the red-stained rock where U(VI) is absorbed onto Fe^{3+}-minerals. This scenario may explain the higher U/Th-ratio in the red-stained rock, since Th is less redox sensitive than U and thus less mobilised during oxidizing conditions. U-rich silicate has also been observed in ongoing studies of fracture fillings in the area /Drake and Tullborg 2006a, 2006b/. It must however be noticed that the U and Th concentrations are very small and the reproducibility too poor to allow unequivocal conclusions to be drawn.

F

The F-content is generally higher in the red-stained rock than in the reference rock (Figure 7-49). There are no differences in F-concentrations in the different rock types, but the Ävrö granite samples show the largest changes between the red-stained samples and the reference samples, with both enrichment (372, 394 and 661) and depletion (144). Quartz monzodiorite sample 62 also shows F-enrichment in the red-stained sample. Sample 62 and 661 are the only samples that are enriched in CaO (Figure 7-37) and a very diffuse correlation between F and CaO changes can be discerned, although the CaO-concentrations are generally much more depleted than the F-concentrations. The major F-bearing minerals in the samples, apart from fluorite that may be present in very small amounts in fractures and voids, are biotite and hornblende. Since these minerals are altered it is highly realistic that F is mobilized. Studies of fracture mineralogy infer that fracture fillings that are coeval with the red-staining event include fluorite /Drake and Tullborg 2004, 2005/. An explanation for the enriched F-concentrations in the red-stained rock may thus be that minute

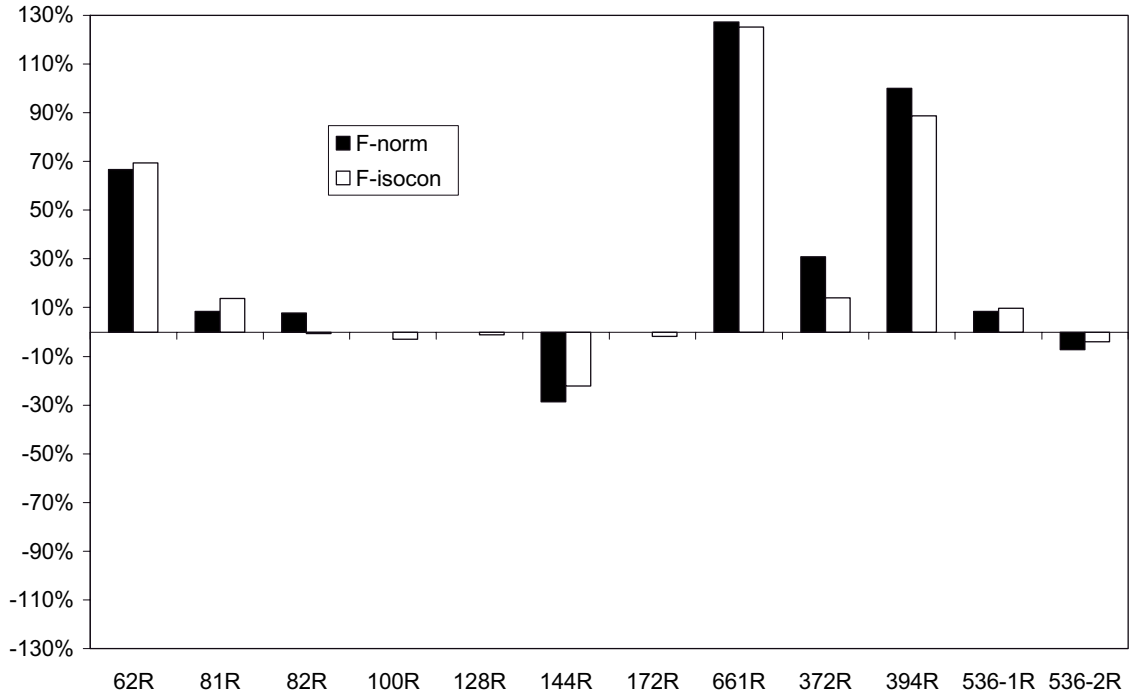

Figure 7-49. *Plot of normative changes of F between red-stained samples and reference samples, using absolute values and isocon-plot values.*

fluorite crystals, in addition to precipitation as constituents in fracture coatings, have precipitated in micro-fractures, minor fractures and voids as a consequence of alteration of biotite and hornblende. Few fluorite crystals have however been observed in the thin section investigations.

Rare Earth Elements (REE)

The Rare Earth Element (REE) content has been analysed in all of the samples. The difference between reference samples and red-stained samples are generally very small, which indicate that these elements are either fixed in minerals that are resistant to alteration or that the elements are redistributed within a very limited rock volume. The REE might be concentrated in the apatite, as suggested by /Landström et al. 2001/ and in titanite as suggested by /Gebel et al. 1999/. Both of these minerals are relatively resistant to alteration, and the REE-content in easily altered minerals such as biotite is low /Gebel et al. 1999/. Two of the red-stained samples show somewhat depleted REE-values. Both of these (81R[2] and 144R) were re-analysed samples and differ significantly from the first analysis of that sample. This may be due to the small sample volumes, and that REE is present in very small amounts. In general, however, the Ävrö granite samples are very homogenous (Figure 7-50) and differ somewhat from the quartz monzodiorite and fine-grained samples which show lower LREE values than the Ävrö granite samples (Figure 7-51 and 7-52). The quartz monzodiorite and fine-grained dioritoid samples also vary more in HREE. Sample 144 does not correlate to the other Ävrö granite samples (Figure 7-53). Noteworthy is that this fairly unchanged behaviour also include the redox sensitive elements such as Ce and Eu, which generally have not been mobilised at all or are redistributed. An exception is the depletion of Eu in sample 81R(2), which differ significantly from 81R and is thus highly uncertain (Figure 7-51). The lack of major fractionation of Eu relative to other REE may further indicate that the hydrothermal event is of low-temperature origin. This is since Eu fractionation is commonly assumed to be associated to high-temperature hydrothermal alteration processes e.g. /Sverjensky 1983/.

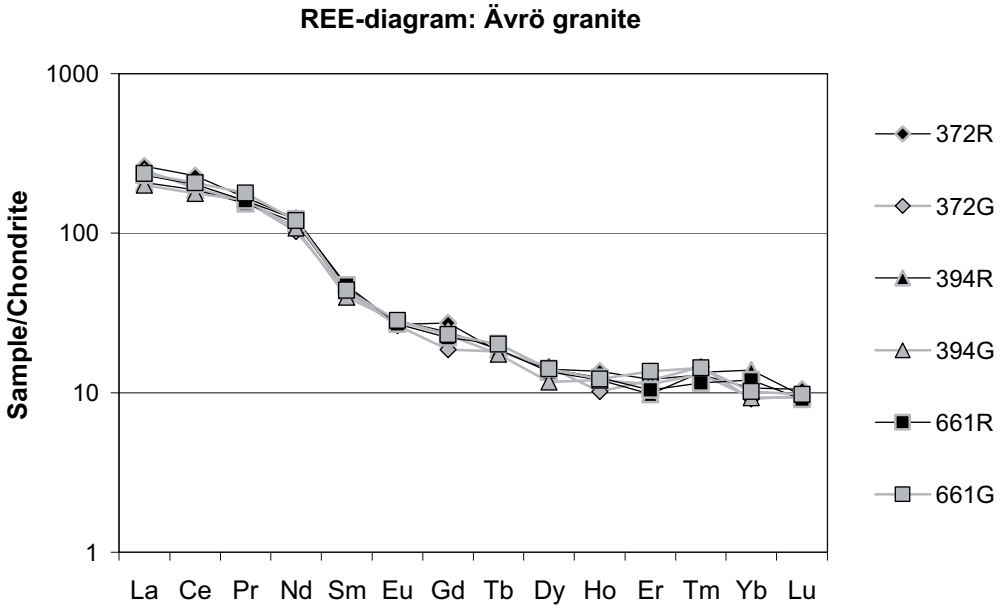

Figure 7-50. *Chondrite normalised REE-plot of Ävrö granite samples 372, 394 and 661 using chondrite values from /Evansen et al. 1978/.*

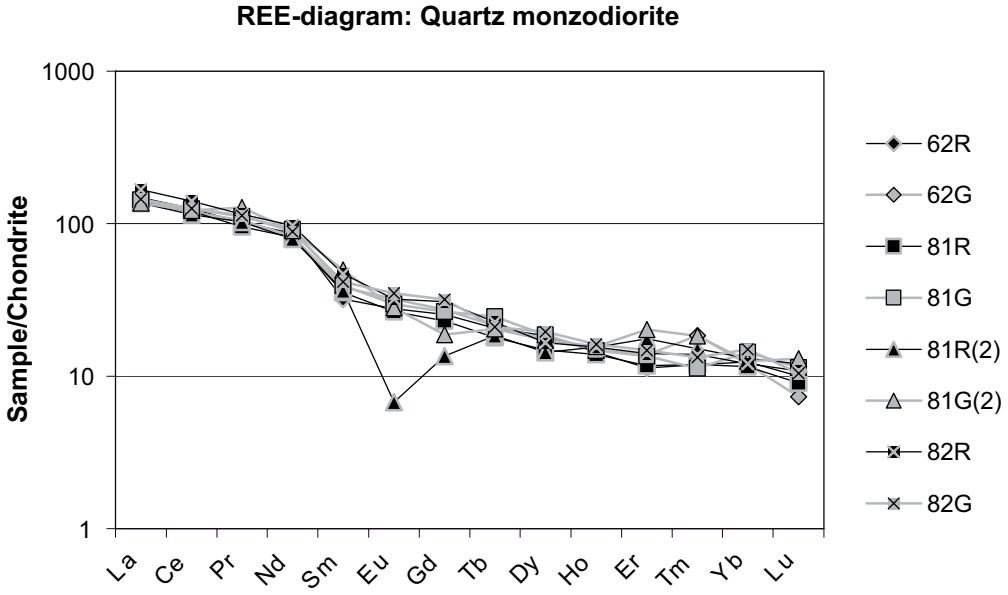

Figure 7-51. *Chondrite normalised REE-plot of quartz monzodiorite samples 62, 81, 81(2) and 82 using chondrite values from /Evansen et al. 1978/.*

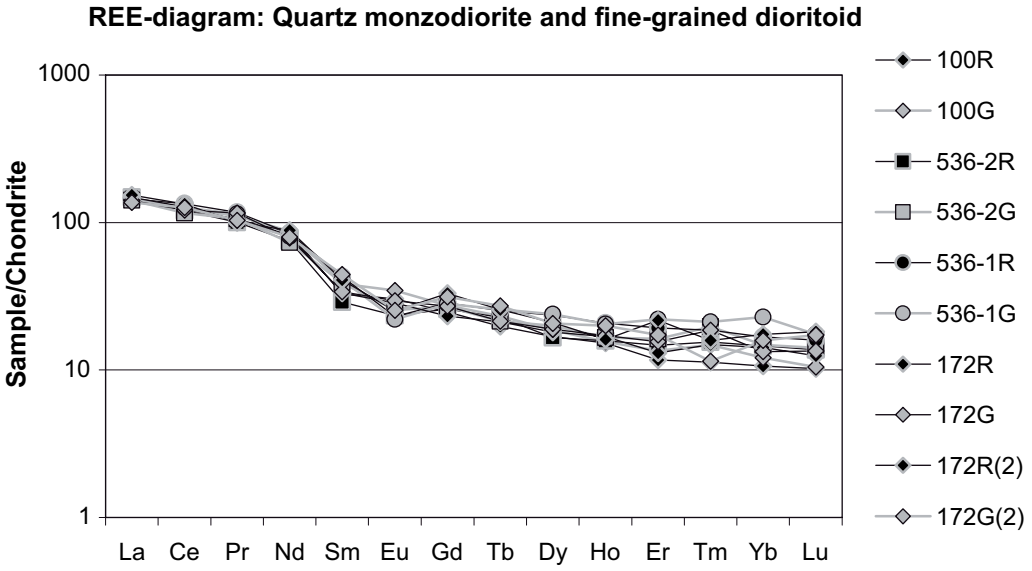

Figure 7-52. *Chondrite normalised REE-plot of quartz monzodiorite samples 100, 172 and 172(2) and fine-grained dioritoid samples 536-1 and 536-2 using chondrite values from /Evansen et al. 1978/.*

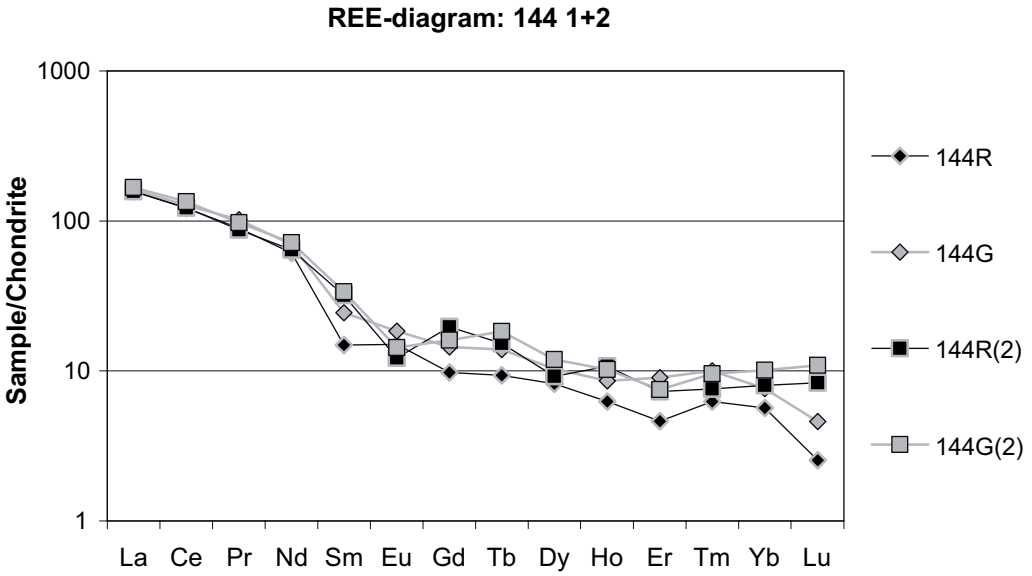

Figure 7-53. *Chondrite normalised REE-plot of Ävrö granite samples 144 and 144(2) using chondrite values from /Evansen et al. 1978/.*

7.5 Mössbauer spectroscopy

Written in cooperation with Hans Annersten, Uppsala University.

Mössbauer spectroscopy analyses were carried out for all the 24 samples (see Section 6.4). The analyses give values of the total $Fe^{3+}/(Fe^{3+} + Fe^{2+})$ (= oxidation factor[total]) in the whole rock sample, in silicates and in oxides, respectively. The oxidation factor (total) is obtained from combining the oxidation factor (silicate) with oxidation (oxide). Oxidation factor (total) provides the most reliable results, since the resolution is better than for e.g. oxidation factor (oxide). All Mössbauer spectroscopy results are shown in Table 7-19.

Table 7-19. Mössbauer spectroscopy results.

Sample	Fe^{3+}-bearing mineral	Oxidation factor (silicate)	Oxidation factor (oxide)	Oxidation factor (total)	Fe_{tot} (wt. %)[a]	Fe^{2+}_{tot} (wt. %)	Fe^{3+}_{tot} (wt. %)
62R	FeMg-s.mt	0.31	0.72	0.41	6.13	3.62	2.52
81R	FeMg-s.mt	0.29	0.74	0.4	6.30	3.78	2.52
82R	FeMg-s.mt	0.24	0.72	0.359	7.20	4.62	2.59
100R	FeMg-s.ep.hem	0.203	1	0.466	6.98	3.73	3.25
128R	FeMg-s.hem	0.165	1	0.304	4.62	3.22	1.41
144R	FeMg-s.epi.hem	0.318	1	0.578	2.57	1.09	1.49
172R	FeMg-s.mt.hem	0.2	0.82	0.386	5.51	3.38	2.12
372R	FeMg-s.epi.hem	0.38	0.92	0.576	3.83	1.63	2.21
394R	FeMg-s.epi.mt	0.52	0.713	0.549	3.69	1.66	2.02
536-1R	FeMg-s.tr mt	0.12	tr mt		5.17		
536-2R	FeMg-s.mt.hem	0.23	0.694	0.28	5.07	3.65	1.42
661R	FeMg-s.epi.mt.hem	0.48	0.77	0.536	3.79	1.76	2.03
62G	FeMg-s.mt	0.25	0.68	0.35	6.34	4.12	2.22
81G	FeMg-s.mt	0.24	0.68	0.36	6.93	4.43	2.49
82G	FeMg-s.mt	0.22	0.62	0.33	7.00	4.69	2.31
100G	FeMg-s.hem	0.15	1	0.42	6.79	3.94	2.85
128G	FeMg-s.mt.hem	0.239	0.81	0.371	4.65	2.93	1.73
144G	FeMg-s.mt.hem	0.28	0.89	0.535	2.74	1.27	1.46
172G	FeMg-s.epi.mt	0.196	0.68	0.32	5.48	3.72	1.75
372G	FeMg-s.epi.mt.hem	0.36	0.75	0.48	3.57	1.86	1.71
394G	FeMg-s.epi.mt	0.44	0.65	0.47	3.49	1.85	1.64
536-1G	FeMg-s.mt.hem	0.2	0.62	0.26	5.10	3.77	1.33
536-2G	FeMg-s.mt.hem	0.226	0.65	0.31	5.53	3.81	1.71
661G	FeMg-s.epi.mt	0.35	0.73	0.43	3.66	2.09	1.57

Abbreviations: FeMg-s = Fe-Mg silicates (mainly chlorite and occasionally biotite, amphibole and clinopyroxene), epi = epidote, mt = magnetite, hem = hematite, tr = trace amounts.

[a] = Fe_20_3*0.6995. No total oxidation factor was yielded for sample 536-1R due to the small amount of oxides.

7.5.1 Silicates

Most of the Fe^{3+} in the silicates is found in Fe-Mg silicates (mainly chlorite), although chlorite contains higher concentrations of Fe^{2+} than Fe^{3+}. The Mössbauer spectra for chlorite overlap with the spectra for other Fe-Mg silicates, e.g. biotite, amphibole and clinopyroxene and it is difficult to separate these minerals in the spectra. However, the thin Mössbauer-lines for Fe-Mg silicates suggest that the major part of the Fe-Mg-silicates is chlorite and other Fe-Mg silicates (biotite, amphibole and clinopyroxene) constitute a small part at most. The Fe^{3+}/Fe_{tot}-ratio of the Fe-Mg-silicates is commonly higher in the red-stained samples than in the reference samples. The Fe^{3+}/Fe_{tot}-ratio of Fe-Mg silicates in the red-stained samples is about 12 to 31%. The Fe^{3+}/Fe_{tot}-ratio of Fe-Mg silicates in the reference samples is about 15 to 25%. In some samples, mostly those of Ävrö granite, epidote was also traced as a major Fe^{3+}-bearing silicate (more than c. 3 vol. %). The Ävrö granite thus have higher oxidation factors (silicate) since epidote contains Fe^{3+} only, while e.g. chlorite contain both Fe^{2+} and Fe^{3+}. /Tullborg 1995/ reports higher Fe^{3+}/Fe_{tot}-contents in wall rock chlorite than in wall rock biotite. A higher amount of chlorite (and epidote) in the red-stained rock compared to the reference rock will result in a higher oxidation factor (silicate) in the

red-stained rock. This is evident in most of the samples in this study (Figure 7-54), except for samples 128 and 536-1, where the oxidation factor (silicate) is higher in the reference sample than in the red-stained sample. Generally the oxidation factor (silicate) is about 0.4–8% higher in the red-stained samples. Outliers are the enriched oxidation factor in sample 394 (13%) and the depletion in oxidation factor in samples 128 (–7.4%) and 536-1 (–8%). The average increase in oxidation factor (silicate) is about 2.5% (including outliers) and about 3.7% (excluding outliers).

7.5.2 Oxides

The most important Fe^{3+}-bearing oxides are magnetite ($Fe^{3+}/Fe_{tot} = 2/3$) and hematite (100% Fe^{3+}). Since magnetite has an oxidation factor of about 0.6667 and hematite has an oxidation factor of 1, the oxidation factor is between 0.6667 and 1 in the samples, and is increased with increasing hematite-content. The oxidation factor for oxides has poor accuracy for many samples since the oxide-content (in vol. %) in the samples often is close to the detection limit. That is for instance the reason why the magnetite content in 100G is left out although thin section investigations show that there is magnetite in this sample. Also sample 536-1R is left out since the oxide content was below the detection limit. It is however evident that there is more hematite in the red-stained samples compared to the reference samples, (Figure 7-55), in accordance with thin sections investigations. Hematite does commonly not replace the whole magnetite content, which also is evident from the characteristic incomplete pseudomorphic replacement of magnetite by hematite that is observed in a most of the red-stained samples. The oxidation factor (oxide) is increased by up to 19% in the red-stained samples compared to the reference samples and the average increase is about 9%.

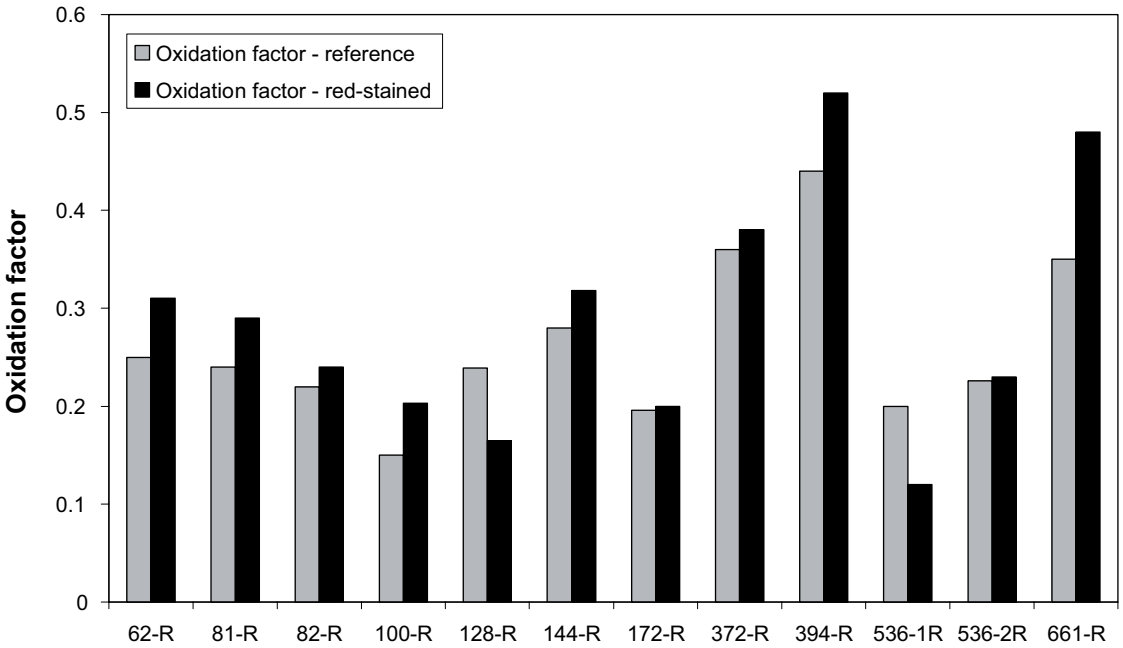

Figure 7-54. *Oxidation factor (silicate) obtained from Mössbauer spectroscopy. Note the higher oxidation factor in the epidote-rich Ävrö granite samples (372, 394 and 661).*

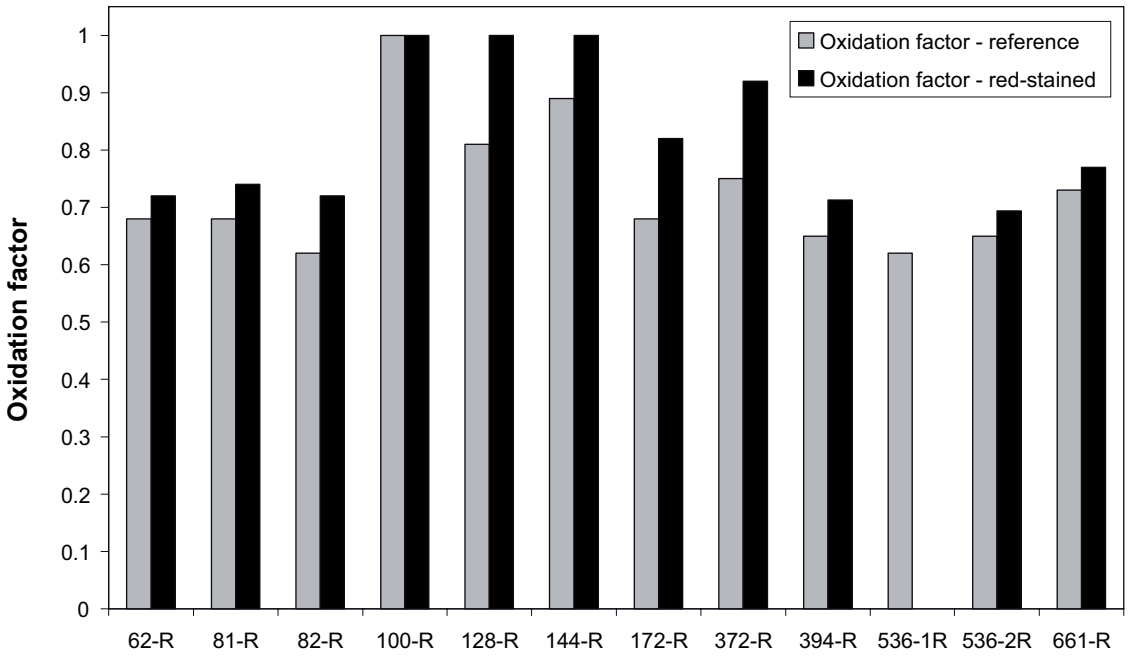

Figure 7-55. *Oxidation factor (oxide) obtained from Mössbauer spectroscopy.*

7.5.3 Total

As stated above the oxidation factor (total) is the most reliable measurement of the oxidation factor and it is obtained by correlating oxidation factor (silicate) and oxidation factor (oxide), which are both described above. The oxidation factor (total) is commonly higher in the red-stained rock than in the reference rock (Figure 7-56). The total oxidation factor is higher in 9 of the red-stained samples (about 3–10%, average about 6%) and is lower in two samples (about 3–7%). Total oxidation factor is not obtained for sample 536-1R since the oxide content was below detection limit. The average change in oxidation factor (total) overall is an increase of about 4.25%. The amount of magnetite and/or hematite may however "hide" the increase in Fe^{3+} in the total oxidation factor since magnetite and hematite have such high oxidation factors compared to chlorite. In sample 536-2R, for instance, both the oxidation factor (oxide) and the oxidation factor (silicate) are higher than in fine-grained dioritoid sample 536-2G, but the oxidation factor (total) is lower in sample 536-2R compared to sample 536-2G since the amount of magnetite in sample 536-2G is so high. The total oxidation factor is generally higher in Ävrö granite samples (144, 372, 394 and 661) than in quartz monzodiorite and fine-grained dioritoid samples, mainly because of higher amounts of epidote in Ävrö granite. The increase in the total oxidation factor is also highest in the Ävrö granite samples (4.3–10.6%, average 8.1) compared to quartz monzodiorite samples (generally 3–6.6% increase, with a 7% decrease in 128R) and fine-grained dioritoid samples. The total amount of Fe^{3+}/Fe_{tot} in Ävrö granite samples is 54–58% (average 56%) in the red-stained samples and 43–53.5% (average 47.9%) in the reference samples. The total amount of Fe^{3+}/Fe_{tot} in quartz monzodiorite samples is 30–41% (average 38.8%) in the red-stained samples and 32–42% (average 35.9%) in the reference samples, while fine-grained dioritoid sample 536-2R has 28% Fe^{3+}/Fe_{tot} (undetectable amounts of oxides in 536-1R) and 536-2G has 31% (536-1G has 26%).

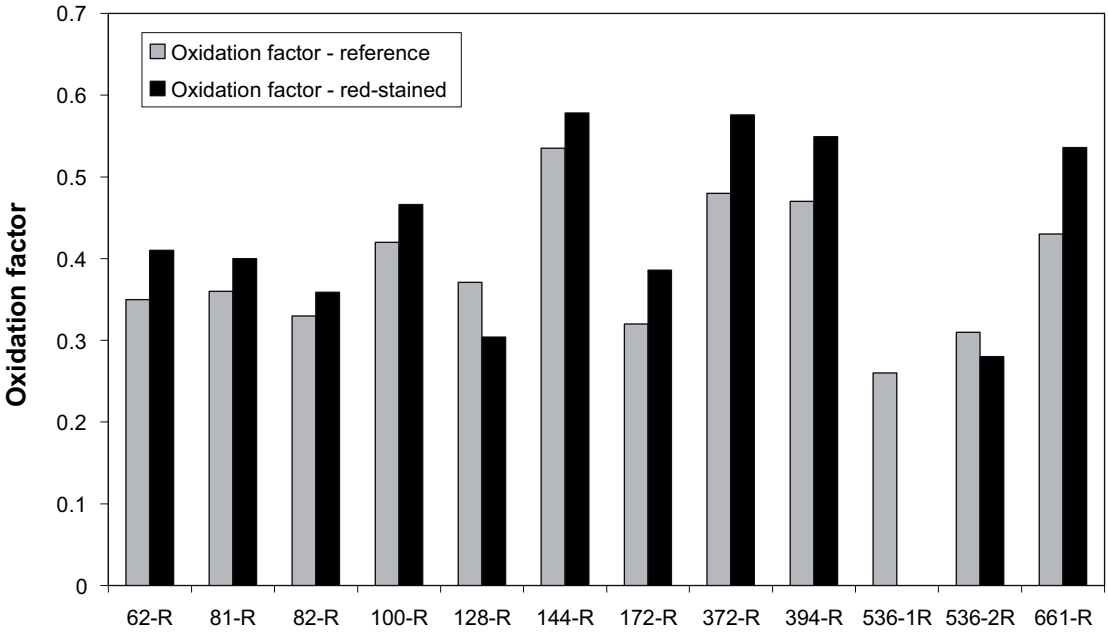

Figure 7-56. *Oxidation factor (total) obtained from Mössbauer spectroscopy.*

8 Summary of the mineralogical and geochemical changes and related changes in redox capacity

The red-staining of the wall rock adjacent to fractures is caused by hydrothermal alteration and associated, usually minor, oxidation. The red-staining is caused by minute inclusions of Fe^{3+}-rich minerals, mainly hematite. These are present in secondary pores, usually hosted in K-feldspar (adularia) and to lesser extent in albite that are replacing primary plagioclase. Accompanying this alteration is hematitization of magnetite, chloritization of biotite (and hornblende and augite) and formation of secondary sericite, prehnite, grothite (titanite) and epidote. An increase in micro-porosity and micro-fractures during alteration is also observed. Minerals like quartz, primary K-feldspar (micro-perthite and groundmass microcline) and titanite remained rather fresh during alteration. The red-staining of feldspar has obviously taken place at hydrothermal conditions and temperatures around 280–400°C are indicated. This is based on temperatures of chloritization, prehnite formation, epidote formation, feldspar composition (thermometry) and the low-temperature paragenesis in general, based on information from /Liou et al. 1983, Nekvasil and Burnham 1987, Frey et al. 1991, Deer et al. 1992, Slaby 1992, Eliasson, 1993, Spear 1993, Lee and Parsons 1997, Bucher and Frey 2002, Wilamowski 2002, Benisek et al. 2004, and this study/. It should be noted that feldspar-thermometers are not calibrated for these temperatures and therefore the estimated temperatures should be considered approximate. The chemistry of chlorite in the altered rock closely resembles the chemistry of early formed chlorite in fracture fillings in the area /Drake and Tullborg 2004, 2005, 2006a/. Intense local red-staining caused by hematite and possibly also Fe-oxyhydroxide in micro-fractures is thought to be formed subsequently to the major red-staining event. /Eliasson 1993/ proposed the latter red-staining to occur at temperatures of about 150–250°C.

The red-stained rock is highly enriched in major elements K, Na, trace element Rb as well as in H_2O. Enrichment of Ba, F and U is also evident in a majority of the samples. The increase in K, Na, Rb and Ba is associated to formation of secondary adularia, albite and subordinately sericite and alteration of biotite in the reference rock. The increase of H_2O is due to the increase in secondary water-bearing minerals like chlorite, prehnite and sericite in the red-stained rock.

The red-stained rock is highly depleted in Ca and trace elements like Sr, Cs, Be, Ga and Cr while moderate depletion is evident for Al, Th, S and possibly Mn. The depletion of these elements is mainly associated to the removal of the anorthite-content from break down of primary plagioclase, alteration of biotite, hornblende and augite and oxidation of magnetite and pyrite.

The total Fe-content as well as related elements such as Ti, Mg, Sc, V and Co remained fairly constant as well as Si, P, Y and REE. These elements are either redistributed and fixed in secondary minerals within a very limited rock volume or completely fixed in resistant primary minerals during alteration. A small enrichment in Fe-contents in three of the red-stained Ävrö granite samples might however be associated with elevated epidote-contents in these samples compared to the reference rock.

Mössbauer analyses reveal that Fe^{3+}-contents are elevated in the red-stained rock compared to the reference rock although the total Fe-content remained fairly constant. This is caused by oxidation of magnetite to hematite and an increase in Fe^{3+}/Fe_{tot}-ratio in the silicates,

partly because of a higher amount of Fe^{3+}-bearing epidote in the red-stained rock. Most of the Fe^{3+} in the silicates is however contained in Fe-Mg silicates (mainly chlorite), although Fe^{2+}-concentrations are higher than Fe^{3+}-concentrations in chlorite. The chlorite is found in higher amounts in the red-stained rock than in the reference rock, thus increasing the Fe^{3+}/Fe_{tot}-ratio in the red-stained rock. The Fe^{3+}-concentrations are also higher in the red-stained samples than in the reference samples. The increase in Fe^{3+} is however not as high as the macroscopic features of the red-stained rock might suggest. The total increase in Fe^{3+}/Fe_{tot} is about 3–10% in most of the samples, although some samples show higher Fe^{3+}/Fe_{tot}-ratio in the reference rock mainly due to higher oxide-contents in these samples. Ävrö granite samples generally have the highest Fe^{3+}/Fe_{tot}-ratios and also the largest increase in Fe^{3+}/Fe_{tot} (average 8.1%), apparently caused by high epidote-contents, which are increased in the red-stained rock. The average total portion of Fe^{3+}/Fe_{tot} in Ävrö granite samples is 56% in the red-stained samples and 47.9% in the reference samples. The average total portion of Fe^{3+}/Fe_{tot} in quartz monzodiorite samples is 38.8% in the red-stained samples and 35.9% in the reference samples, while the fine-grained dioritoid samples have Fe^{3+}/Fe_{tot} values of 26–31% (in both red-stained samples and reference samples). A schematic summary of how the Fe^{3+}/Fe_{tot}-ratios and related mineralogy have changed in the different rock types in the red-stained samples compared to the reference samples is shown in Table 8-1.

Usually the “unaltered” reference wall rock samples in this study was not completely unaltered and are characterized by chloritization of biotite and partial alteration of plagioclase. These samples are however not extensively oxidized which shows that the hydrothermal alteration often reaches further into the wall rock than the oxidation does, which is in agreement with studies of /Landström et al. 2001/. A schematic illustration of the characteristic features of the red-staining is found in Figure 8-1.

Table 8-1. Schematic summary of the changes in Fe^{3+}/Fe_{tot}-ratios and related mineralogy in the different rock types. Values in brackets are average values.

Sample	Silicates				Oxides					Total			
	Biotite (vol. %)	Chlorite (vol. %)	Epidote (vol. %)	Fe^{3+}/Fe_{tot} silicate (%)	Oxides [a] (vol. %)	Magnetite (vol. %)[b]	Hematite (vol. %)[b]	Mt+Hem (vol. %)[b]	Fe^{3+}/Fe_{tot} oxide (%)	Fe^{3+}/Fe_{tot} total (%)	Fe_{tot} (wt. %)[c]	Fe^{2+}_{tot} (wt. %)	Fe^{3+}_{tot} (wt. %)
Dioritoid reference	6.7–15.4 (11.1)	0.8–6.7 (3.8)	0.1–0.2 (0.15)	20–22.6 (21.3)	0.6–0.7 (0.65)	60–72.7 (66.4)	10–18.2 (14.1)	9.1–30 (19.5)	62–65 (63.5)	26–31 (28.5)	5.10–5.52 (5.31)	3.77–3.81 (3.79)	1.33–1.71 (1.52)
Dioritoid red-stained	1–1.4 (1.2)	13.4–14.4 (13.9)	0.3–0.8 (0.6)	12–23 (17.5)	0.3–1.2 (0.72)	16.7–25 (20.8)	0–25 (12.5)	50–83.3 (66.7)	69.4*	28*	5.07*	3.65*	1.42*
QMD reference	0.3–11.8 (4.4)	0.9–17.2 (10.4)	0.1–1.4 (0.5)	15–25 (21.6)	0.3–3.2 (1.8)	2–100 (72.8)	0–9.8 (2.9)	0–88.2 (24.3)	62–100 (74.2)	32–42 (35.9)	4.65–7.00 (6.20)	2.93–4.69 (3.97)	1.73–2.85 (2.22)
QMD red-stained	0.1–1.8 (0.6)	9.1–17.7 (12.5)	1–3.2 (1.6)	16.5–31 (23.5)	0.6–3.6 (1.9)	0–80 (22.8)	7.1–32.3 (15.8)	0–92.9 (61.5)	72–100 (85.2)	30.4–46.6 (38.8)	4.62–7.20 (6.12)	3.22–4.62 (3.72)	1.41–3.25 (2.40)
Ävrö granite reference	0.6–2 (1.3)	3.2–11.5 (8.8)	0.2–10.3 (5.1)	28–44 (35.8)	0.6–1.4 (1.1)	0–100 (50.9)	0–31.8 (9.4)	0–90.5 (39.7)	65–89 (75.5)	43–53.5 (47.9)	2.74–3.66 (3.36)	1.27–2.09 (1.77)	1.46–1.71 (1.60)
Ävrö granite red-stained	0.1–0.6 (0.2)	5.4–12.3 (8.5)	1.1–9.4 (5.7)	31.8–52 (42.5)	0.3–2.3 (1.0)	0–60 (30.3)	10–55.6 (25.4)	25–77.8 (44.3)	71.3–100 (85.1)	53.6–57.8 (56)	2.57–3.83 (3.47)	1.09–1.76 (1.53)	1.49–2.21 (1.94)

Abbreviations: QMD = Quartz monzodiorite, Mt+Hem = magnetite partially replaced by hematite. * = Based on sample 536-2R, since sample 536-1R only included trace amounts of oxides it was left out. [a] = Magnetite and hematite (ilmenite is excluded), [b] = % of counted oxide vs. total counts of magnetite, hematite and magnetite+hematite, [c] = Fe_2O_3 multiplied by 0.6995. Dioritoid samples are 536-1 and 536-2 m. QMD samples are 61, 81, 82, 100, 128 and 172 m. Ävrö granite samples are 144, 372, 394 and 661 m. Pyrite is commonly present in very small amounts in the samples (< 0.25 vol. %) and is thus not included in Table 8-1. However, both point-counting and whole rock chemical analyses show that pyrite and sulphur is generally depleted in the red-stained rock compared to the reference rock.

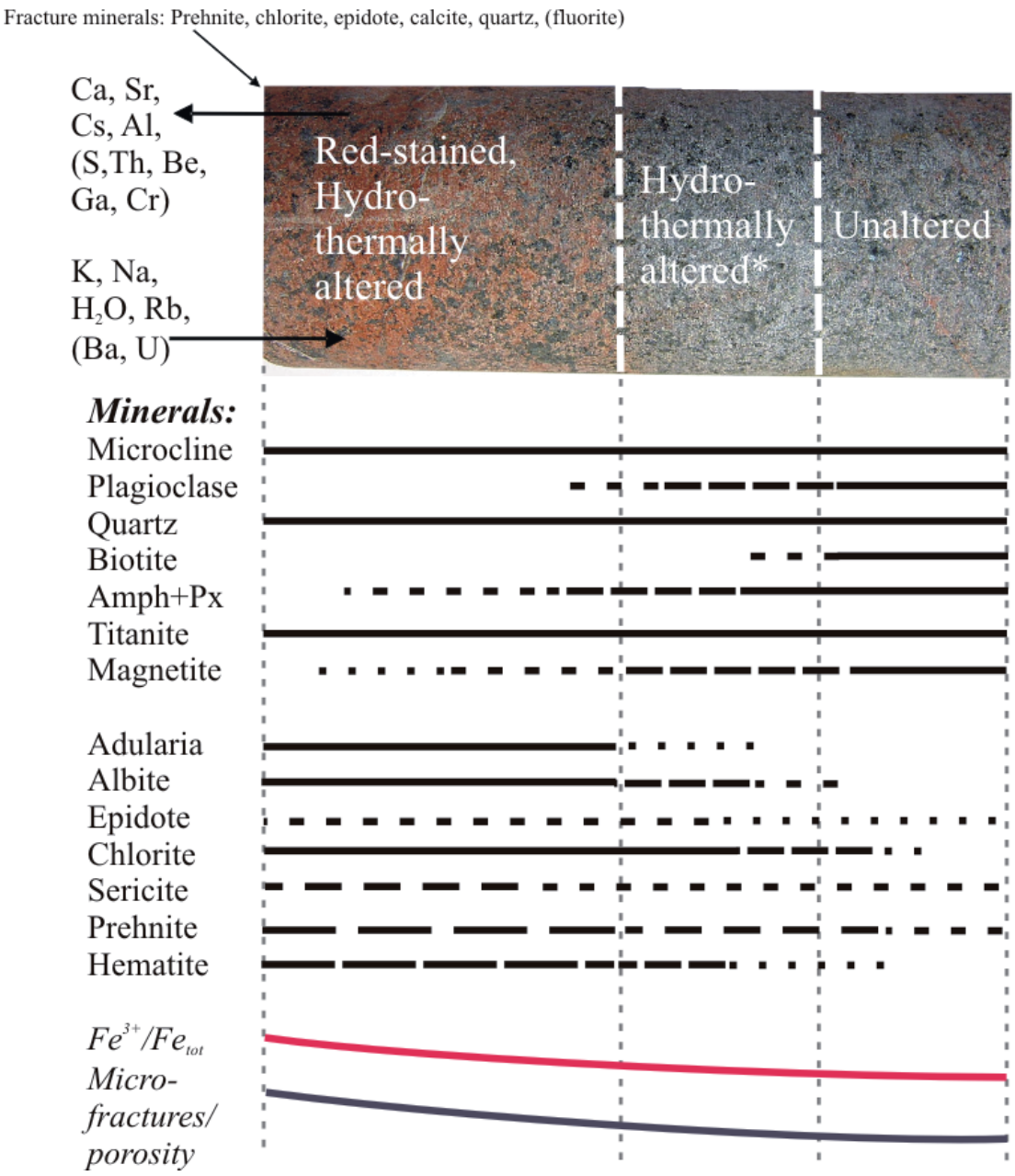

Figure 8-1. *Tentative sketch of the major features of the wall rock. Vertically stippled lines indicate which part that is red-stained due to oxidation/hydrothermal alteration, hydrothermally altered (but not red-stained(*)) and fairly unaltered, respectively. The fracture rim is at the left side of the sketch. Arrows indicate which element that is enriched or depleted in the red-stained rock compared to the reference rock. The horizontal lines (partly stippled), show where the major minerals occur in the different zones adjacent to the fracture. The red and black lines at the bottom illustrate the change in Fe^{3+}/Fe_{tot} and the amount of micro-fractures/porosity from the fracture surface into the wall rock.*

9 Changes in properties of concern for a deep repository for spent radioactive fuel

The oxidation and hydrothermal alteration described in this study has resulted in changed properties of the rock, potentially influencing several parameters that need to be considered for the planning and modelling of a nuclear waste repository. These parameters are reducing capacity, porosity, sorption, thermal conductivity and rock strength. The possible effects caused by the alteration are discussed below. Since no detailed study of changing rock strength properties (rock mechanics) of altered, oxidized rock compared to unaltered rock has been carried this is not discussed here. However, the higher porosity in the red-stained rock may lead to lower rock strength.

9.1 Reducing capacity

At the planned depth of a repository (approx. 500 m) reduced groundwater is a prerequisite. In order to maintain the stability of the canister it is important that groundwaters do not contain dissolved O_2 during the life time of the repository. Oxygen will be introduced during the construction and operation of the repository. This oxygen will be consumed by the inorganic (mainly Fe^{2+}) and organic redox buffers. Experiments have previously been carried out on Äspö in order to prove this /Puigdomenech et al. 2001/. Another scenario which may introduce oxygenated water into the bedrock is glacial meltwater. The basic idea is that such meltwater can contain more dissolved O_2 than the present recharge and in addition, the organic buffer may be severely reduced below the ice. Furthermore high hydraulic heads beneath the inland ice sheet may force this oxygen-rich water to large depth in the bedrock. The extent and potential for O_2 intrusion to large depth, related to the glacial scenario is debated but nevertheless it is of importance to show that Fe^{2+} is available in the bedrock and along the fractures in order to provide enough reducing capacity. One of the tasks of the present study is to determine how much reducing capacity is left in the oxidised and hydrothermally altered red stained parts of the wall rock compared to fresh host rock. The results are summarised below:

1) The main Fe^{2+}-bearing minerals in the relatively fresh rock in the Simpevarp subarea are commonly biotite, chlorite, magnetite, amphibole (mainly hornblende). In addition, the quartz monzodiorite and fine-grained dioritoid also contain some pyroxene (mainly augite). In the altered and red stained samples the most common Fe^{2+} mineral is chlorite.
2) The change in Fe^{3+}/Fe_{tot} ratio is relatively small between the relatively fresh samples and the red-stained and altered samples (mean values for each rock type);
   a) Quartz monzodiorite; 35.9% Fe^{3+}/Fe_{tot} increased to 38.8% in the red-stained samples.
   b) Ävrö granite; 47.9% Fe^{3+}/Fe_{tot} increased to 56% in the red-stained samples.
   c) Dioritoid; the silicates and oxides in the red-stained samples are moderately enriched in Fe^{3+}/Fe_{tot}. However, the small and highly variable oxide content makes it impossible to obtain conclusive results of the total changes in Fe^{3+}/Fe_{tot}.
3) The available Fe^{2+} varies between 3.72 to 3.97 wt. % in fresh and red-stained Quartz monzodiorite respectively, and 1.53 to 1.77 wt. % in fresh and red-stained Ävrö granite. The dioritoid showed Fe^{2+} content of 3.65 to 3.79 wt. %. It can thus be concluded that red-stained samples of the quartz monzodiorite and dioritoid contain significantly more Fe^{2+} than the Ävrö granite samples in this study.
4) Pyrite has been documented in small amounts in most samples (< 0.25%). Based on S contents the amounts of sulphide are however, mostly lower in the red-stained samples.

The overall conclusion is that the decrease in reducing capacity in the oxidized wall rock is not as high as macroscopic observations might suggest. Instead, the mineralogical changes in combination with the modest oxidation and formation of minute hematite grains have produced the red-staining.

9.2 Porosity

The mineralogical changes related to hydrothermal alteration usually increase the porosity, but most of all changes the structure and distribution of the pores. This is also the case for the alteration/oxidation observed within the Simpevarp area. Diffusion and sorption are the two main retention mechanisms for radionuclides considered in the safety assessment modelling. Porosity is a key parameter for both:

1) Diffusion depends to a large extent on the amounts of connected pores and their shape.
2) Sorption is dependent on mineral composition but also on the surface area available, which in turn is related to the porosity.

Studies of connected porosities have been carried out within the Oskarshamn site investigations on drill core samples from KSH01, KSH02 at Simpevarp, KLX02, KLX03, KLX04, KLX05 and KLX06 at Laxemar /Savukoski 2004, Savukoski and Carlsson 2004, Börjesson and Gustavsson 2005, Savukoski 2005ab/. These studies did not focus on comparisons of porosity differences between red-stained and fresh rock. However, some of the samples in these studies are clearly red-stained (oxidized) and comparisons of red-stained and fresh samples based on results from the above mentioned studies are evaluated briefly in this report. Sample descriptions from (Gustavsson, pers. comm.) were also used. It should be noted that the samples measured for porosity in the above mentioned studies are quite thin (about 1/2 the drill core diameter). This might give higher porosity values than expected, especially for the heterogeneous and coarse-grained Ävrö granite cf. e.g. /Tullborg and Larson 2005/. The results from the above mentioned studies show that the red-stained samples generally have higher porosities than the fairly fresh rock and that the porosity is generally highest in Ävrö granite samples. For the major rock types these porosities were measured:

1. Ävrö granite:
   - Fresh: 0.2 to 0.6% (average = 0.34%, 13 samples, KLX03, KLX05).
   - Red-stained: 0.5 to 0.8% (average: 0.59%, 15 samples, KLX04).
2. Quartz monzodiorite:
   - Fresh: 0.1 to 0.4% (average = 0.23%, 15 samples, KSH01, KLX03, KLX05).
   - Red-stained: 0.2 to 0.4% (average = 0.3%, 5 samples, KSH01, KLX03).
3. Fine-grained diorite:
   - Fresh: 0.1 to 0.3% (average = 0.2%, 8 samples, KSH01, KLX05).
   - Red-stained: 0.2 to 0.4% (average = 0.3%, 2 samples, KSH01).

In the drill core KSH02 at Simpevarp it was shown that the porosity is higher in altered fine-grained dioritoid (porosity = 1 to 2.5%) compared to fresh fine-grained dioritoid (porosity = 0.2 to 1%) /Mattsson and Thunehed 2004/.

In studies at Äspö HRL it has been shown that the porosity is higher in altered, oxidized granitic rock adjacent to fractures (porosity = 0.15 to 0.83%, average 0.35%) compared to fresh granitic rock further away from the fractures (porosity = 0.13 to 0.20) /Eliasson 1993/.

Distribution of the pores and the textures of the connected pores can be studied using different impregnation techniques. Such studies have been carried out on altered and fresh rock samples from Äspö /Mazurek et al. 1995, Byegård et al. 1998, Johansson 2000/.

These studies show that the distribution of pores is heterogeneous and that the orientation effects may be considerable. A higher porosity close to the fracture wall is shown in PMMA studies on Äspö /Kelokaski et al. 2001/, where the porosity in some wall rock samples is due to connected pores with preferred orientation. This porosity is increased in connection to micro-fractures which are more common in the altered wall rock. Results from impregnation studies also show that connected porosity in crystalline rock is mainly made up of micro-fractures and to some extent porous minerals (often secondary or altered minerals) /Mazurek et al. 1995, Johansson 2000/. Frequency, size and orientation of the micro-fractures are crucial for the connectivity of the pores. At Äspö, the connected porosity shows a distinct decrease from the partly gouge filled breccia centre of water conducting structures through the altered wall rock and further into unaltered fresh bedrock /Andersson et al. 2002/.

Introduction of new micro-fractures caused by drilling and disturbances of the samples due to stress release might however influence the porosity of the samples.

No measurements of total porosity have been carried out in this study. However, micro-porosity-features have been found to be more prominent in the red-stained samples than in the reference samples, sometimes high-lightened by ink-impregnation. The main porosity-affecting features of the red-stained rock compared to the reference rock are:

- Higher amount of micro-fractures through crystals (particularly quartz and subordinately K-feldspar phenocrysts) and along grain boundaries in the red-stained rock.
- Higher porosity of secondary and altered minerals, especially in plagioclase pseudomorphs, chlorite and prehnite.
- Grain expansion associated to chloritization of biotite, resulting in radial fractures.

These features are thought to increase the total porosity and the micro-porosity in the red-stained rock to a higher degree than in the reference samples, in accordance to other studies in the area (see above).

9.3 Sorption

Sorption of radionuclides on the fracture walls combined with diffusion into the fracture coatings and further into micro-fractures in the wall rock is the main retardation factors for nuclide transport. Sorption capacity for each trace element is dependent on the water/mineral system present. Therefore are changes in wall rock mineralogy related to changes in the sorption capacity.

Laboratory and in situ experiments studying the sorption of different tracers have been carried out on altered and fresh Äspö diorite at the Äspö HRL /Byegård et al. 1998/. These batch experiments showed that the sorptivity of the tracers increases in the order $^{22}Na^{+}$ $< {}^{47}Ca^{2+} \approx {}^{85}Sr^{2+} < {}^{86}Rb^{+} \approx {}^{133}Ba^{2+} < {}^{137}Cs^{+}$ (both in laboratory and in situ). This study also indicates that the sorption is stronger in the fresh Äspö diorite compared to the altered Äspö diorite. The lower sorptivity in the altered rock is supposed to be due to the alteration of biotite to chlorite, since biotite has much higher sorption capacity than chlorite, especially regarding Cs^{+}. Subsequent sorption studies on gouge and rim zone (altered wall rock) materials from the TRUE Block Scale site in the Äspö Hard Rock laboratory show more complex patterns. These indicate similar or slightly higher sorption coefficients in the rim zone material compared to the fresh host rock /Byegård and Tullborg, in manuscript/. Concerning very altered and red stained sections of the bedrock, the fine grained hematite present in the altered feldspar grains may enhance the sorption of some tracers (e.g. U and Ra). Red-stained samples are included in the presently running laboratory program of the site investigations.

The effective sorption is related to available surfaces and therefore the net effect of the alteration can not only be described in terms of changed mineralogy. Within the ongoing site investigation programme batch sorption experiments on samples from fracture zones, altered wall rock and fresh host rock are carried out. BET surface measurements on this type of materials are compiled in the background report for transport modelling /Byegård et al. in manuscript/ and show significantly higher areas for the altered material than for the fresh host rock, i.e. a larger active surface as a result of alteration.

9.4 Thermal properties

The thermal properties of the rock influence the planning of a repository for spent nuclear fuel. Heat is produced by the spent fuel and preferable the buffer and the rock surrounding the canister should be kept at temperatures below 100° C. The capability of the rock to transfer the heat from the deposition holes and further into the bedrock away form the repository is therefore an important parameter. Low thermal conductivity, low thermal diffusivity and high thermal capacity in rock surrounding the deposition holes will require a larger distance between the holes.

The thermal properties of the rock depend on e.g. mineralogy. For example, quartz has a high thermal conductivity compared to other minerals and therefore a rock with high quartz content (granitic to granodioritic) usually has a higher thermal conductivity than quartz monzodiorite.

Studies of thermal properties at the Äspö HRL showed that samples of altered Äspö diorite had higher thermal conductivity, higher thermal diffusivity and lower thermal capacity than fresh Äspö diorite ("Äspö diorite" is here synonymous to Ävrö granite of quartz monzodioritic composition) /Sundberg and Gabrielsson 1999/. The thermal conductivity is 2.70 W/m°C for the altered Äspö diorite and 2.32 W/m°C for the fresh Äspö diorite (based on mean calculated values and laboratory measurements). The difference in thermal properties between the altered rock and the fresh rock is mainly depending on the higher content of chlorite, which has replaced biotite, in the altered rock /Sundberg and Gabrielsson 1999/. Chlorite has considerably higher thermal conductivity (5.1 W/m°C) than biotite (2.0 W/m°C) /Horai and Simmons 1969, Horai 1971/. The higher thermal conductivity in the altered Äspö diorite compared to the fresh Äspö diorite may also depend on the replacement of plagioclase by albite in the altered rock /Sundberg and Gabrielsson 1999/. This is because the thermal conductivity of albite (2.1 W/m°C) is higher than that of plagioclase with an An-content of 25% (1.61 W/m°C) /Horai and Simmons 1969, Horai 1971/. The Äspö diorite samples investigated in the study at Äspö HRL are similar in chemistry and mineralogy to samples 128, 372, 394 and 661 in the present study at Simpevarp.

The changes in thermal properties of the oxidized and hydrothermally altered rock adjacent to fractures compared to the fairly fresh reference samples in the present study can be estimated hypothetically by comparing mineralogical changes. The major changes in thermal properties are probably due to the replacement of biotite by chlorite and leads to increased thermal conductivity in the red-stained samples. The replacement of plagioclase by albite and K-feldspar (2.51 W/m°C, /Horai and Simmons 1969, Horai 1971/) also leads to higher thermal conductivity of the red-stained rock compared to the reference rock. However, biotite is already partially replaced by chlorite in some of the reference samples. This decreases the difference in thermal conductivity between the reference samples and the related red-stained samples. So far, the thermal conductivity measurements carried out within the site investigations program have not been interpreted based on sample specific mineralogical compositions and therefore the significance of the changes in thermal conductivity caused by the hydrothermal alteration can not be evaluated properly at this stage.

10 Acknowledgements

We would like to thank the staff at the SKB Simpevarp site investigations for their support. Analytica AB is thanked for whole rock chemical analyses. Prof. Hans Annersten, Uppsala University is thanked for carrying out Mössbauer spectroscopy, writing of the method description and for contributing to Section 7.5. Kjell Helge (Minoprep AB) is thanked for carrying out sample preparation. Prof. Sven Åke Larson, Göteborg University is thanked for having improved the manuscript and contributing constructive comments. Thomas Eliasson, SGU, Dr. Jesper Petersson, Swedpower AB, Assoc. Prof. Susan Stipp, Copenhagen University and Björn Sandström, Göteborg University kindly provided some references. Dr. Artur Benisek, Kiel University is thanked for support with feldspar thermometry. Dr. Cees-Jan de Hoog, Göteborg University is thanked for useful comments. Fredrik Hartz, SKB, kindly helped us with the map for the area.

11 References

Alderton D H M, Pearce J A, Potts P J, **1980.** Rare earth element mobility during granite alteration; evidence from Southwest England, Earth and Planetary Science Letters, 49, p. 149–165.

Andersson P, Byegård J, Dershowitz B, Doe T, Hermanson J, Meier P, Tullborg E-L, Winberg A, 2002. Final report of the TRUE Block Scale project, 1. Characterisation and model development. SKB TR-02-13. 224 pp. Svensk Kärnbränslehantering AB.

Bailey J C, 1971. Geochemistry of igneous rocks. Division of petrology, Geology Institute, Copenhagen University, Öster Voldgade 10, DK-1350 Copenhagen., 287 pp.

Baker J H, **1985.** Rare earth and other trace element mobility accompanying albitization in a Proterozoic granite, W. Bergslagen, Sweden, Mineralogical Magazine, 49, Part 1, p. 107–115.

Barnes J D, Selverstone J, Sharp Z D, **2004.** Interactions between serpentinite devolatization, metasomatism and strike-slip strain localization during deep-crustal shearing in the Eastern Alps, Journal of Metamorphic Geology, 22, p. 283–300.

Beane R E, Titley S R, **1981.** Porphyry copper deposits; Part II. Hydrothermal Alteration and Mineralization, Economic Geology, 75th Anniversary Volume, p. 235–269.

Benisek A, Kroll H, Cemic L, **2004.** New developments in two-feldspar thermometry, American Mineralogist, 89, p. 1496–1504.

Bucher K, Frey M, 2002. Petrogenesis of Metamorphic Rocks. Springer-Verlag. Berlin, Heidelberg, 341 pp.

Busenberg E, Clemency C V, **1976.** The dissolution kinetics of feldspars at 25 degrees C and 1 atm CO (sub 2) partial pressure, Geochimica et Cosmochimica Acta, 40, p. 41–49.

Byegård J, Johansson H, Skålberg M, Tullborg E-L, 1998. The interaction of sorbing and non-sorbing tracers with different Äspö rock types, Sorption and diffusion experiments in the laboratory scale. TR-98-18. 111 pp. Svensk Kärnbränslehantering AB.

Byegård J, Tullborg E-L, in manuscript. Sorption experiments and leaching studies using fault gouge material and rim zone material from the Äspö Hard Rock Laboratory. IPR-06-xx. Svensk Kärnbränslehantering AB.

Byegård J, Gustavsson E, Tullborg E-L, Crawford J, in manuscript. Bedrock transport properties. Preliminary site description Laxemar subarea – version 1.2. SKB R-06-xx. Svensk Kärnbränslehantering AB.

Börjesson S, Gustavsson E, 2005. Laboratory data from the site investigation programme for the transport properties of the rock. Data delivery for data freeze Laxemar 2.1. Oskarshamn site investigation. SKB P-05-106. 23 pp. Svensk Kärnbränslehantering AB.

De Albuquerque C A R, **1975.** Partition of trace elements of co-existing biotite, muscovite and potassium feldspar of granitic rocks, northern Portugal, Chemical Geology, 16, p. 89–108.

Debon F, Le F P, **1982.** A chemical-mineralogical classification of common plutonic rocks and associations, Transactions of the Royal Society of Edinburgh: Earth Sciences, 73, p. 135–149.

Deer W A, Howie R A, Zussman J, 1992. An introduction to the rock-forming minerals. Longman Scientific & Technical;Wiley. Harlow, Essex, England; New York, NY, 696 pp.

Dipple G M, Wintsch R P, Andrews M S, **1990.** Identification of the scales of differential element mobility in a ductile fault zone, Journal of Metamorphic Geology, 8, p. 645–661.

Drake H, Tullborg E-L, 2004. Fracture mineralogy and wall rock alteration, results from drill core KSH01A+B. SKB P-04-250. 120 pp. Svensk Kärnbränslehantering AB.

Drake H, Tullborg E-L, 2005. Fracture mineralogy and wall rock alteration, results from drill cores KAS04, KA1755A and KLX02. SKB P-05-174. 69 pp. Svensk Kärnbränslehantering AB.

Drake H, Tullborg E-L, 2006a. Fracture mineralogy, Results from drill core KSH03A+B. SKB P-06-03. Svensk Kärnbränslehantering AB, Submitted to SKB.

Drake H, Tullborg E-L, 2006b. Fracture mineralogy of the Götemar granite, Results from drill cores KKR01, KKR02 and KKR03. SKB P-06-04. Svensk Kärnbränslehantering AB, submitted to SKB.

Drake H, Tullborg E-L, 2006c. Mineralogical, chemical and redox features of red-staining adjacent to fractures, Results from drill core KLX04. SKB P-06-02. Svensk Kärnbränslehantering AB, Submitted to SKB.

Ehrenborg J, Stejskal V, 2004a. Boremap mapping of core drilled boreholes KSH01A and KSH01B. Oskarshamn site investigation. SKB P-04-01. 28 pp. Svensk Kärnbränslehantering AB.

Ehrenborg J, Stejskal V, 2004b. Boremap mapping of core drilled boreholes KSH03A and KSH03B. Oskarshamn site investigation. SKB P-04-132. 24 pp. Svensk Kärnbränslehantering AB.

Eliasson T, 1993. Mineralogy, geochemistry and petrophysics of red coloured granite adjacent to fractures. SKB TR-93-06. 68 pp. Svensk Kärnbränslehantering AB.

Elkins L T, Grove T L, **1990.** Ternary feldspar experiments and thermodynamic models, American Mineralogist, 75, p. 544–559.

Ellis A J, Mahon W A J, 1977. Geochemistry and Geothermal System. Academic Press. New York, N.Y., 392 pp.

Ennis D J, Dunbar N W, Campbell A R, Chapin C E, **2000.** The effects of K-metasomatism on the mineralogy and geochemistry of silicic ignimbrites near Socorro, New Mexico, Chemical Geology, 167, p. 285–312.

Essaifi A, Capdevila R, Fourcade S, Lagarde J L, Ballevre M, Marignac C, **2004.** Hydrothermal alteration, fluid flow and volume change in shear zones; the layered mafic-ultramafic Kettara Intrusion (Jebilet Massif, Variscan Belt, Morocco), Journal of Metamorphic Geology, 22, p. 25–43.

Evansen N M, Hamilton P J, O'Nions R K, **1978.** Rare Earth Abundances in Chondritic Meteorites, Geochimica et Cosmochimica Acta, 42, p. 1199–1212.

Ferry J M, **1979.** Reaction mechanisms, physical conditions, and mass transfer during hydrothermal alteration of mica and feldspar in granitic rocks from South-central Maine, USA, Contributions to Mineralogy and Petrology, 68, p. 125–139.

Frey M, de C C, Liou J G, 1991. A new petrogenetic grid for low-grade metabasites. In,1991, Sixth meeting of the European Union of Geosciences. 3; 1. p. 106. Blackwell Scientific Publications, Oxford, International

Fuhrman M L, Lindsley D H, **1988.** Ternary-feldspar modeling and thermometry, American Mineralogist, 73, p. 201–215.

Gaal G, Gorbatschev R, 1987. An outline of the Precambrian evolution of the Baltic Shield. In,1987, Precambrian geology and evolution of the central Baltic Shield; 1st Symposium on the Baltic Shield. 35. p. 15–52. Elsevier, Amsterdam, International

Gebel A, Stosnach H, Mengel K, Schmidt K H, **1999.** Trace element analysis of granitoid minerals using Laser-Ablation ICP-MS. EUG10, Strasbourg, March 28–April 1, Journal of Conference Abstracts, 4(1), p. 795.

Grant J A, **1986.** The isocon diagram; a simple solution to Gresens' equation for metasomatic alteration, Economic Geology and the Bulletin of the Society of Economic Geologists, 81, p. 1976–1982.

Gresens R L, **1967.** Composition-volume relationships of metasomatism, Chemical Geology, 2, p. 47–65.

Helgeson H C, Murphy W M, Aagaard P, **1984.** Thermodynamic and kinetic constraints on reaction rates among minerals and aqueous solutions; II, Rate constants, effective surface area, and the hydrolysis of feldspar, Geochimica et Cosmochimica Acta, 48, p. 2405–2432.

Holness M B, **2003.** Growth and albitization of K-feldspar in crystalline rocks in the shallow crust: a tracer for fluid circulation during exhumation? Geofluids, 3, p. 89–102.

Horai K i, Simmons G, **1969.** Thermal conductivity of rock-forming minerals, Earth and Planetary Science Letters, 6, p. 359–368.

Horai K i, **1971.** Thermal conductivity of rock-forming minerals, Journal of Geophysical Research, 76, p. 1278–1308.

Hughes C J, **1973.** Spilites, keratophyres, and the igneous spectrum, Geological Magazine, 109, p. 513–527.

Johansson H, 2000, Retardation of tracers in crystalline rocks, PhD Thesis. Series 1582,Chalmers University of Technology, Göteborg, Sweden.

Kastner M, Siever R, **1979.** Low temperature feldspars in sedimentary rocks, American Journal of Science, 279, p. 435–479.

Kelokaski M, Oila E, Siitari-Kauppi M, 2001. Investigation of porosity and microfracturing in granitic fracture wall rock and fault breccia specimens using the PMMA technique, TRUE Block Scale project, Äspö Hard Rock Laboratory. 57 pp. Svensk Kärnbränslehantering AB.

Kerrich R, Fryer B J, **1979.** Archaean precious-metal hydrothermal systems, Dome Mine, Abitibi greenstone belt; II, REE and oxygen isotope relations, Canadian Journal of Earth Sciences = Journal Canadien des Sciences de la Terre, 16, p. 440–458.

Kornfält K A, Wikman H, 1987. Description of the map of solid rocks around Simpevarp. SKB PR-25-87-02. 45 pp. Svensk Kärnbränslehantering AB.

Kornfält K A, Persson P O, Wikman H, **1997.** Granitoids from the Äspo area, southeastern Sweden; geochemical and geochronological data, Gff, 119, p. 109–114.

Krauskopf K B, Bird D K, 1995. Introduction to Geochemistry, third edition. McGraw-Hill Book Co. Singapore. 647 pp.

Kresten P, Chyssler J, **1976,** The Götemar Massif in south-eastern Sweden; a reconnaissance survey, Geologiska Föreningen i Stockholm Förhandlingar, 98, Part 2, p. 155–161.

Lagache M, Weisbrod A, **1977.** The system: two alkali feldspars-KCl-NaCl-H (sub 2) O at moderate to high temperatures and low pressures, Contributions to Mineralogy and Petrology, 62, p. 77–101.

Landström O, Tullborg E-L, 1991. Results of mineralogical studies and trace element analyses (U, Th and REEs) of fracture coatings, groundwaters and rock samples. In: Tullborg E-L, Wallin B, and Landström O, (1991); Hydrogeochemical studies of fracture minerals from water conducting fractures and deep groundwaters at Äspö. SKB PR-25-90-01. pp. Svensk Kärnbränslehantering AB.

Landström O, Tullborg E-L, 1995. Interactions of trace elements with fracture filling minerals from the Äspö Hard Rock Laboratory. SKB TR-95-13. 71 pp. Svensk Kärnbränslehantering AB.

Landström O, Tullborg E-L, Eriksson G, Sandell Y, 2001. Effects of glacial/post-glacial weathering compared with hydrothermal alteration - implications for matrix diffusion. Results from drillcore studies in porphyritic quartz monzodiorite from Äspö SE Sweden. SKB R-01-37. 60 pp. Svensk Kärnbränslehantering AB.

Larson S A, Berglund J, **1992.** A chronological subdivision of the Transscandinavian igneous belt three magmatic episodes? Geologiska Föreningen i Stockholm Förhandlingar, p. 459–461.

Larsson D, Gronvold K, Oskarsson N, Gunnlaugsson E, **2002.** Hydrothermal alteration of plagioclase and growth of secondary feldspar in the Hengill volcanic centre, SW Iceland, Journal of Volcanology and Geothermal Research, 114, p. 275–290.

Le Maitre R W (Ed.), 1989. A Classification of Igneous Rocks and Glossery of Terms. Oxford, Blackwell. 193 pp.

Le Maitre R W (Ed.), 2002. Igneous Rocks: A Classification and Glossary of Terms: Recommendations of the International Union of Geological Sciences Subcommission on the Systematics of Igneous Rocks. Cambridge University Press. 240 pp.

Lee M R, Parsons I, **1997.** Dislocation formation and albitization in alkali feldspars from the Shap Granite, American Mineralogist, 82, p. 557–570.

Lee M R, Parsons I, **1998.** Microtextural controls of diagenetic alteration of detrital alkali feldspars; a case study of the Shap Conglomerate (Lower Carboniferous), Northwest England, Journal of Sedimentary Research, Section A: Sedimentary Petrology and Processes, 68, p. 198–211.

Liou J G, Kim H S, Maruyama S, **1983.** Prehnite - epidote equilibria and their petrologic applications, Journal of Petrology, 24, p. 321–342.

Ludden J, Gelinas L, Trudel P, **1982.** Archean metavolcanics from the Rouyn-Noranda District, Abitibi greenstone belt, Quebec; 2, Mobility of trace elements and petrogenetic constraints, Canadian Journal of Earth Sciences = Journal Canadien des Sciences de la Terre, 19, p. 2276–2287.

Maddock R H, Hailwood E A, Rhodes E J, Muir Wood R, 1993. Direct fault dating trials at the Äspö Hard Rock Laboratory. SKB TR-93-24. 189 pp. Svensk Kärnbränslehantering AB.

Maghraoui M E, Joron J L, Raimbault L, Treuil M, **2002.** Element mobility during metasomatism of granitic rocks in the Saint-Chely d'Apcher area (Lozere, France), Environment International, 28, p. 349–357.

Marquer D, Burkhard M, 1992. Fluid circulation, progressive deformation and mass-transfer processes in the upper crust; the example of basement-cover relationships in the External Crystalline Massifs, Switzerland. In,1992, Mechanical instabilities in rocks and tectonics; a selection of papers. 14; 8–9. p. 1047–1057. Pergamon, Oxford-New York, International

Mattsson H, Thunehed H, 2004. Interpretation of geophysical borehole data and compilation of petrophysical data from KSH02 (80–1,000 m) and KAV01. Oskarshamn site investigation. SKB P-04-77. 70 pp. Svensk Kärnbränslehantering AB.

Mazurek M, Bossart P, Eliasson T, 1995. Classification and characterization of water-conducting fractures at Äspö: Results of phase 1 investigations. SKB PR 25-95-03. 76 pp. Svensk Kärnbränslehantering AB.

Middelburg J J, Van d W C H, Woittiez J R W, **1988.** Chemical processes affecting the mobility of major, minor and trace elements during weathering of granitic rocks, Chemical Geology, 68, p. 253–273.

Mongelli G, **1993.** REE and other trace elements in a granitic weathering profile from "Serre", southern Italy, Chemical Geology, 103, p. 17–25.

Morad S, Bergan M, Knarud R, Nystuen J P, **1990.** Albitization of detrital plagioclase in Triassic reservoir sandstones from the Snorre Field, Norwegian North Sea, Journal of Sedimentary Petrology, 60, p. 411–425.

Nekvasil H, Burnham C W, 1987. The calculated individual effects of pressure and water content on phase equilibria in the granite system. In,1987, Magmatic processes; physico-chemical principles; a volume in honor of Hatten S Yoder, Jr. 1. p. 433–445. Geochemical Society, University Park, PA, United States.

Nesbitt H W, **1979.** Mobility and fractionation of rare earth elements during weathering of a granodiorite, Nature (London), 279, p. 206–210.

Nesbitt H W, Markovics G, **1997.** Weathering of granodioritic crust, long-term storage of elements in weathering profiles, and petrogenesis of siliciclastic sediments, Geochimica et Cosmochimica Acta, 61, p. 1653–1670.

Nilsson K P, Bergman T, Eliasson T, 2004. Bedrock mapping 2004 – Laxemar subarea and regional model area. Outcrop data and description of rock types. Oskarshamn site investigation. SKB P-04-221. pp. Svensk Kärnbränslehantering AB.

O'Neil J R, **1977.** Stable isotopes in mineralogy, Physics and Chemistry of Minerals, 2, p. 105–123.

Orville P M, **1963.** Alkali ion exchange between vapor and feldspar phases, American Journal of Science, 261, p. 201–237.

Parneix J C, Beaufort D, Dudoignon P, Meunier A, **1985.** Biotite chloritization process in hydrothermally altered granites, Chemical Geology, 51, p. 89–101.

Parry W T, Downey L M, **1982.** Geochemistry of hydrothermal chlorite replacing igneous biotite, Clays and Clay Minerals, 30, p. 81–90.

Petersson J, Eliasson T, **1997.** Mineral evolution and element mobility during episyenitization (dequartzification) and albitization in the postkinematic Bohus Granite, southwest Sweden, Lithos, 42, p. 123–146.

Puigdomenech I, Ambrosi J-P, Eisenlohr L, Lartigue J-E, Banwart S A, Bateman K, Milodowski A E, West J M, Griffault L, Gustafsson E, Hama K, Yoshida H, Kotelnikova S, Pedersen K, Michaud V, Trotignon L, Rivas Perez J, 2001.
O_2 depletion in granitic media. The REX project. SKB TR-01-05. 86 pp.
Svensk Kärnbränslehantering AB.

Putnis A, 2002. Mineral replacement reactions; from macroscopic observations to microscopic mechanisms. In,2002, Mineralogy for the new millennium. 66; 5. p. 689–708. Mineralogical Society, London, United Kingdom.

Raimbault L, Burnol L, 1998. The Richemont rhyolite dyke, Massif Central, France; a subvolcanic equivalent of rare-metal granites. In,1998, Granitic pegmatites; the Cerny-Foord volume. 36, Part 2. p. 265–282. Mineralogical Association of Canada, Ottawa, ON, Canada.

Saigal G C, Morad S, Bjorlykke K, Egeberg P K, Aagaard P, **1988.** Diagenetic albitization of detrital K-feldspar in Jurassic, Lower Cretaceous, and Tertiary clastic reservoir rocks from offshore Norway; I, Textures and origin, Journal of Sedimentary Petrology, 58, p. 1003–1013.

Savukoski M, 2004. Drill hole KLX04A. Determining of porosity by water saturation and density by buoyancy technique. Oskarshamn site investigation. SKB P-04-268. 28 pp. Svensk Kärnbränslehantering AB.

Savukoski M, 2005a. Drill hole KLX03A. Determination of porosity by water saturation and density by buoyancy technique. Oskarshamn site investigation. SKB P-05-94. 26 pp. Svensk Kärnbränslehantering AB.

Savukoski M, 2005b. Drill hole KLX05A. Determination of porosity by water saturation and density by buoyancy technique. Oskarshamn site investigation. SKB P-05-127. 28 pp. Svensk Kärnbränslehantering AB.

Savukoski M, Carlsson L, 2004. Drill hole KSH01A. Determining of porosity by water saturation and density by buoyancy technique. Oskarshamn site investigation. SKB P-04-56. 30 pp. Svensk Kärnbränslehantering AB.

Slaby E, Lensch G, Mihm A, **1990.** Metasomatic aplites from Rauschermuehle and Kreimbach, Palatinate, West Germany, Neues Jahrbuch fuer Mineralogie, Monatshefte. 1990, p. 343–352.

Slaby E, **1992.** Changes in the structural state of secondary albite during progressive albitization, Neues Jahrbuch fuer Mineralogie, Monatshefte. 1992, p. 321–335.

Spear F S, **1993.** Metamorphic phase equilibria and pressure-temperature-time paths., Mineralogical Society of America Monograph Series, 1, p. 799.

Stanfors R, Rhen I, Tullborg E L, Wikberg P, 1999. Overview of geological and hydro-geological conditions of the Aspo Hard Rock Laboratory site. In,1999, Geochemistry of the Aspo Hard Rock Laboratory, Sweden. 14; 7. p. 819–834. Pergamon, Oxford-New York-Beijing, International

Stosnach H, Mengel K, 1998. An assessment of the distribution of trace elements in Äspö granitoids: Implication for the use of granites as geological barrier. HRL 98-02. pp.

Streckeisen A, **1976.** To each plutonic rock its proper name, Earth-Science Reviews, 12, p. 1–33.

Streckeisen A, **1978.** IUGS Subcommission on the Systematics of Igneous Rocks; classification and nomenclature of volcanic rocks, lamprophyres, carbonatites and melilitic rocks; recommendation and suggestions, Neues Jahrbuch fuer Mineralogie, Abhandlungen. 134, p. 1–14.

Sundberg J, Gabrielsson A, 1999. Laboratory and field measurements of thermal properties of the rocks in the prototype repository at Äspö HRL. IPR-99-17. 67 pp. Svensk Kärnbränslehantering AB.

Sverjensky D A, **1983.** Europium redox equilibria in aqueous solution, Earth and Planetary Science Letters, Volume 67, p. 70–78.

Taboada T, Garcia C, **1999.** Pseudomorphic transformation of plagioclases during the weathering of granitic rocks in Galicia (NW Spain), Catena, 35, p. 291–302.

Tullborg E-L, 1995. Chapter 4. Mineralogical/Geochemical Investigations in the Fracture Zone. In: Banwart S,1995, The Redox experiment in block scale. SKB PR 25-95-06. p. 81–101. Svensk Kärnbränslehantering AB.

Tullborg E L, 1997. Recognition of low-temperature processes in the Fennoscandian Shield: Doctoral thesis, Earth Science Centre A17, Göteborg University, 35 pp.

Tullborg E-L, 2002. Matrix Fluid Chemistry Report, Borehole KF0051A01:4 – Results from chemical and SEM/EDS analyses and porosity/density measurements, Äspö Hard Rock Laboratory. SKB ITD-02-04. 18 pp. Svensk Kärnbränslehantering AB.

Tullborg E-L, Larson S Å, **2005.** Porosity in crystalline rocks – a matter of scale, Engineering geology, in press, p.

Tulloch A J, **1979.** Secondary Ca-Al silicates as low-grade alteration products of granitoid biotite, Contributions to Mineralogy and Petrology, 69, p. 105–117.

Wahlgren C-H, Ahl M, Sandahl K-A, Berglund J, Petersson J, Ekström M, Persson P-O, 2004. Bedrock mapping 2003 – Simpevarp subarea. Outcrop data, fracture data, modal and geochemical classification of rock types, bedrock map, radiometric dating. Oskarshamn site investigation. SKB P-04-102. 59 pp. Svensk Kärnbränlehantering AB.

Van Baalen M R, 1993. Titanium mobility in metamorphic systems; a review. In,1993, Geochemistry of accessory minerals; papers presented at the Third V M Goldschmidt conference. 110; 1–3. p. 233–249. Elsevier, Amsterdam, Netherlands.

van der Weijden C H, van der Weijden R D, 1995. Mobility of major, minor and some redox-sensitive trace elements and rare-earth elements during weathering of four granitoids in central Portugal, Chemical Geology, 125, p. 149–167.

van Gaans P F M, Vriend S P, Poorter R P E, 1995. Hydrothermal processes and shifting element association patterns in the W-Sn enriched granite of Regoufe, Portugal. In,1995, Geochemical exploration 1993. 55; 1–3. p. 203–222. Elsevier, Amsterdam-New York, International.

Wilamowski A, **2002.** Chloritization and polytypism of biotite in the Lomnica granite, Karkonosze Massif, Sudetes, Poland: Stable isotope evidence, Chemical Geology, 182, p. 529–547.

Wollast R, Chou L, 1985. Kinetic study of the dissolution of albite with a continuous flow-through fluidized bed reactor. In,1985, The chemistry of weathering. Series C: Mathematical and Physical Sciences. 149. p. 75–96. D Reidel Publishing Company, Dordrecht-Boston, International.

Åberg G, **1978.** A geochronological study of the Precambrian of southeastern Sweden., Geologiska Föreningens i Stockholm Förhandlingar, 100, p. 125–154.

Åberg G, **1988.** Middle Proterozoic anorogenic magmatism in Sweden and worldwide., Lithos, p. 279–289.

Åberg G, Löfvendahl R, Levi B, **1984.** The Götemar granite-isotopic and geochemical evidence for a complex history of an anorogenic granite, Geologiska Föreningen i Stockholm Förhandlingar, 106, p. 327–333.

Åhäll K I, Larson S A, **2000.** Growth-related 1.85–1.55 Ga magmatism in the Baltic Shield; a review addressing the tectonic characteristics of Svecofennian, TIB 1-related, and Gothian events, GFF, 122, p. 193–206.

Åhäll K-I, 2001. Åldersbestämning av svårdaterade bergarter i sydöstra Sverige. SKB R-01-60. 28 pp. Svensk Kärnbränslehantering AB.

Appendix 1

Element changes for each sample

In this section the normative element changes (from absolute concentrations) of selected elements in each sample is presented.

Sample KSH03 – 62

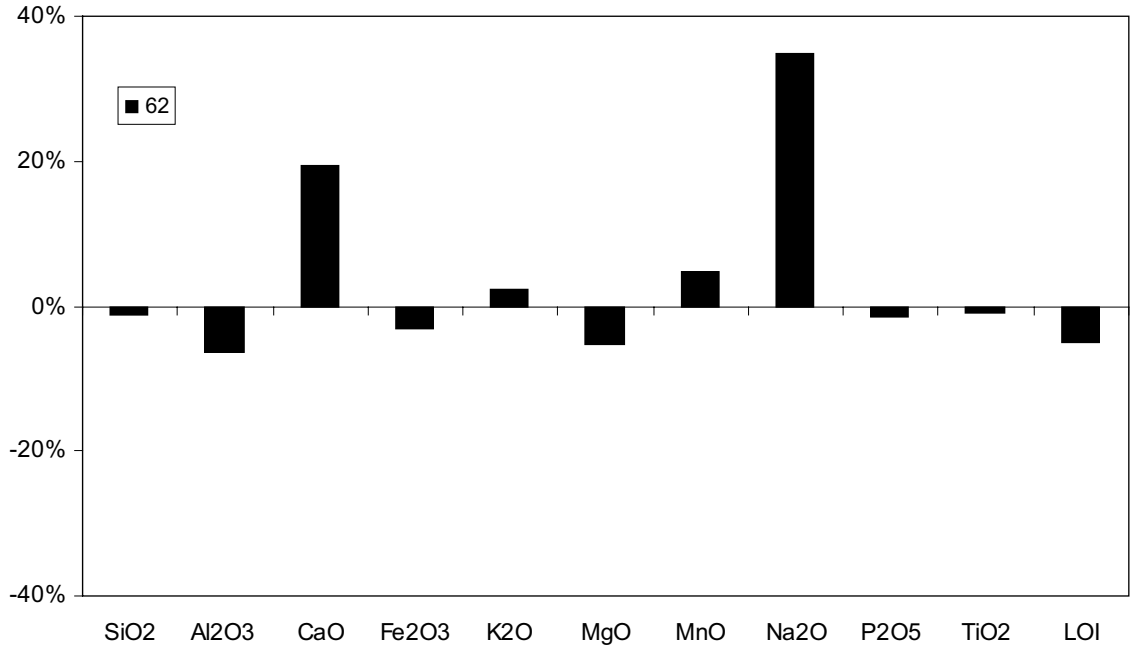

***62**: Major elements, minor elements and loss on ignition (LOI).*

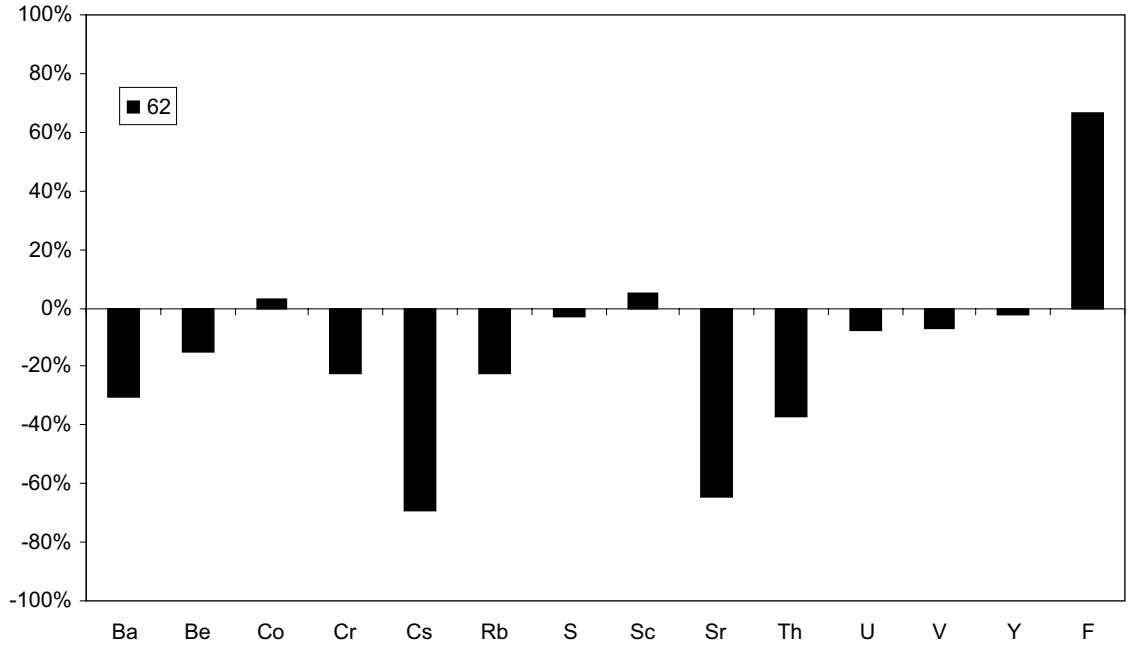

***62**: Selected trace elements.*

Sample KSH03 – 81

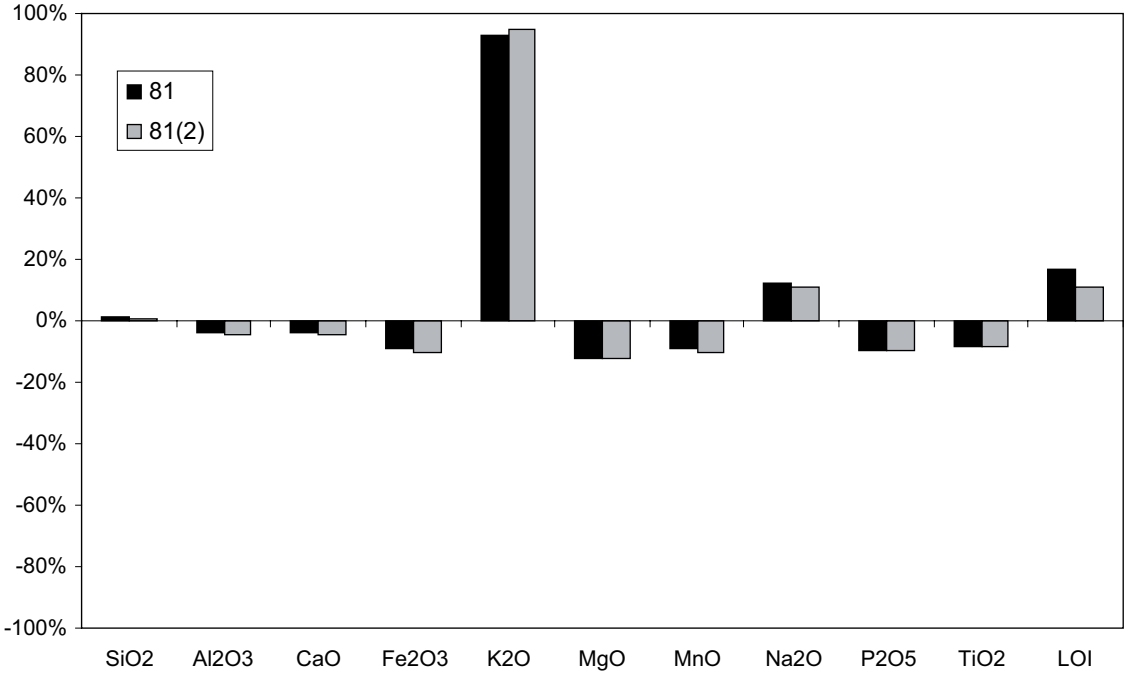

***81**: Double analyses of major elements, minor elements and loss on ignition (LOI).*

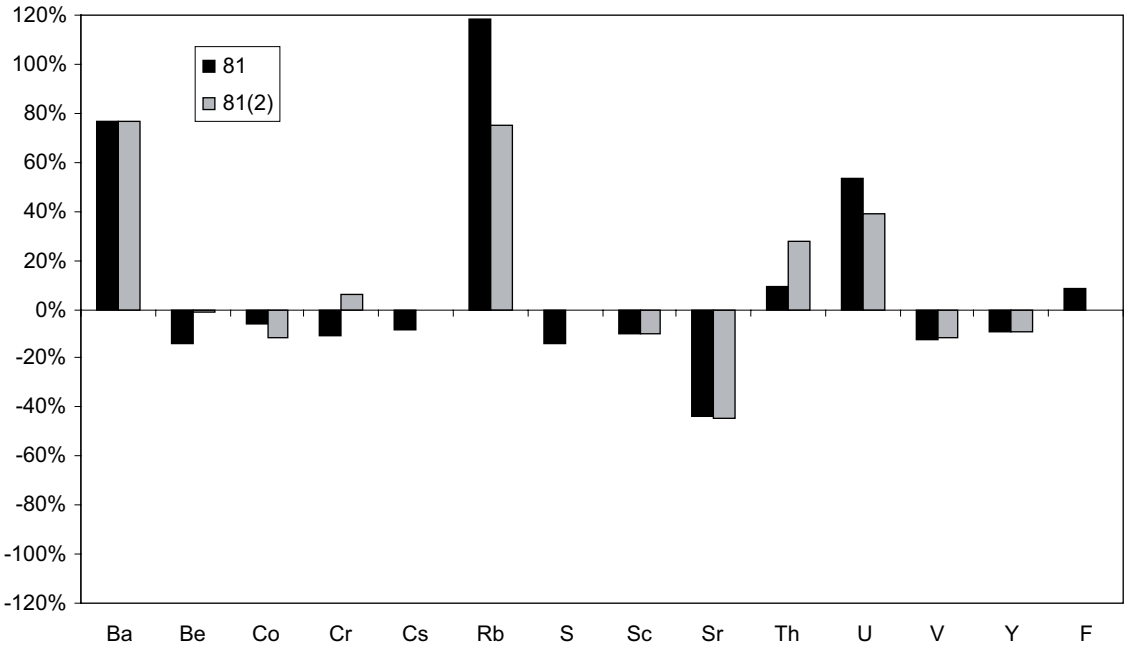

***81**: Double analyses of selected trace element, excluding Cs, S and F in the second analysis.*

Sample KSH03 – 82

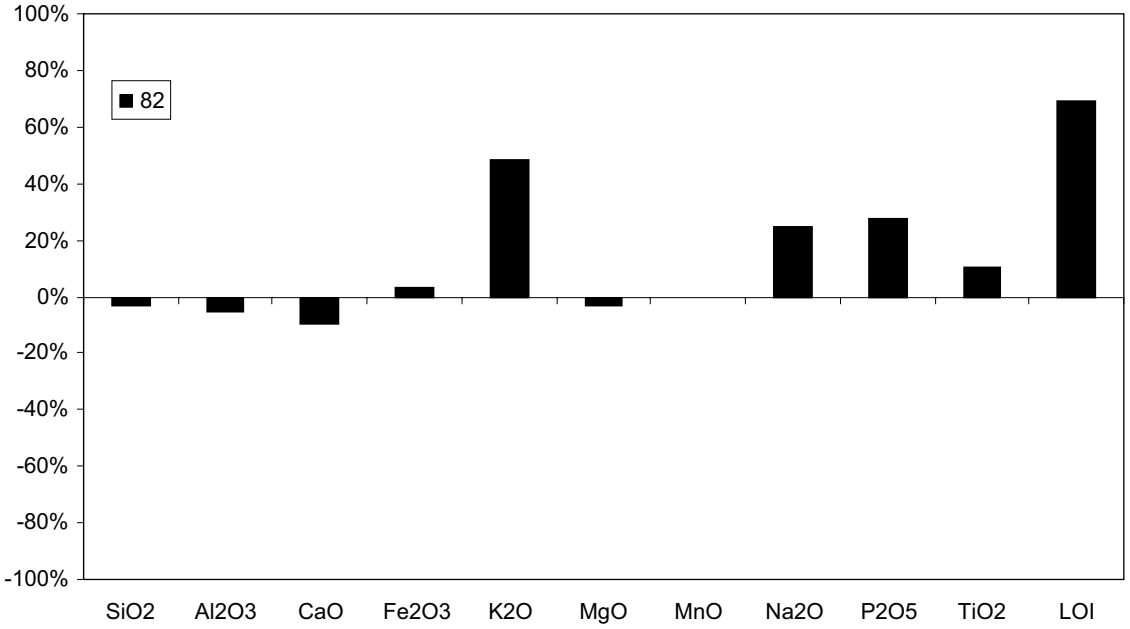

***82**: Major elements, minor elements and loss on ignition (LOI).*

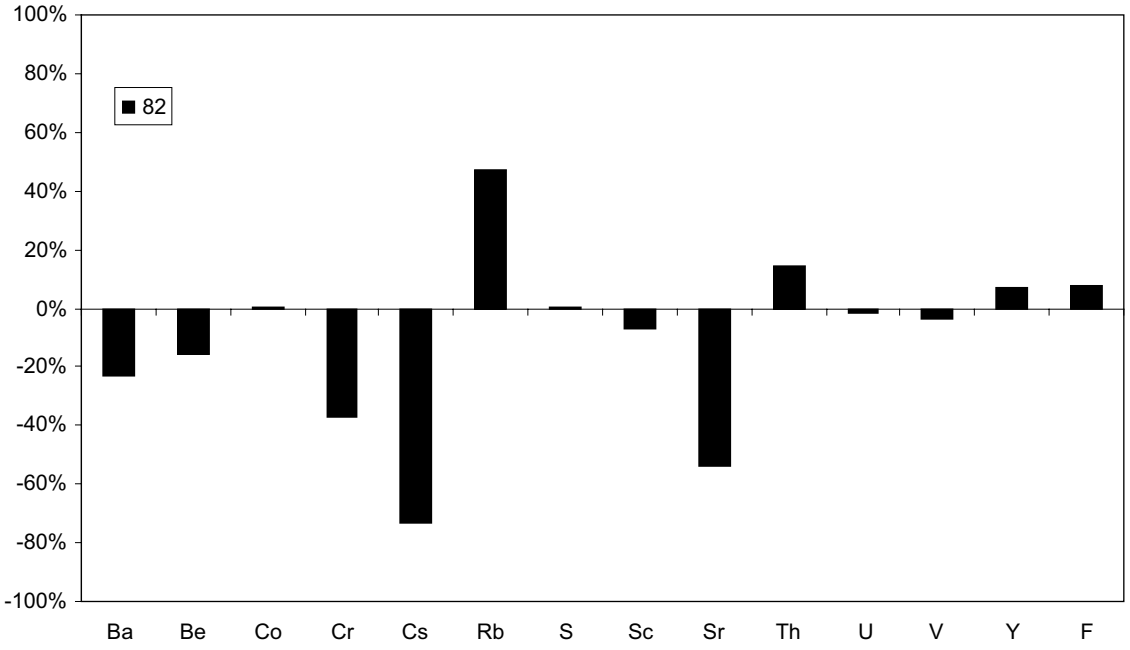

***82**: Selected trace elements.*

Sample KSH03 – 100

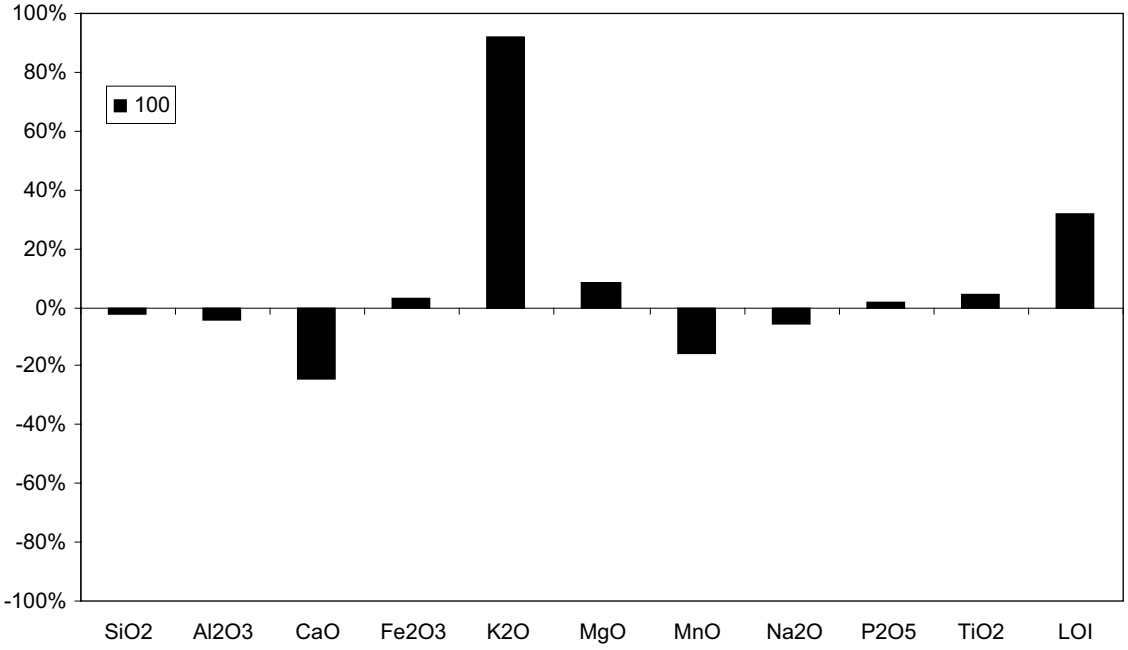

100: *Major elements, minor elements and loss on ignition (LOI).*

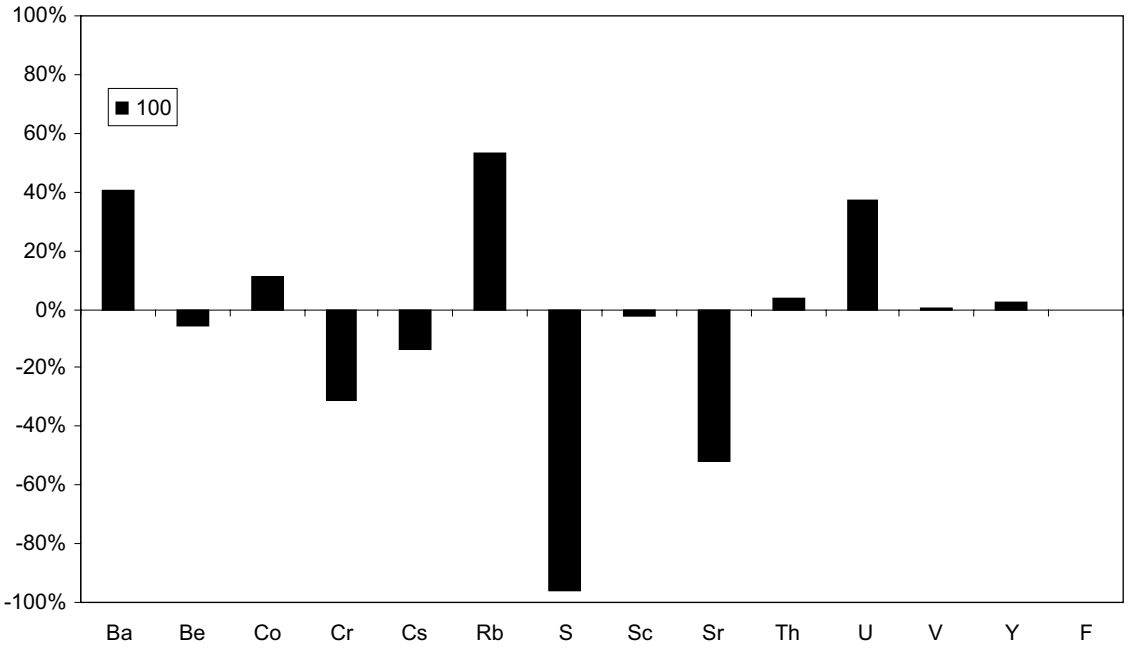

100*: Selected trace elements.*

Sample KSH03 – 128

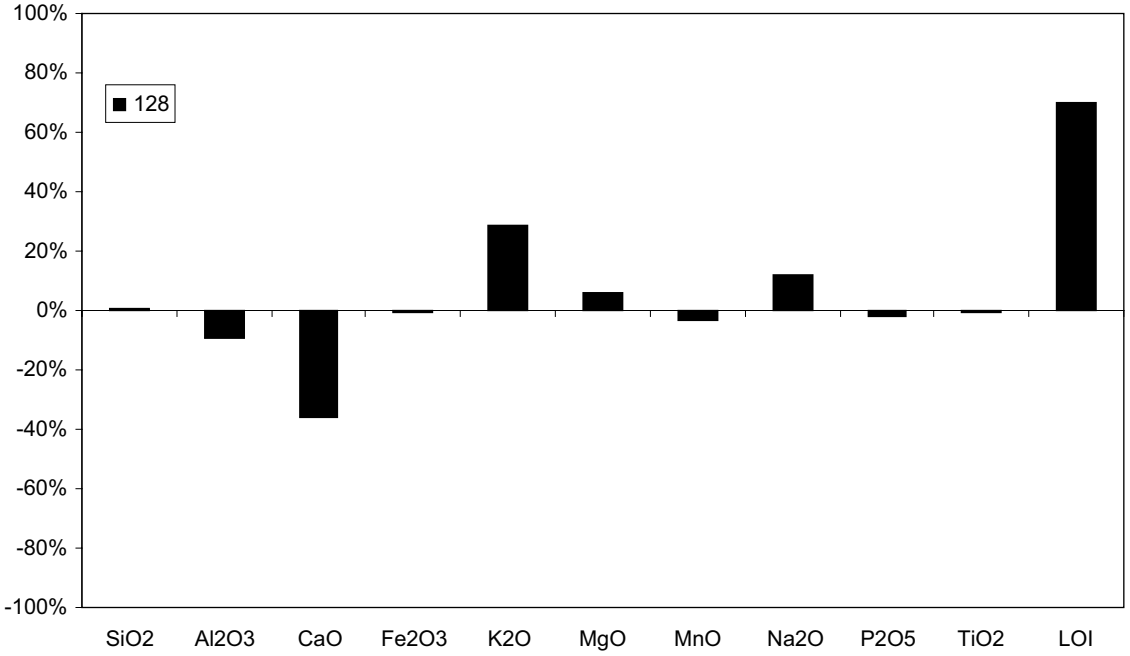

***128**: Major elements, minor elements and loss on ignition (LOI).*

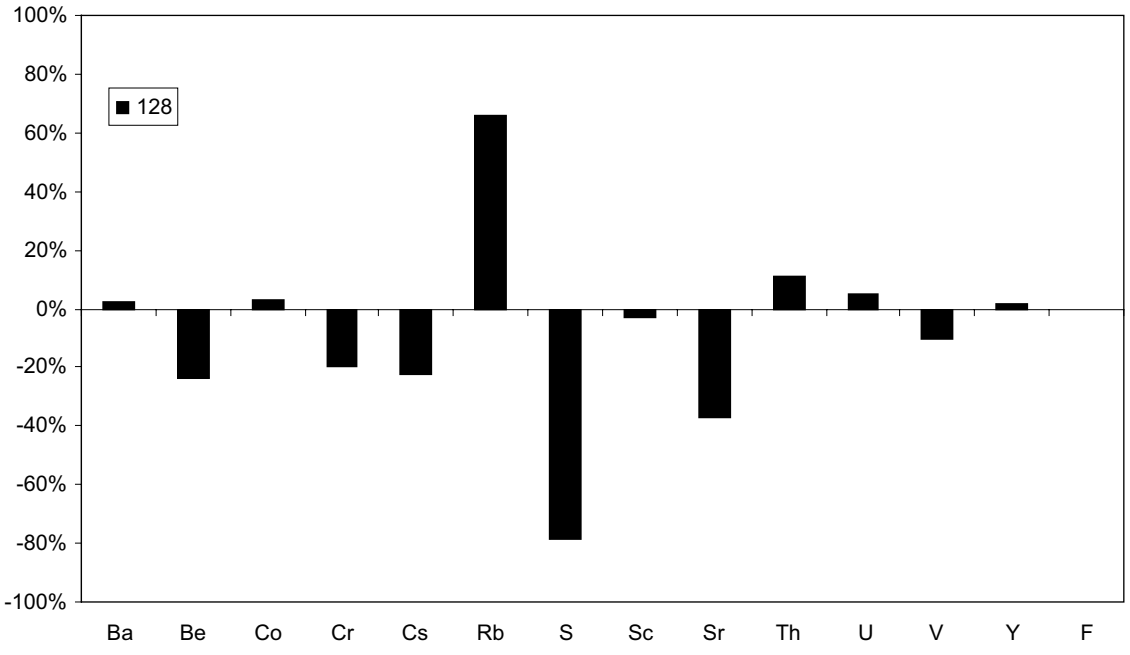

***128**: Selected trace elements.*

Sample KSH03 – 144

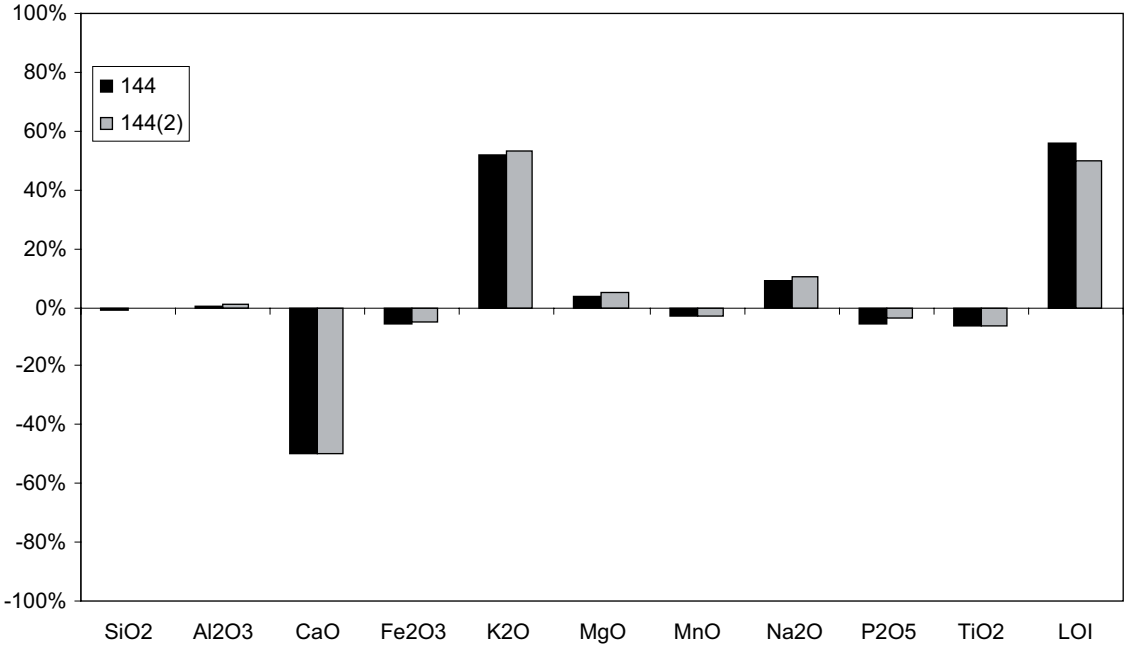

***144**: Double analyses of major elements, minor elements and loss on ignition (LOI).*

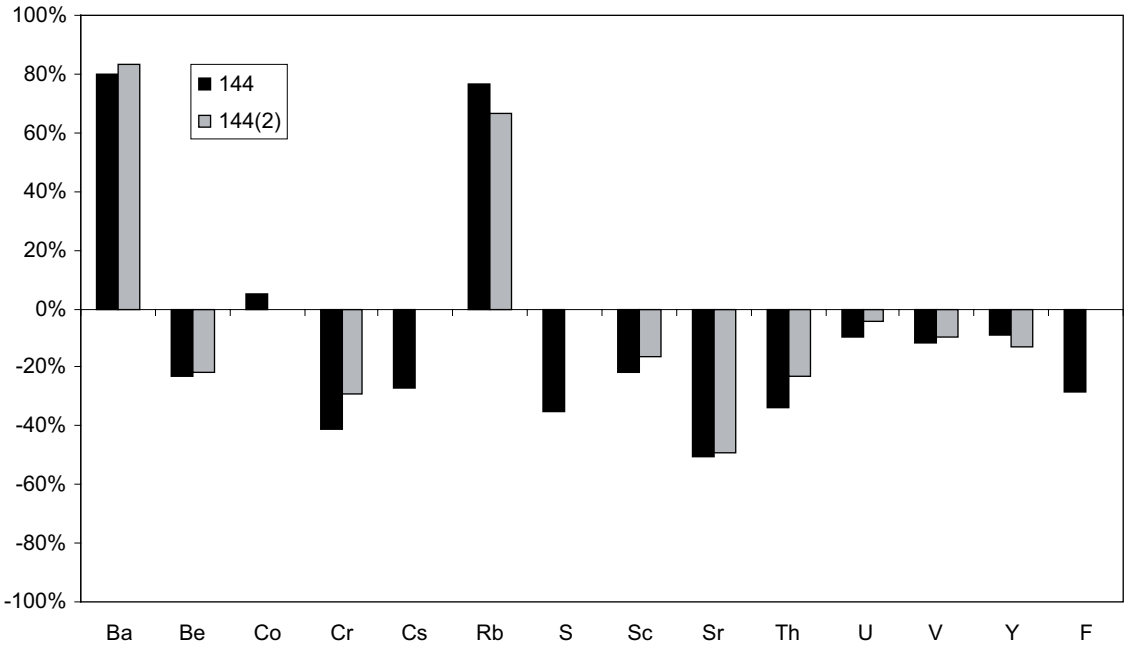

***144**: Double analyses of selected trace element, excluding Cs, S and F in the second analysis.*

Sample KSH03 – 172

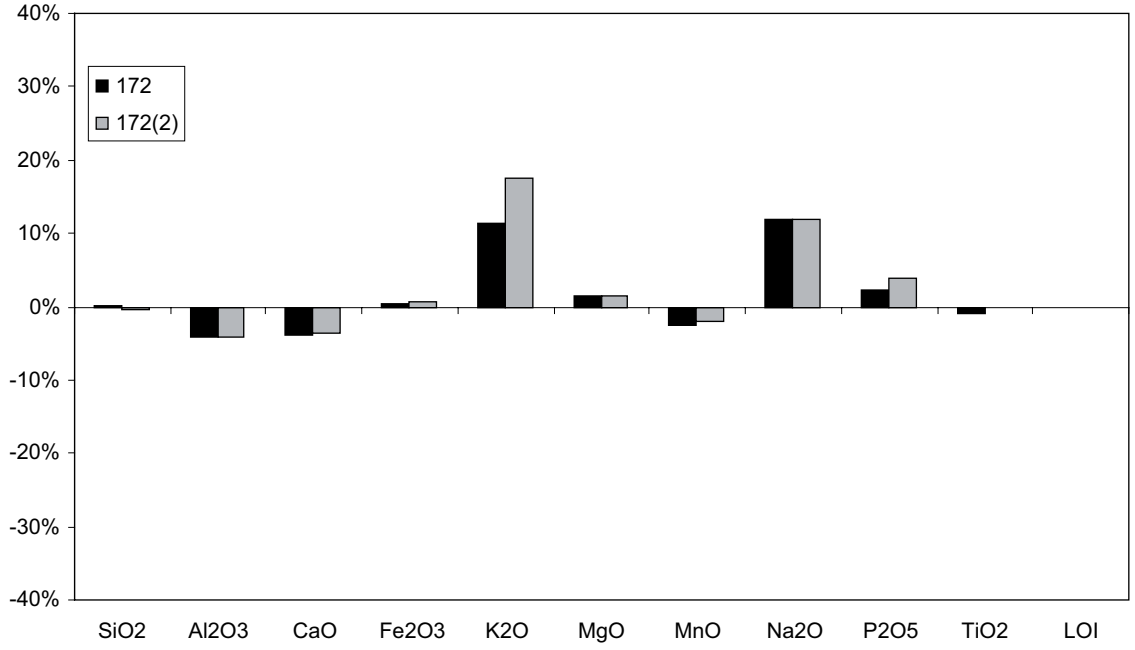

***172**: Double analyses of major elements, minor elements and loss on ignition (LOI).*

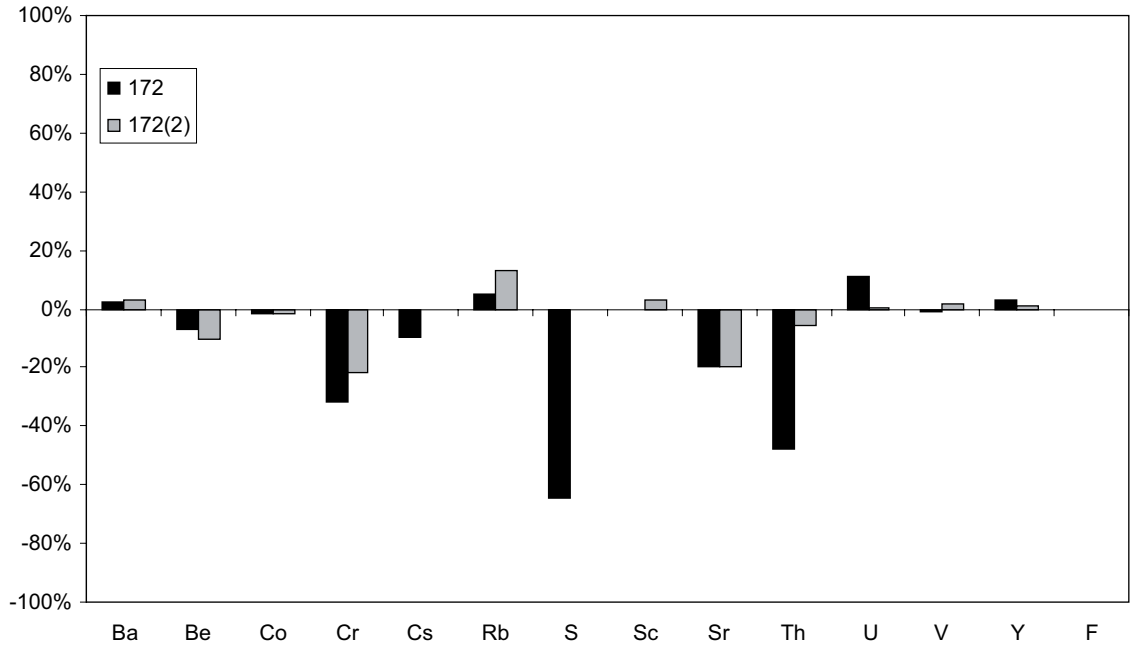

***172**: Double analyses of selected trace element, excluding Cs, S and F in the second analysis.*

Sample KSH03 – 372

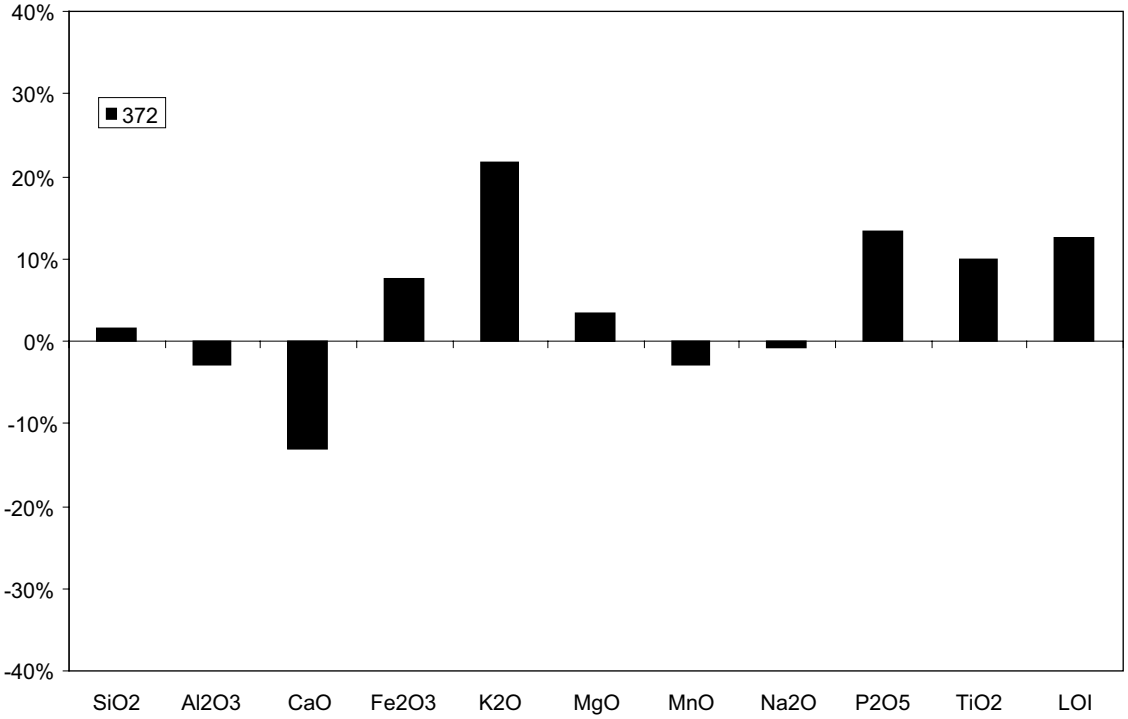

***372**: Major elements, minor elements and loss on ignition (LOI).*

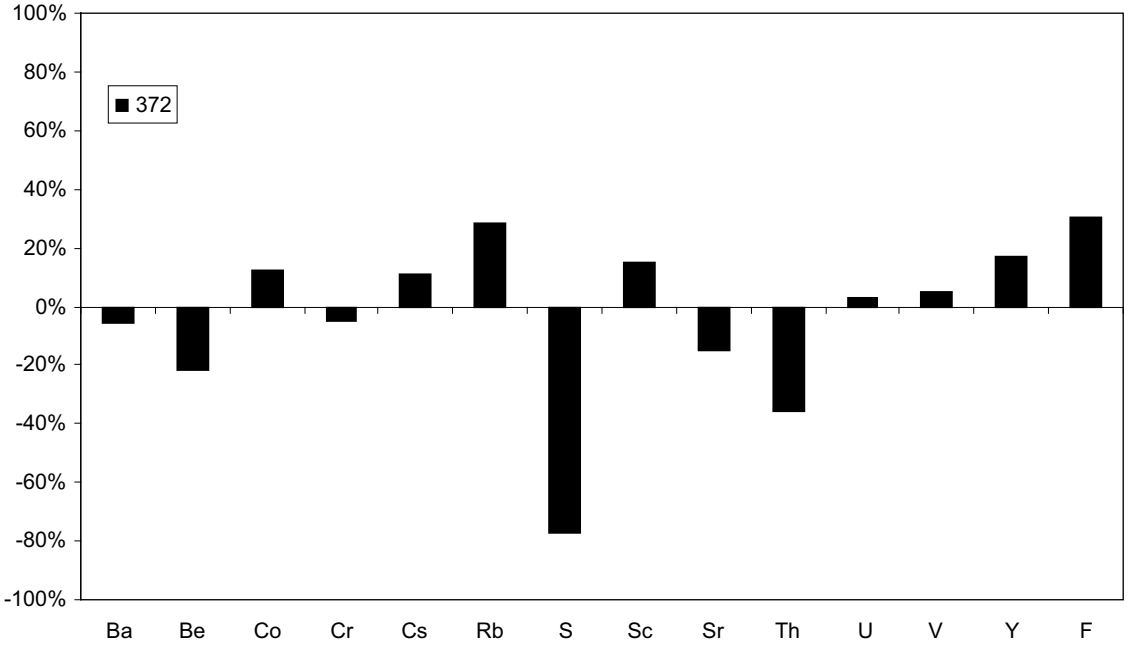

***372**: Selected trace elements.*

Sample KSH03 – 394

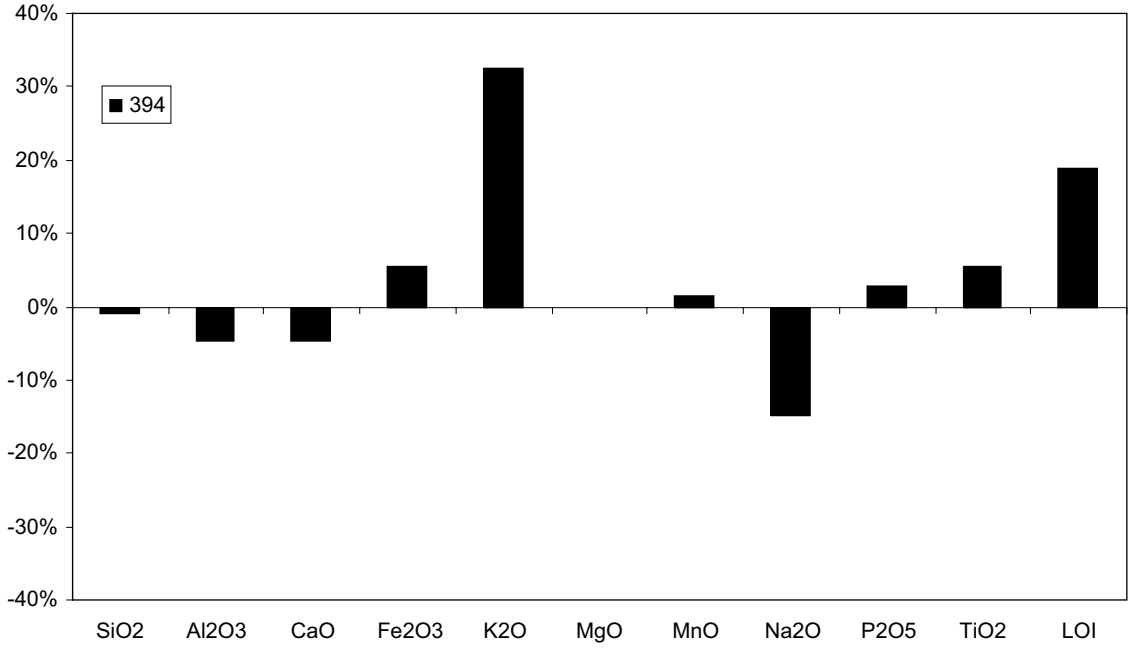

***394**: Major elements, minor elements and loss on ignition (LOI).*

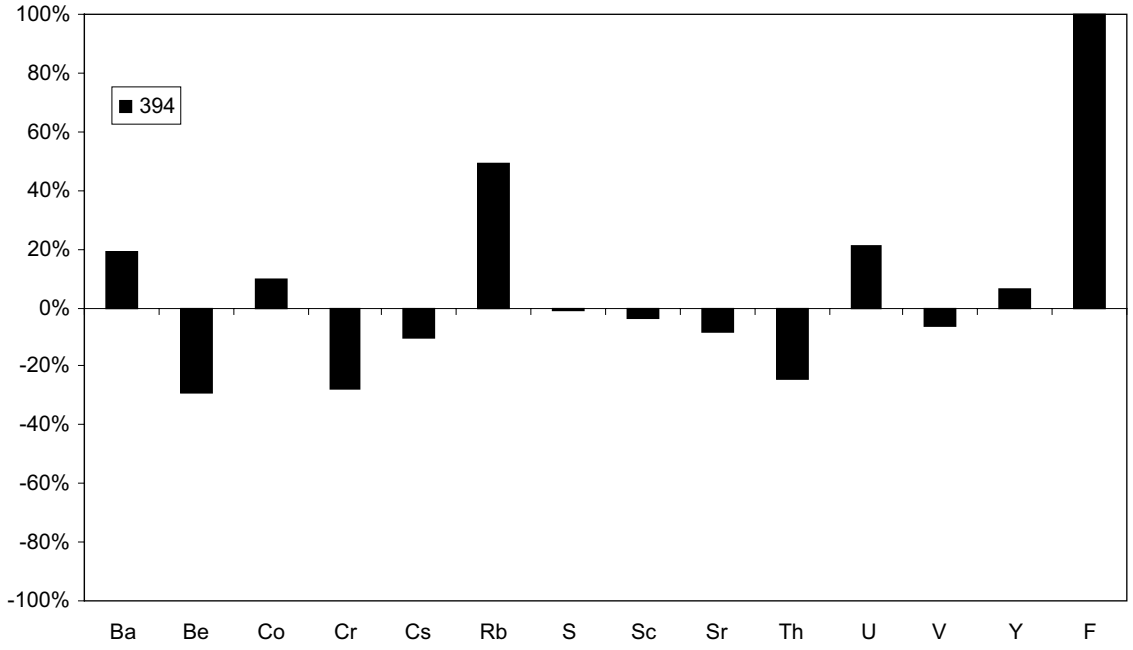

***394**: Selected trace elements.*

Sample KSH03 – 661

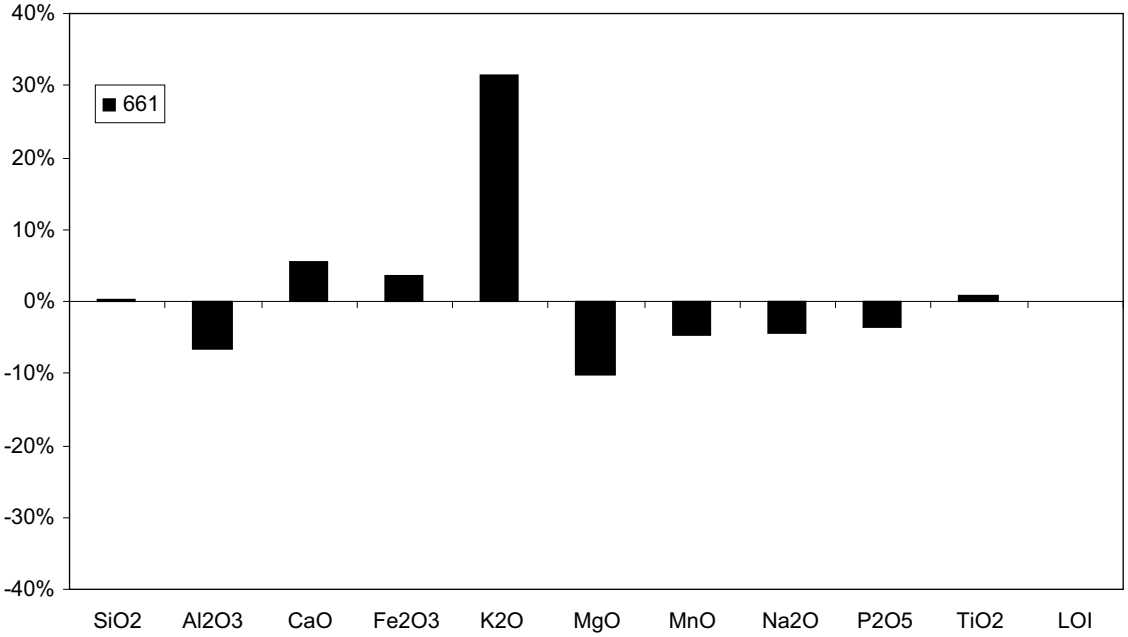

***661**: Major elements, minor elements and loss on ignition (LOI).*

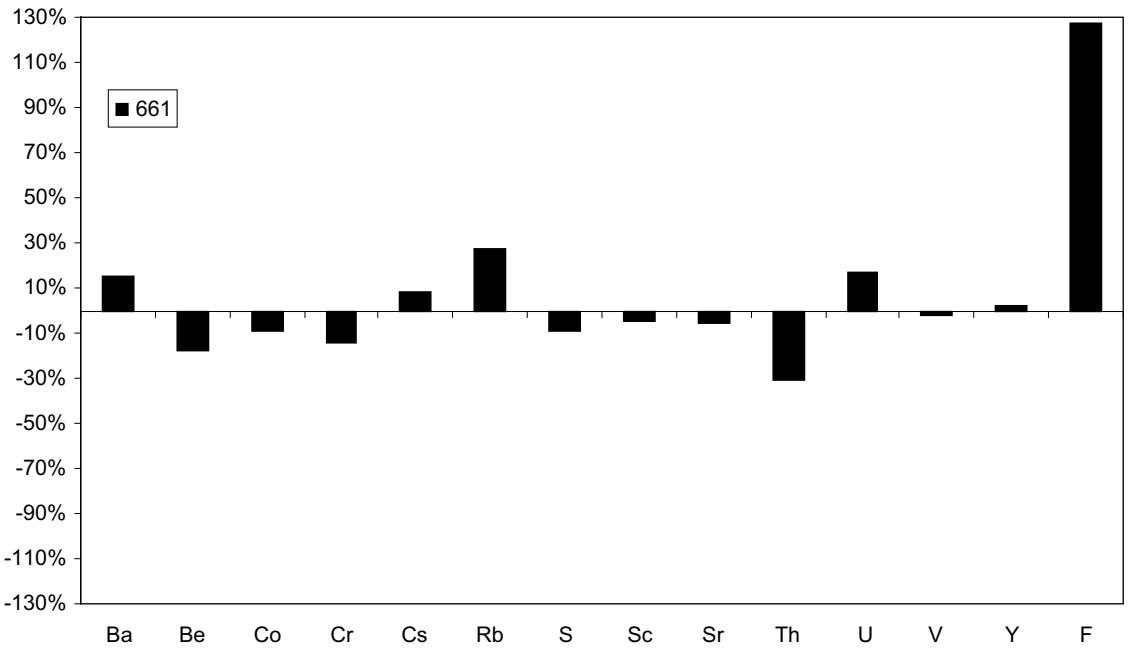

***661**: Selected trace elements.*

Sample KSH01 – 536-1

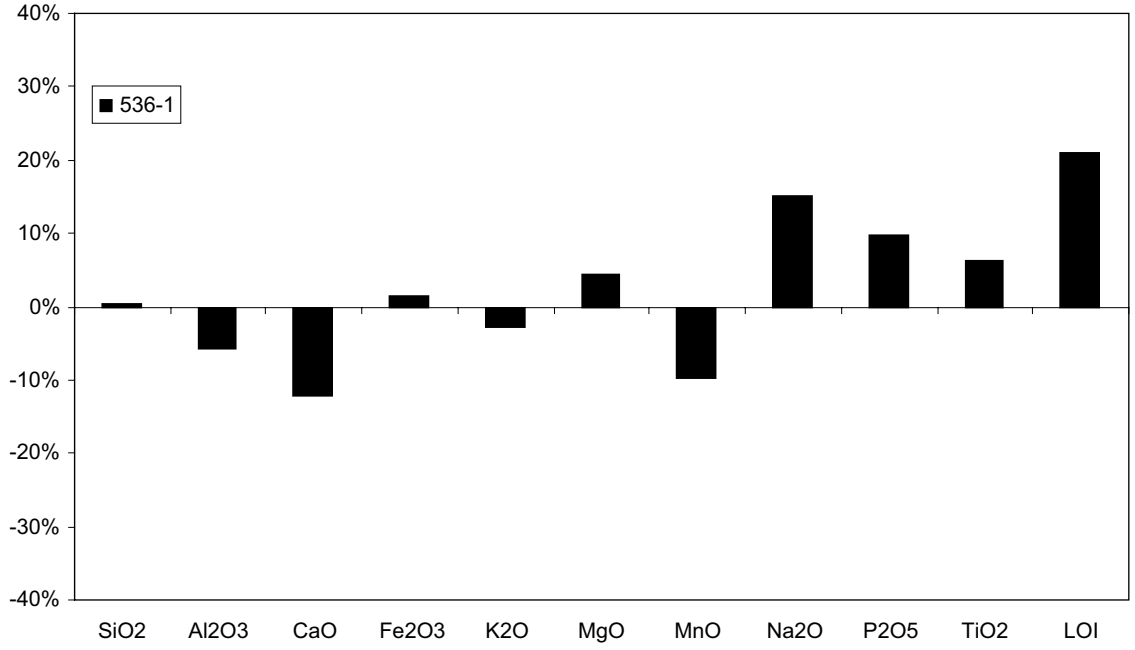

536-1: *Major elements, minor elements and loss on ignition (LOI).*

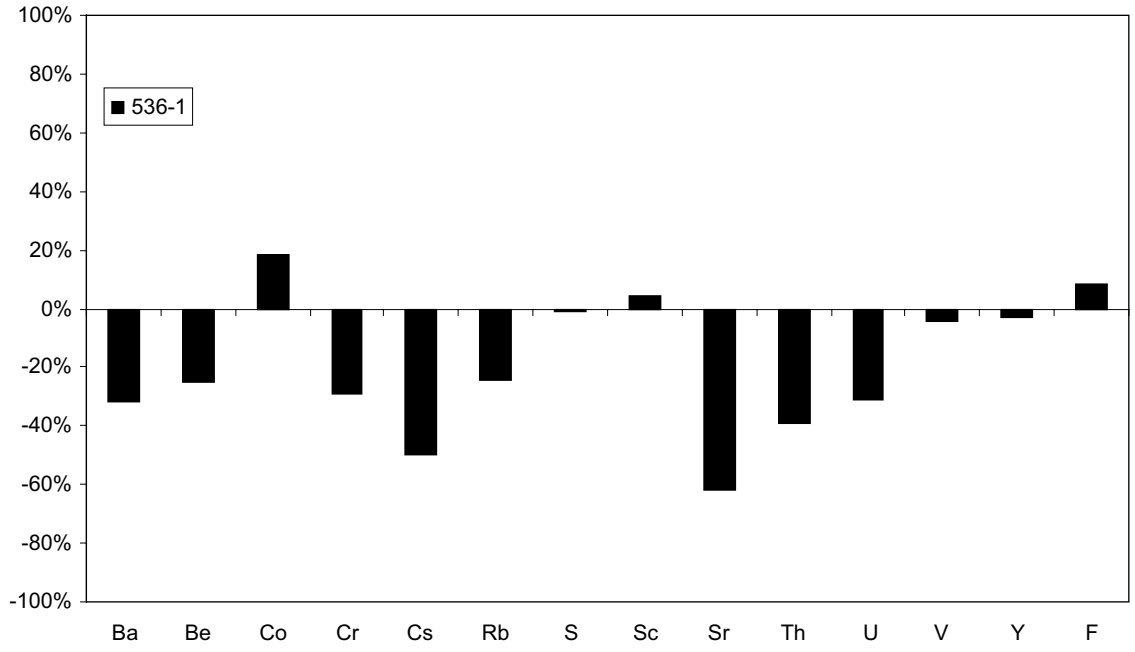

536-1*: Selected trace elements.*

Sample KSH01 – 536-2

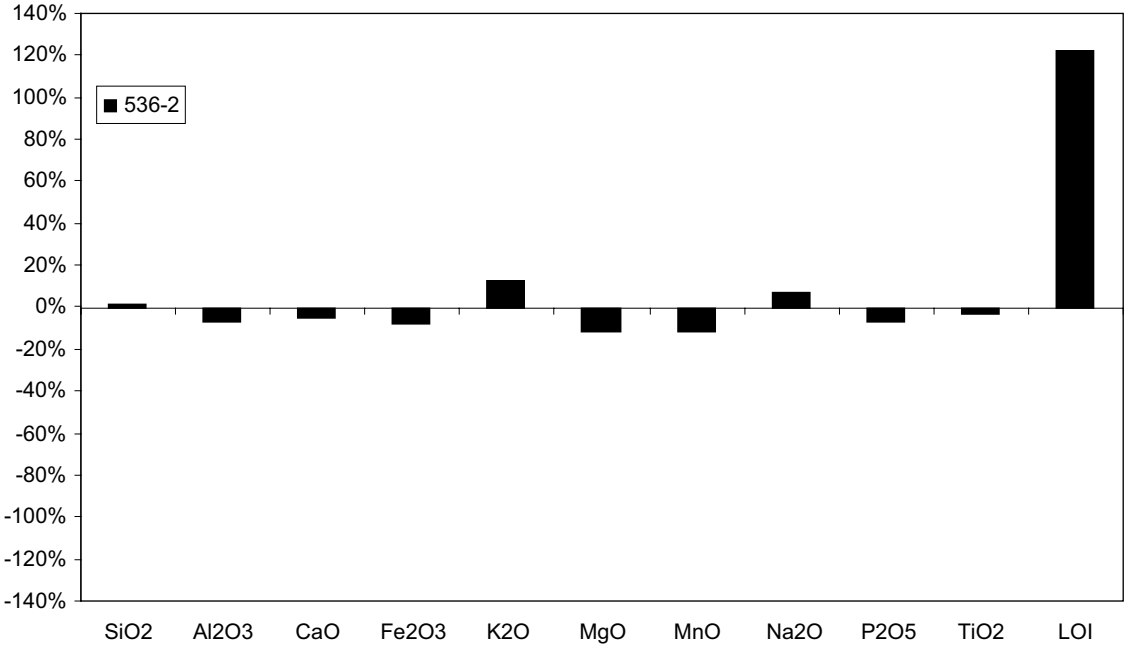

536-2: *Major elements, minor elements and loss on ignition (LOI).*

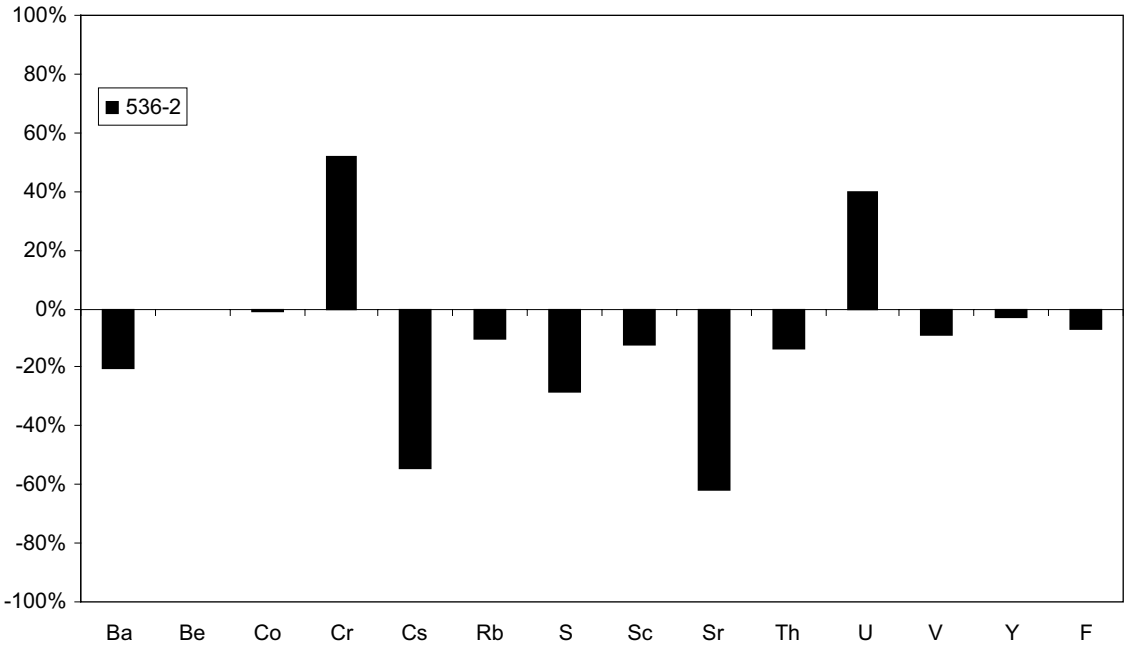

536-2*: Selected trace elements.*

Appendix 2

SEM-EDS analyses

SEM-EDS analyses of K-feldspar, plagioclase, albite, whole plagioclase crystals (in reference samples; G), and whole plagioclase crystals (in red-stained samples; R). * = below detection limit of SEM-EDS. Abbreviations: Whole = analyses of the whole crystal (as oppose to spot analyses) Ser = sericite, Kfsp = K-feldspar, Plag = plagioclase, Preh = prehnite, Chl = chlorite and Epi = epidote.

K-feldspar	Na_2O	Al_2O_3	SiO_2	K_2O	CaO	FeO	BaO	Total	Comments
82R	0.73	19.23	63.60	15.57	*	0.20	0.23	99.55	in albititized plagioclase
100R-1	*	18.91	63.97	16.20	*	0.05	0.63	99.70	in albititized plagioclase
100R-2	0.33	20.57	61.49	15.46	*	0.39	0.76	99.00	in albititized plagioclase
100R-3	0.34	19.04	65.16	16.45	*	0.14	0.22	101.35	in albititized plagioclase
128R-1	0.42	19.19	64.16	15.84	*	0.21	*	100.03	in albititized plagioclase
128R-2	*	19.25	65.22	16.62	*	0.43	*	101.53	in albititized plagioclase
128R-3	*	19.04	65.83	16.85	*	0.05	*	101.76	in albititized plagioclase
128R-4	0.50	18.73	64.30	15.18	*	0.29	0.36	99.37	in albititized plagioclase
128R-5	*	18.76	64.66	16.53	*	0.23	*	100.18	in albititized plagioclase
128R-6	*	18.83	62.73	15.90	0.18	0.34	0.51	98.74	in albititized plagioclase
128R-7	*	19.88	63.14	15.88	0.10	0.22	*	99.33	in albititized plagioclase
144G-1	0.71	19.37	65.22	16.09	*	*	0.53	101.92	Fresh perthite
144G-3	0.85	19.39	65.69	15.51	*	*	0.52	101.69	Groundmass microcline(whole)
144R-1	0.87	19.24	64.40	15.07	*	0.21	1.42	101.21	Perthite phenocryst (whole)
144R-2	0.68	19.34	64.39	15.46	*	*	1.90	101.77	Fresh perthite
144R-3	0.47	19.39	65.63	16.36	*	0.05	*	101.84	in albititized plagioclase
144R-4	0.55	18.48	62.99	15.42	*	*	0.39	97.84	Groundmass microcline
372G-1	0.95	19.04	63.46	14.78	*	*	1.74	99.97	K-feldspar-rich part of perthite
372R-1	*	19.06	65.21	15.69	*	0.14	0.29	100.40	in albititized plagioclase
394G-1	0.53	19.57	63.58	15.42	*	*	2.26	101.36	Fresh perthite
394R-1	0.66	19.34	63.92	15.04	*	*	1.99	100.95	Fresh perthite
661R-1	0.67	18.69	61.66	14.81	*	*	1.25	97.09	K-feldspar-rich part of perthite
661R-2	0.71	18.58	61.09	14.74	*	*	1.34	96.46	K-feldspar-rich part of perthite
661R-3	2.39	18.19	61.86	12.35	*	*	0.59	95.39	K-feldspar-rich part of perthite
661R-4	*	19.47	63.80	16.05	*	0.05	0.65	99.97	in albititized plagioclase
536-1G	1.21	19.38	65.35	14.92	0.16	*	0.64	101.66	Groundmass microcline
536-1R-1	*	18.53	63.85	16.48	*	0.30	0.33	99.48	Red-stained coarse-grained
536-1R-2	*	18.65	64.27	16.55	*	0.50	0.29	100.26	Red-stained coarse-grained
536-1R-3	*	18.65	64.25	16.66	*	0.26	*	99.82	Red-stained coarse-grained
536-1R-4	*	18.85	65.23	16.73	*	0.05	*	100.81	in albititized plagioclase
536-1R-5	*	18.98	64.74	16.36	0.15	*	0.31	100.55	Red perthite phenocryst (whole)
536-2R-1	*	19.24	64.86	16.63	0.30	0.22	0.57	101.83	Red perthite phenocryst (whole)
536-2R-2	0.40	19.12	64.89	16.21	0.17	0.19	0.55	101.53	Red perthite phenocryst (whole)

Plagioclase	Na_2O	Al_2O_3	SiO_2	K_2O	CaO	FeO	Total	An%
81G-1	6.82	26.29	57.38	0.14	7.78	0.13	98.53	39
81G-2	6.93	26.00	58.56	0.10	7.32	0.26	99.18	37
81G-3	6.24	27.92	56.30	0.16	9.29	0.16	100.06	45
81G-4	7.39	26.53	59.44	0.24	7.16	0.12	100.89	35
82G-1	6.91	26.84	58.94	0.15	7.88	0.17	100.88	39
82G-2	7.58	25.73	60.84	0.16	6.62	0.18	101.12	32
128G	6.94	26.72	58.86	0.19	7.46	0.17	100.33	38
144G	6.97	26.66	59.79	0.34	7.29	0.22	101.26	37
172G	6.36	27.70	56.96	0.12	8.61	0.05	99.75	43
394G	8.09	25.39	62.04	0.17	5.83	0.14	101.67	28
394R	8.39	24.58	62.06	0.11	5.27	0.05	100.41	26
661G	8.12	24.79	61.21	*	5.56	0.16	99.85	27
536-2G-1	6.25	27.79	57.51	0.22	8.87	0.05	100.65	43
536-2G-2	6.21	27.87	57.82	0.29	8.90	0.17	101.26	44
536-2G-3	6.52	27.38	57.72	0.32	8.45	0.20	100.59	42

Albite	Na_2O	Al_2O_3	SiO_2	K_2O	CaO	FeO	Total
82R-1	11.15	20.03	68.01	*	0.08	*	99.27
82R-2	10.79	20.05	68.97	*	0.20	*	100.07
100R-1	10.88	20.00	67.24	*	0.32	*	98.44
100R-2	11.12	19.79	68.07	*	0.12	*	99.10
100R-3	11.36	20.10	68.70	*	0.23	*	100.39
128R-1	11.10	20.34	68.46	*	0.47	*	100.37
128R-2	11.15	20.61	68.72	*	0.34	*	100.82
128R-3	11.27	20.03	68.92	*	0.18	*	100.40
128R-4	11.00	19.81	66.77	*	0.53	*	98.11
128R-5	11.06	20.04	67.56	*	0.42	*	99.08
128R-6	10.75	20.29	66.95	0.13	0.56	*	98.68
128R-7	10.90	19.86	66.80	*	0.60	*	98.16
394R	11.19	20.17	67.59	*	0.70	0.39	100.04
661R	9.79	21.88	64.85	1.40	0.99	0.39	99.30
536-2R	10.23	20.90	67.76	0.84	0.17	*	99.90

Whole plag[G]	Na_2O	MgO	Al_2O_3	SiO_2	K_2O	CaO	FeO	BaO	Total	Comments
62G-1	5.33	*	26.72	57.36	4.27	4.49	0.41	0.20	98.78	
62G-2	6.19	0.21	26.15	57.56	2.16	5.61	0.63	*	98.50	
62G-3	5.56	*	29.00	57.10	2.96	5.72	0.54	*	100.88	
81G-1	4.94	0.33	27.81	56.56	3.68	6.19	0.76	*	100.44	plag+kfsp+ser+preh+chl
81G-2	5.30	0.22	27.67	57.09	3.36	6.18	0.92	*	100.74	
81G-3	4.10	*	28.20	56.39	5.12	5.77	0.14	*	100.58	ser-rich(+kfsp) plag
82G-1	5.59	*	27.64	56.79	1.82	7.32	0.51	*	99.69	
82G-2	4.48	0.27	28.07	56.14	4.43	5.82	0.69	*	99.90	ser-rich(+kfsp)
82G-3	5.03	*	27.42	57.67	3.83	5.17	0.65	*	100.11	
100G-1	6.89	0.35	27.68	60.23	2.24	4.10	0.30	*	101.78	
100G-2	6.95	*	26.58	59.47	1.21	5.86	0.23	*	100.29	
100G-3	4.94	0.40	27.88	55.67	3.59	5.40	0.83	*	98.71	
100G-4	6.10	*	27.10	57.25	1.12	7.23	0.34	*	99.14	
128G-1	5.02	1.23	25.46	53.74	2.20	5.87	4.26	*	97.77	ser-rich(+chl)
128G-2	5.66	*	28.20	56.57	0.65	9.03	0.16	*	100.26	
128G-3	5.07	0.30	27.42	55.98	2.95	6.14	1.30	*	99.15	
128G-4	5.98	*	27.34	57.25	0.73	8.15	0.43	*	99.89	
128G-5	6.66	*	27.21	58.60	0.38	7.82	0.19	*	100.86	
128G-6	4.54	0.32	27.48	56.88	3.87	6.34	0.70	*	100.13	
144G-1	7.34	0.20	25.84	61.04	1.28	5.09	0.19	*	100.97	
144G-2	7.50	*	26.37	60.74	0.75	6.10	0.28	*	101.74	
144G-3	7.17	*	26.94	60.87	0.49	6.95	0.19	*	102.62	
144G-4	7.84	0.28	24.94	61.61	1.54	4.75	0.49	*	101.45	
172G-1	5.55	0.23	27.42	56.53	2.24	6.26	0.39	*	98.75	Sericite-rich
172G-2	5.79	1.30	25.53	56.74	1.50	6.79	1.27	*	98.92	Ser/chl-rich
172G-3	6.01	*	27.13	57.19	1.72	6.58	0.38	*	99.00	
172G-4	6.22	*	26.30	58.15	1.85	6.71	0.34	*	99.57	
172G-5	4.64	*	26.99	57.36	4.99	4.41	0.64	*	99.20	Kfsp-rich
172G-6	6.62	*	26.96	58.36	0.51	7.56	0.18	*	100.19	Fresh
372G-1	5.97	*	25.42	57.95	3.74	3.96	0.41	*	97.45	
372G-2	7.40	*	24.38	58.65	1.45	5.33	0.43	*	97.64	
372G-3	6.68	*	24.89	58.78	2.97	4.34	0.43	*	98.10	
372G-4	7.22	*	25.27	60.06	1.67	5.29	0.35	*	99.87	
394G-1	7.64	*	24.70	60.86	1.19	4.62	0.33	*	99.33	
394G-2	7.48	*	24.19	60.86	1.63	3.98	0.42	*	98.56	
394G-3	7.66	0.23	24.77	61.06	1.51	4.70	0.49	*	100.42	
661G-1	7.24	*	23.20	61.72	2.29	3.68	0.55	0.24	98.91	
661G-2	7.42	0.32	23.78	62.35	3.11	2.34	0.62	*	99.94	
661G-3	7.90	*	25.05	60.66	0.84	5.12	0.23	*	99.80	Fresh
661G-4	7.42	*	25.60	61.24	2.10	4.08	0.34	*	100.78	
661G-5	7.87	*	24.62	60.52	1.26	4.73	0.25	*	99.25	
536-1G-1	6.54	0.21	26.55	58.58	2.35	5.21	0.40	*	99.84	
536-1G-2	6.00	*	27.20	57.58	2.90	5.11	0.36	*	99.16	
536-1G-3	6.29	*	26.72	58.16	2.25	5.58	0.39	*	99.38	
536-1G-4	6.12	*	25.65	56.73	2.71	5.30	0.43	*	97.10	
536-2G-1	6.74	*	26.83	58.42	0.42	8.33	0.13	*	100.86	Fresh

Whole plag[R]	Na_2O	MgO	Al_2O_3	SiO_2	K_2O	CaO	FeO	BaO	Total	Comments
62R-1	4.03	0.38	26.27	58.04	8.50	0.53	1.06	*	98.81	
62R-2	5.40	*	23.14	61.71	7.29	0.79	0.57	0.26	99.17	
62R-3	4.16	0.33	23.65	60.11	8.73	0.67	0.95	*	98.61	
62R-4	5.57	0.24	21.81	62.52	7.46	0.89	0.73	0.23	99.45	
62R-5	5.05	0.35	23.41	60.13	7.38	0.88	0.93	*	98.15	
81R-1	3.67	0.33	23.88	60.83	9.81	0.51	0.94	0.23	100.22	Kfsp-rich(+ser)
81R-2	3.03	0.62	22.67	60.83	10.74	0.84	1.45	0.69	100.89	Kfsp-rich(+ser)
81R-3	2.22	0.36	25.28	56.92	9.38	3.67	1.19	0.50	99.50	
81R-4	3.01	0.32	24.15	60.13	10.09	1.35	0.83	0.54	100.43	
82R-1	7.20	*	21.04	64.36	5.53	0.39	0.93	0.14	99.59	
82R-2	8.76	*	19.88	65.95	3.88	0.47	0.56	*	99.50	
82R-3	7.54	*	19.62	65.98	5.62	0.77	0.62	*	100.15	
82R-4	3.02	*	19.95	63.99	11.76	1.02	0.84	0.34	100.92	Kfsp-rich
82R-5	8.24	*	19.91	66.47	4.56	0.50	0.70	*	100.39	Albite-rich
100R-1	8.12	*	23.15	63.48	3.40	0.89	0.67	*	99.72	
100R-2	8.00	0.39	24.65	63.62	3.47	0.84	0.71	*	101.68	
100R-3	6.61	0.35	25.89	62.08	5.07	1.26	0.82	0.33	102.42	
100R-4	4.08	0.51	24.25	59.00	8.70	0.62	1.49	0.53	99.18	
100R-5	2.55	0.42	25.54	57.18	10.17	0.74	1.06	*	97.66	
128R-1	8.02	*	20.61	64.72	4.09	0.38	0.80	*	98.61	
128R-2	4.95	0.30	20.65	63.09	8.48	0.55	1.25	*	99.27	
128R-3	6.10	*	20.04	66.17	6.70	0.45	0.68	*	100.14	
128R-4	3.33	0.47	23.40	60.55	10.19	0.57	1.33	0.33	100.17	
128R-5	7.54	0.27	23.87	62.13	3.66	1.08	1.35	*	99.90	
128R-6	6.16	0.28	24.08	61.83	6.07	0.90	1.02	*	100.34	
128R-7	4.65	*	21.34	63.79	9.45	0.20	1.07	*	100.51	
128R-8	4.96	*	21.05	63.52	8.46	0.23	1.14	*	99.37	
128R-9	4.19	0.37	22.89	62.17	8.46	0.93	1.11	*	100.13	Sericite-rich
128R-10	4.28	*	20.37	65.16	10.48	0.32	0.30	0.15	101.08	
144R-1	7.31	*	20.45	65.81	5.74	0.39	0.96	*	100.67	Kfsp/Fe-rich
144R-2	10.44	*	20.58	67.60	0.77	0.56	0.15	*	100.08	Albite-rich (+kfsp/Fe)
144R-3	8.63	*	20.82	66.26	3.16	0.59	0.40	*	99.85	
144R-4	7.57	0.52	22.23	62.22	3.41	2.80	0.88	*	99.64	Ser/albite-rich+preh(?)
144R-5	8.62	*	20.85	63.63	2.99	0.31	0.56	*	96.98	
172R-1	3.88	0.34	26.12	58.68	7.64	2.63	0.99	*	100.28	Ser/Kfsp-rich+preh
172R-2	4.44	*	25.17	59.52	6.48	3.68	0.67	0.33	100.30	(Ser)/Kfsp-rich+preh
172R-3	3.33	0.20	25.54	57.21	7.32	4.41	0.74	*	98.76	Ser/Kfsp-rich+preh
172R-4	3.33	0.29	27.47	56.06	6.62	4.35	0.72	0.26	99.10	Ser/Kfsp-rich+preh
172R-5	2.98	0.29	24.16	60.56	10.14	0.85	0.69	0.37	100.04	
372R-1	6.51	0.24	23.66	60.56	4.68	3.27	0.74	0.18	99.91	Ser/Kfsp-rich+preh
372R-2	5.41	0.40	21.30	62.36	7.39	1.22	0.65	*	98.73	Ser/Kfsp-rich+preh
372R-3	3.14	0.28	21.76	63.37	9.91	1.05	0.52	*	100.02	Kfsp-rich
372R-4	4.30	0.19	21.84	62.73	9.40	0.85	0.38	0.18	99.87	Kfsp-rich
394R-1	8.63	*	23.93	62.67	2.28	1.28	0.63	*	99.43	Rel. fresh alb+ser/kfsp/preh(?)
394R-2	7.00	0.23	24.08	60.44	2.87	3.41	0.38	*	98.40	Rel. fresh alb+ser/kfsp/preh(?)
394R-3	7.81	*	19.89	66.50	3.14	1.28	0.81	*	99.43	Rel. fresh alb+ser/kfsp/preh(?)
394R-4	6.01	0.33	23.26	62.03	5.77	1.75	0.34	0.26	99.74	Ser/Kfsp-rich+preh

Whole plag[R]	Na_2O	MgO	Al_2O_3	SiO_2	K_2O	CaO	FeO	BaO	Total	Comments
661R-1	4.85	0.40	20.59	63.99	8.98	0.55	0.61	*	99.97	
661R-2	4.65	0.31	20.42	64.10	9.47	0.68	0.80	*	100.43	
661R-3	4.59	*	22.14	63.25	8.81	0.50	0.48	*	99.76	
661R-4	5.44	0.26	20.59	63.76	8.23	0.62	0.46	*	99.36	
661R-5	7.28	*	19.81	68.66	3.91	0.86	0.25	*	100.77	
661R-6	3.28	*	20.14	62.65	10.67	1.24	0.40	*	98.36	
661R-7	2.04	*	19.56	62.26	13.22	0.33	0.58	*	97.99	
536-1R-1	5.71	0.32	20.23	62.77	6.39	3.58	1.38	0.35	100.72	(Ser)/kfsp-rich+preh+some epi
536-1R-2	4.18	*	19.03	64.91	8.90	1.53	1.49	0.17	100.21	(Ser)/kfsp-rich+preh(+ epi+chl)
536-1R-3	4.34	0.42	19.81	65.43	9.72	0.66	1.45	*	101.83	(Ser)/kfsp+preh+epi
536-1R-4	4.26	0.53	20.07	62.86	9.20	1.34	2.05	*	100.31	(Ser)/kfsp-rich+preh(+ epi+chl)
536-1R-5	5.29	*	18.76	67.67	7.78	1.45	0.66	*	101.61	(Ser)/kfsp-rich+preh+ epi(+qz)
536-2R-2	7.94	*	19.99	67.87	3.79	1.14	0.35	*	101.08	(Ser)/kfsp+preh(+epi)
536-2R-3	8.78	*	21.19	66.88	3.59	0.33	0.58	*	101.35	Ser/Kfsp-rich(+preh)
536-2R-4	7.47	*	21.63	63.04	3.65	3.31	0.87	*	99.96	(Ser)/kfsp+preh(+epi)